# Study of thermal transitions in polymers by a multifrequency modulated DSC technique

Autor : Iria Fraga Rivas

Departament de Màquines i Motors Tèrmics. Grupo TERFIQ.

Escola Tècnica Superior d'Enginyeries Industrial i Aeronàutica de Terrassa

Director: John M. Hutchinson
Co- Director: Salvador Montserrat Ribas

Tutor: Miguel Mudarra López
Departament de Física i Enginyeria Nuclear

*Programa de Doctorat: Física Computacional i Aplicada.*

**Tesi presentada per obtenir el grau del Doctora amb menció europea per la Universitat Politècnica de Catalunya**

**Terrassa, Gener 2010**

*Le savant n'étudie pas la nature parce que cela est utile ; il l'étudie parce qu'il y prend plaisir et il y prend plaisir parce qu'elle est belle. Si la nature n'était pas belle, elle ne vaudrait pas la peine d'être connue, la vie ne vaudrait pas la peine d'être vécue. Je ne parle pas ici, bien entendu, de cette beauté qui frappe les sens, de la beauté des qualités et des apparences ; non que j'en fasse fi, loin de là, mais elle n'a rien à faire avec la science; je veux parler de cette beauté plus intime qui vient de l'ordre harmonieux des parties, et qu'une intelligence pure peut saisir.*

*Scientists do not study nature because it is useful; they study it because they delight in it, and they delight in it because it is beautiful. If nature were not beautiful, it would not be worth knowing; and if nature were not worth knowing, life would not be worth living. I am not talking about, of course, the beauty which strikes the senses, the one of qualities and appearances. I am far from despising this, but it has nothing to do with science. What I mean is that more intimate beauty which comes from the harmonious order of its parts, and which a pure intelligence can grasp.*

*Los científicos estudian la naturaleza no porque sea útil, sino porque encuentran placer en ello, y encuentran placer porque es hermosa. Si no lo fuera, no merecería la pena conocerla, y si la naturaleza no mereciera la pena, la vida tampoco. No me refiero, claro está a la belleza que estimula los sentidos, la de las cualidades y las apariencias; no es que menosprecie tal belleza, nada más lejos de mi intención, mas ésta nada tiene que ver con la ciencia; me refiero a esa hermosura más profunda que emana del orden armonioso de las partes, susceptible de ser captada por una inteligencia pura.*

*Jules Henri Poincaré*. Science et mèthode. Paris: Ernest Flammarion ed. 1908.

A todos los maestros que han pasado por mi vida, empezando por mis padres,

ya que a su esfuerzo, dedicación y conocimiento debo todo lo que sé…

Aunque realizada íntegramente en la ETSEIAT de Terrassa, la historia de esta tesis tiene un capítulo previo en la Universidad de Santiago de Compostela; es por ello por lo que siento que he de comenzar los agradecimientos en mi tierra:

A Lisardo, in memoriam, él tuvo la capacidad de ver mi potencial y supo convertir a una licenciada en Física en un motivado proyecto de científica.

A María, que me cogió de la mano cuando comenzaba a dar mis primeros y tambaleantes pasos en el metódico mundo del laboratorio, y me enseñó, paciente y tan bien a caminar sola de manera firme y segura. Y porque más allá de hacer de simple mentora, surgió a la vez una sincera y mutua relación de amistad.

A Jose y Xurxo, qué-altos-qué-fuertes, por su música de fondo, por estar dispuestos siempre a ayudar a dos damas en apuros, por su comprensión con la raza de las cotorras y por regalarnos un estupendo viaje-congreso a Polonia.

A mis padres, por ser siempre, en los momentos de pérdida de rumbo y tempestad, el faro guía que devuelve con seguridad el barco a puerto seguro.

A mis hermanos, Diego y Nela, por admirarme y creer en mí más que yo misma. Por sus ánimos en todo momento, y por no dudar nunca (no como yo) que lo conseguiría.

A Marc; a él le tocó la peor parte de la tesis, la de los nervios y los agobios. Gracias por saber secar y hacer desaparecer lágrimas de impotencia y cansancio en los momentos de flaqueza y mantenerte en todo momento inmune a mis gruñidos. Por la risoterapia permanente y por formar conmigo el mejor de los equipos. T'estimo.

To Mettler-Toledo, thanks for the important economical and scientific support.

To the people in Rostock: the laboratory staff (with special mention to the head Prof. Schick) and also the visitors during my stay and to the friends in Justus-von-Liebeg-Weg (Marta, Sophie, Lin-Lin, Ely, Susanne, Monika…). Thanks to Carmen, who helped me and answered my questions before my arrival, and finally when we met, we get friends from the very first moment. My research there was not as successful as we expected, but during those four months, I learnt some thinks about Physics, computers! and life that are not reflected in any diploma.

A Gloria, por su hospitalidad y tantos meses de risas, juergas, amistad y confesiones de banqueta. A Luis y Lola, por hacer de padres postizos. Al resto de familia peregrina por hacerme sentir desde el primer momento en casa y sacarme a pasear los fines de semana. A Ramón, por ayudarme a poner bonito todo este contenido que se me antojaba indominable al principio.

A Clara, por ser como es y por estar siempre ahí para mí aguantando lo inaguantable, aunque sea en la distancia. Gracias por los años compartidos en Santiago.

Thanks to Gosia: she had the same doubts as I had, she thought the same as I did and finally both took the same decision. Thanks to those secret talks in the sun full of confessions.

A Frida, por hacer de "madre" de laboratorio, por estar siempre pendiente de que todo esté en orden y de que funcione. Sin ella el laboratorio no tendía sentido (ni

estaría entero). Es un placer compartir despacho y trabajar en un equipo tan bien coordinado (a pesar del desorden natural de John y el mío propio…).

A Pilar, por las comidas compartidas y los consejos regalados. Por alegrarse con mis alegrías y preocuparse por mis (pocos) problemas. Al resto de "gente de comedor" que "fueron apareciendo" poco a poco: Bea, Vane, Miquel, David, Mari, Inés… gracias por compartir sonrisas, comidas, confidencias, coral, actividades UNIVERS y alguna que otra cenita. La Escuela es más humana (¡y amena!) junto a vosotros.

Al Departamento de Física Aplicada por las facilidades para presentar mi tesis en él y convalidar mis cursos anteriores. Especial mención a Isabel Mercader, encargada de la aprobación inicial para poder presentar el proyecto de tesis aquí y a Esther Cantos, a la que he mareado de todas las maneras posibles que se me ocurren y siempre ha atendido a mis e-mails, llamadas, súplicas, preguntas y papeleos varios al momento y de la manera más rápida, fácil y eficiente.

Y por último, y por ello el que es el agradecimiento más importante, a John y Salvador, porque cuando aparecí por el laboratorio pidiendo un proyecto creyeron en mí desde el primer momento y me "enchufaron" el TOPEM, sin garantías de que pudiese obtener nada de él. Afortunadamente, cuatro años después siento, entre orgullosa y sorprendida, que a un aparato que hubiese tirado por la ventana muy a gusto el primer año, hasta es posible cogerle cariño. A ambos debo mi primer artículo como primera autora con la satisfacción que ello conlleva. Tras decidir quedarme y continuar con la tesis he de agradecerles el haber hecho todo lo posible (sobre todo económicamente) para que esto saliese adelante y porque desde el primer día me han estado enseñando tanto en tantos aspectos. Ha sido un placer aprender a su lado. Salvador se retira, pero con John aún me quedan muchas cosas (¡y muchas ganas!) para seguir investigando.

# INDEX

# 1. Motivation

# 2. Introduction

# 3. Application to the glass transition of Polycarbonate

# 4. Vitrification during the isothermal cure of a thermoset

# 5. Vitrification and devitrification during the non-isothermal cure of a thermoset

# LIST OF ACRONYMS AND ABBREVIATIONS USED

$A_T$: temperature amplitude/ pulse amplitude
ADSC: Alternating Differential Scanning Calorimetry
CHT: Continuous Heating Transformation (cure diagram)
$C_p$: Heat Capacity
$C'_p$: in-phase heat capacity.
$C''_p$: out-of-phase heat capacity
$c_p(f)$: specific heat capacity frequency-dependent.
$C_{pg}$: heat capacity in the glassy state
$C_{pl}$: heat capacity in the glassy state
$c_p(f)$: specific heat capacity angular frequency-dependent
$C^*_p$: complex heat capacity
$C_{p0}$: quasi-static heat capacity
c.w.: calculation window
DEA: dielectric analysis
$\Delta C_p$ vit: heat capacity change in the vitrification
$\Delta H_{tot}$: total heat flow
$\Delta H_v$: heat flow in the vitrification
DF: Diffusion factor
DGEBA: diglycidyl ether of bisphenol A
DSC: Differential Scanning Calorimetry
$E_c$: Activation energy
Ee: epoxi equivalent
g(t): transfer function
HF: heat flow
$HF_{non\ rev}$: non- reversing heat flow
$HF_{rev}$: reversing heat flow
LMDSC: Light Modulated Differential Scanning Calorimetry
MDSC: Modulated Differential Scanning Calorimetry
MF: mobility factor
PC: Polycarbonate
PEM: Parameter Estimation Method
PEN: Poly(ethylene 2,6-naphthalene dicarboxilate)
PET: poly(ethylene terephthalate)
PLA: Polylactide
s.i.: sampling interval
s.t.r.: switching time range.
Std: Standard
$T_g$: glass transition temperature.
$T_{g0}$: glass transition temperature of an uncured system resin + hardener
$T_{g\infty}$: glass transition temperature of the fully cured system resin + hardener
$T_c$: cure temperature
$T_f$: fictive temperature
$T_{mid}$: mid-point temperature
$t_{cw}$: calculation window time
TGAP: triglycidyl ether of para-aminophenol
TMDSC: Temperature Modulated Differential Scanning Calorimetry

TOPEM: Temperature Modulated DSC with PEM
TTT: Time Temperature Transformation (cure diagram)
$t_{devit}$: devitrification time
$t_v$: vitrification time
UV: Ultra Violet
VTF: Vogel-Tammann-Fulcher
WLF: Williams-Landel-Ferry
WOK: Web of Knowledge.
wt%: weight percent
x: non-linearity parameter.

$\alpha$: degree of cure
$\alpha_v$: degree of cure at vitrification
$\beta$: non-exponencial parameter
$\beta_u$: underlying heating (cooling) rate
$\delta$: phase angle
$\lambda$: diBenedeto parameter
$\omega$: angular frequency
$\Phi$, $\phi$: heat flow

# CHAPTER 1
# MOTIVATION

Differential Scanning Calorimetry (DSC) is one of the most widely used thermal analysis techniques for the study of transitions and relaxation processes in polymers and also in other materials. It measures the heat flow as a function of time and/or temperature, and determines the energy released or absorbed by a sample. Its advantages are that it is fast and sensitive, the amount of sample needed is small (of the order of mg) and the sample preparation is easier than for some other techniques. It is used not only for general Thermal Analysis, but also to test for Quality Control or Research and Development of different types of materials. A wider description of the technique is given in the next chapter.

As an illustration of the evolution through the years and the research areas where
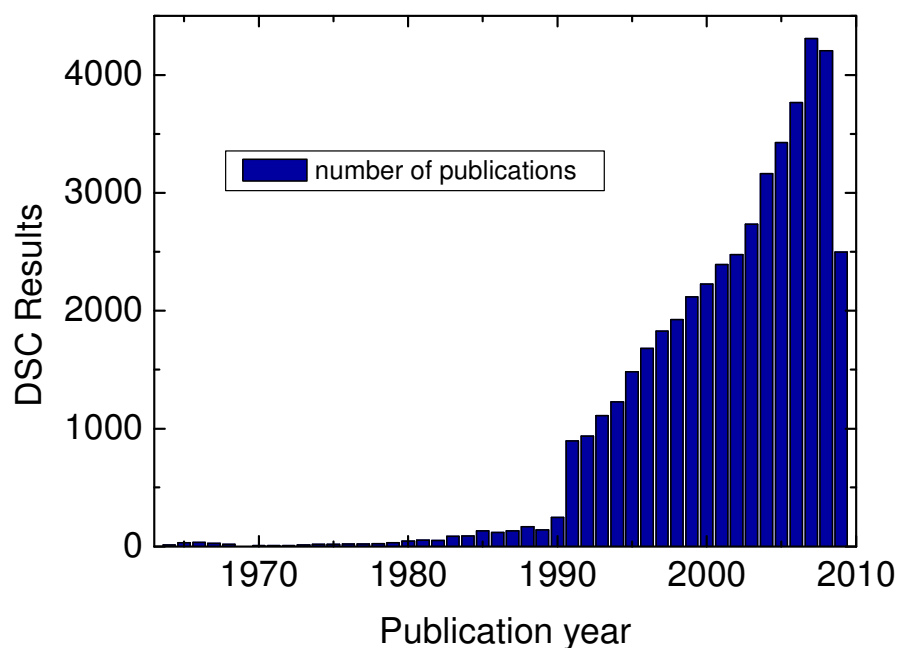
Figure 1.1. Number of Publications classified by year. Results were obtained in a search in the Web of Knowledge using the Topic "DSC" and making a filter of Science and Technology and excluding medical articles (DSC also means dynamic-susceptibility-contrast magnetic resonance).

1

this technique is applied, a simple search in the Web of Knowledge (WOK) database using the keyword "DSC" with a filter in Science and Technology results in more than 45,000 references for a technique that was introduced in 1963, some 45 years ago [1]. The evolution since its introduction until the present can be seen in Figure 1.1. It is clear that the use of this technique has been growing at an ever increasing rate with time. It should be noted that the count of the last year is incomplete, and would increase when the database is updated.

If these results are analyzed in Subject Areas, with a filter of a minimum of 1500 results, we can observe that the Chemistry and the Polymer Science Groups represent the main part, closely followed by that of Materials Science. These Results are shown in Figure 1.2.
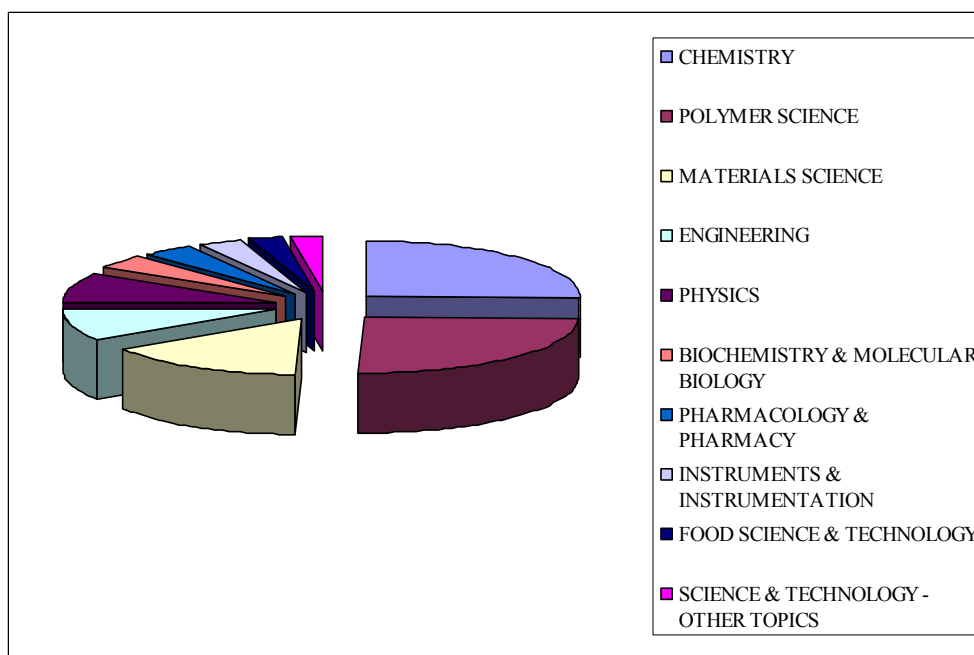


Figure 1.2. Classification of the previous results of the search by areas of application.

More recently, in 1993, a new technique was commercialised in which a periodic temperature modulation of small amplitude is superimposed on the underlying rate

2

of conventional DSC [2,3]. Several versions of this exist in the market, including Modulated DSC (MDSC, from TA Instruments) and Alternating DSC (ADSC, from Mettler-Toledo), and they are usually referred to generically as Temperature Modulated DSC techniques (TMDSC).

Despite their differences, all are fundamentally based upon the same principle, which involves a Fourier Transformation of the modulated heating rate and heat flow signals, from which one can obtain certain information additional to that available from conventional DSC. In a single experiment it is possible to determine the response of the polymer on two different time/frequency/rate scales, which has been shown to offer advantages in a number of different areas [e.g. 4-7], and in particular in its application to cross-linking reactions [8-15] and the glass transition [16-21]. A more detailed description of the technique is given in the next chapter.

Nevertheless, the impact of TMDSC does not appear to have been as dramatic as it could have been. A new search in the Web of Knowledge database [22] using the combination of keywords "TMDSC or MDSC or ADSC" yields fewer than 600 references, a strike rate considerably less than that for "DSC" above. The subject areas of publication are the same as in the case of the previous DSC search. The evolution with time of the TMDSC publications is shown in Figure 1.3, together with the earlier results for DSC for comparison.

In the first place, it can be clearly observed in Figure 1.3 that the number of publications of Modulated DSC is insignificant compared with the DSC results obtained. Secondly, it can be seen in the inset that the number of publications rose rapidly initially, but reached a plateau at about 1998, and thereafter has remained rather constant at about $55 \pm 15$ publications per year. One possible reason for this is

3
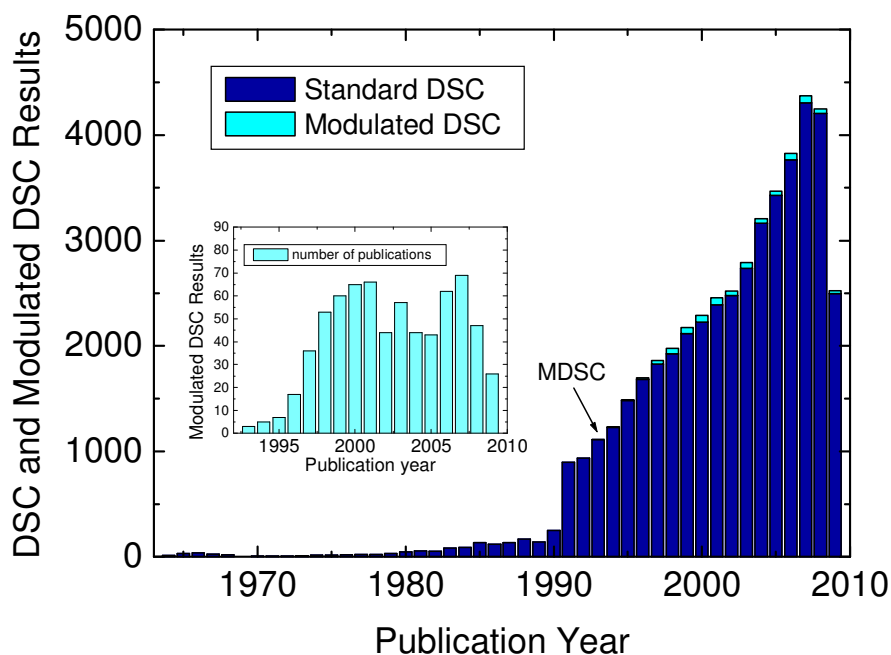
Figure 1.3. Number of Publications classified by year. Results were obtained in a search in the Web of Knowledge using the Topic "MDSC" or "ADSC" or "TMDSC" and selecting the same filter as in the previous search of "DSC". Dark Blue corresponds to DSC Results and Cyan corresponds to Temperature Modulated DSC Results.

that, despite the advantages afforded by TMDSC in various areas, and particularly in those specifically mentioned above, it is not a particularly convenient technique to use. Perhaps of major importance here, at least in respect of ADSC, is that it requires a minimum of two separate scans, a "blank" and a "sample", for any given set of experimental parameters, which results in a very time-consuming procedure if one wishes to study, for example, the frequency dependence of a certain phenomenon. Thus any technique that could overcome this drawback would be welcome, and this is just what TOPEM can offer.

The principles of TOPEM [23] are described in detail in the next chapter, but here it can be stated simply that the fundamental idea is that instead of being based upon a periodic modulation of the heating rate, as is the situation with TMDSC techniques, TOPEM uses a stochastic modulation of the heating or cooling rate by means of random pulses of temperature. This stochastic perturbation introduces a broad frequency spectrum in the response, which implies that *TOPEM is apparently able to determine the complex heat capacity over a range of frequencies in a single scan.*

In the present thesis, a detailed description of the basis and operation of TOPEM is presented. In an initial study, the influence of all the different parameters (experimental and calculation) on the results of an experiment is analyzed. Following this initial study, and with a more profound understanding of the technique as a result, different transitions of polymers are selected and investigated, these results then being compared with those obtained by modulated DSC (in the present case, ADSC). In some cases, additional simulations were made for comparison with the experimental results, to complete and/or justify them.

The advantages, precision, limitations and applications of this new technique are analyzed and presented here. The limitations observed are planned to be studied in the future. The advantages observed will be useful for the application of this technique to analyze different materials as those studied in the present work. Perhaps in a few years, a search in the WOK will give a significantly different result from that presented in Figure 1.4, in which TOPEM results have been added to the Temperature Modulated DSC results previously presented in the inset of Figure 1.3.
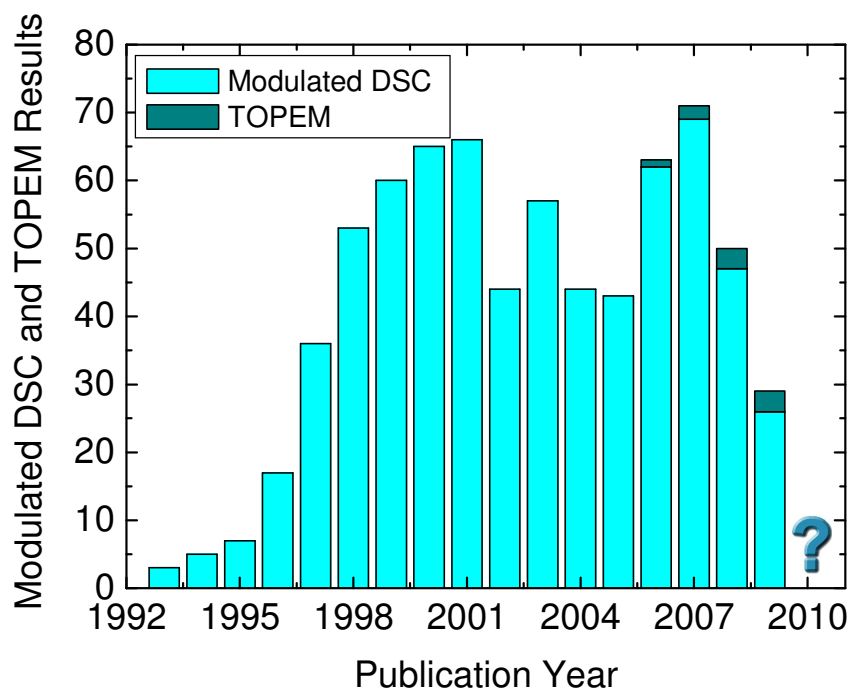
Figure 1.4. Number of Publications classified by year. Results are the same as in the previous search, and the results from the TOPEM search are added. Cyan corresponds to Modulated DSC Results and Dark Cyan to TOPEM Results.

All the experimental part was made in the same calorimeter, a DSC823$^{e}$ from Mettler-Toledo equipped with sample robot and Julabo FT400 intracooler, and with STAR$^{e}$ software for control of the experimental conditions and for data analysis. The same calorimeter can be used for conventional DSC, for ADSC or for TOPEM; the difference lies only in the software. This has the advantage of permitting the comparison between the two modulated techniques to be made without any differences arising due to the use of two different calorimeters.

# References

1. E. S. Watson, M. J. O'Neill, J. Justin and N. Brenner; *Anal. Chem. 36,* **1964**, 1233.

2. P.S. Gill, S.R. Sauerbrunn and M. Reading; *J. Thermal. Anal. 40,* **1993**, 931.

3. M. Reading, D. Elliot and V.L. Hill; *J.Thermal Anal. 40,* **1993**, 949.

4. M. Reading; *Trends in Polymer Science, 1* (1993) 248.

5. J. E. K. Schawe and G. W. H. Höhne; *Thermochim. Acta, 304/305,* **1997**, 111.

6. K. J. Jones, I. Kinshott, M. Reading, A. A. Lacey, C. Nikolopoulos and H. M. Pollock*; Thermochim. Acta, 304/305,* **1997**, 187.

7. M. Angiuli, C. Ferrari, L. Lepori, E. Matteoli, G. Salvetti, E. Tombari, A. Banti and N. Minnaja; *J. Thermal Anal. Calorim., 84,* **2006**, 105.

8. S. Montserrat and I. Cima; *Thermochim. Acta, 330,* **1999**, 189.

9. S. Swier and B. Van Mele; *Thermochim. Acta, 330,* **1999**, 175.

10. W. Jenninger, J. E. K. Schawe and I. Alig; *Polymer, 41,* **2000**, 1577.

11. G. Van Assche, E. Verdonck and B. Van Mele; *J. Thermal Anal. Calorim., 59,* **2000**, 305.

12. S. Montserrat and J. G. Martin; *J. Appl. Polym. Sci., 85,* **2002**, 1263.

13. S. Montserrat and J. G. Martin; *Thermochim. Acta, 388,* **2002**, 343.

14. M. Villanueva, L. Núñez, M. R. Núñez, B. Rial, L. Fraga and S. Montserrat; *J. Thermal Anal. Calorim., 79,* **2002**, 45.

15. J. M. Salla, X. Ramis, J. M. Morancho and A. Cadenato; *Thermochim. Acta, 388,* **2002**, 355.

16. J. M. Hutchinson and S. Montserrat; *J. Thermal Anal., 47,* **1996**, 103.

17. B. Wunderlich, A. Boller, I. Okazaki and S. Kreitmeier; *J. Thermal Anal., 47,* **1996**, 1013.

18. S. Weyer, A. Hensel and C. Schick; *Thermochim. Acta, 305,* **1997**, 267.

19. J. M. Hutchinson and S. Montserrat; *Thermochim. Acta, 305,* **1997**, 257.

20. J. M. Hutchinson; *Thermochim. Acta, 324,* **1998**, 165.

21. S. Weyer, H. Huth and C. Schick; *Polymer 46,* **2005**, 12240.

22. Search in the web of knowledge connected trough the FECYT (Spanish Fundation for Science and Technology) and the MICINN (Spanish Ministry of Science and Innovation) http://www.accesowok.fecyt.es/login/ Searches updated: SEP 2009.

23. J.E.K. Schawe, T. Hütter, C. Heitz, I. Alig and D. Lellinger; *Thermochim. Acta 446*, **2006**, 147.

# CHAPTER 2
# INTRODUCTION

## 2.1. Definition of Thermal Analysis

Thermal analysis covers a group of techniques in which a physical property of a substance is measured as a function of temperature whilst the substance is subjected to a controlled temperature program [1].

## 2.2. Differential Scanning Calorimetry

Differential Scanning Calorimetry (DSC) is a thermal analysis technique in which the difference in energy input into a substance and a reference is measured as a function of temperature whilst they are subjected to a controlled temperature programme. Two modes can be distinguished depending on the method of measurement used: Power-Compensation DSC and Heat-Flux DSC [1]. The second one, heat-flux DSC, is the mode of the calorimeter used in the present thesis.

In a heat-flux DSC, sample (S) and reference (R) are placed in small crucibles and positioned on a heat-flux plate placed inside a furnace. The plate generates a very controlled heat flow from the furnace wall to the sample and reference. Temperature measurement also takes place at this plate, directly below the crucible. In the case of the calorimeter used for the present work, there are 56 thermocouples for each crucible. This design eliminates the influence of changes in the thermal resistance of the system. In this way, enthalpy changes in the sample can be measured accurately [2]. If the sample undergoes any transition or reaction, there is a difference in the temperatures of the sample and reference that is related with the heat flow released (exothermic process) or absorbed (endothermic process) by the sample. This heat flow is directly measured by the calorimeter as a function of time and/or temperature. The experiments are performed in an inert atmosphere of Nitrogen. Figure 2.1 shows a furnace cross section of the calorimeter [3] with a detail of the

9

sensor and a picture of two aluminium crucibles, a sample and a reference, situated on the plate.



**Key**

1. Furnace lid
2. Crucibles on the DSC sensor
3. Silver furnace
4. PT100 of furnace
5. Flat heater between two insulating disks
6. Thermal resistance for cooler
7. Cooling flange
8. Compression spring construction
9. Cooling flange PT100
10. DSC raw signal for amplifier
11. Dry gas inlet
12. Purge gas inlet
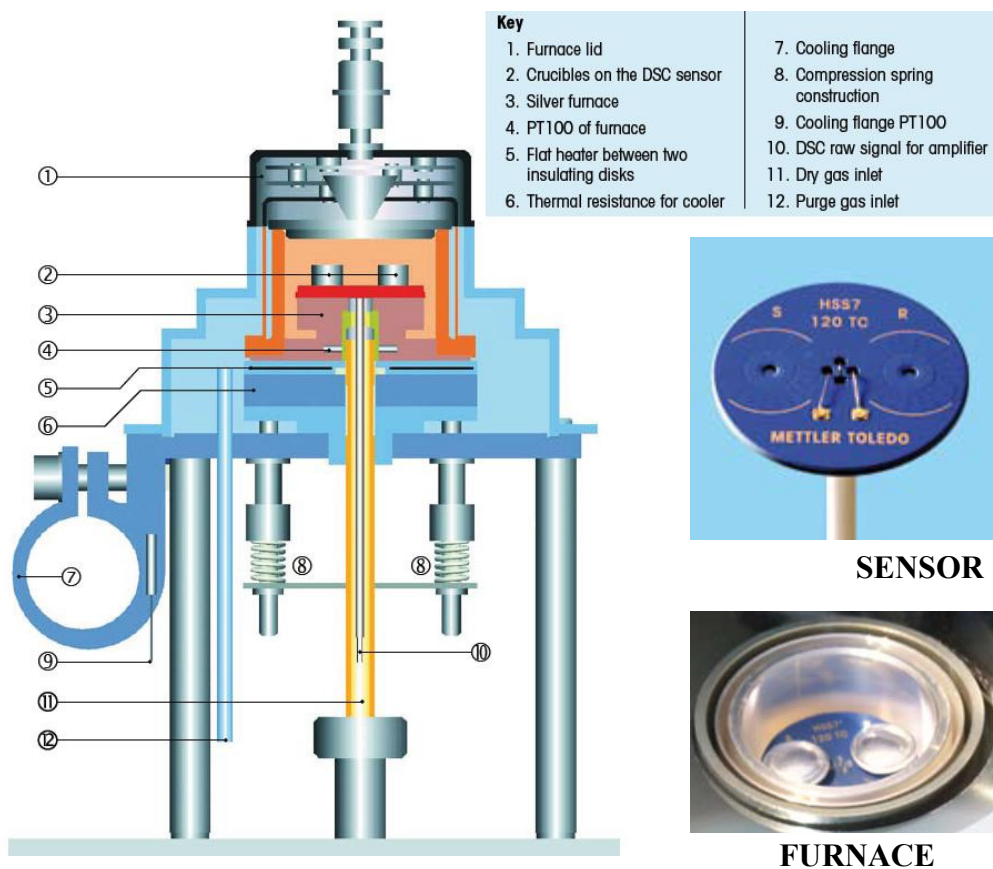
**SENSOR**

**FURNACE**

Figure 2.1. Furnace Cross Section of the calorimeter used. The upper Figure on the right shows a detail of the sensor with the thermocouples, and the locations of the sample (S) and the reference (R). The lower Figure shows the furnace with sample and reference inside aluminium crucibles.

In a conventional DSC experiment, a sample and a reference (normally a crucible with a sample with no thermal activity into the studied temperature range; generally, an empty crucible is used) are heated or cooled at a linear rate, or maintained at a constant temperature in an isothermal experiment.

A temperature programme of a standard DSC experiment can be described by Equation (1):

$$T(t) = T_0 + \beta_u \cdot t \qquad (2.1)$$

where $T_0$ is the initial temperature and $\beta_u$ the underlying heating (cooling) rate. In the case of an isothermal experiment, $\beta_u$ is zero.

Figure 2.2 shows schematic temperature programmes for standard DSC basic experiments: isothermal and heating at a constant rate. It is also possible to programme scans on cooling, and to combine different types of scans (called segments) in the same experiment.
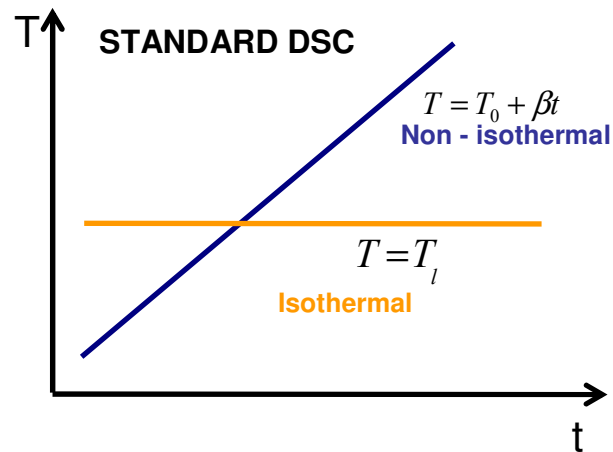


Figure 2.2- Schematic temperature programmes for isothermal and non-isothermal experiments in standard DSC.

From the response of the sample to the temperature programme, namely the heat flow as a function of time or temperature, it is possible to obtain information about the thermodynamic processes such as melting, crystallization, and glass transitions or kinetic processes such as cure and physical aging, that have taken place during the

experiment. Likewise, it is also possible to measure absolute values of, and changes in, thermal properties such as heat capacity and thermal conductivity but not in a single scan.

As an example of a typical DSC measurement, Figure 2.3 shows the heat flow obtained on heating Polyethylene-terephthalate (PET) from ambient temperature to 290 ºC at 10 K/min. PET is a semi-crystalline polymer that shows three different transitions: the first transition is the glass transition with an enthalpic relaxation, the second one is cold crystallization and the last one corresponds to melting.
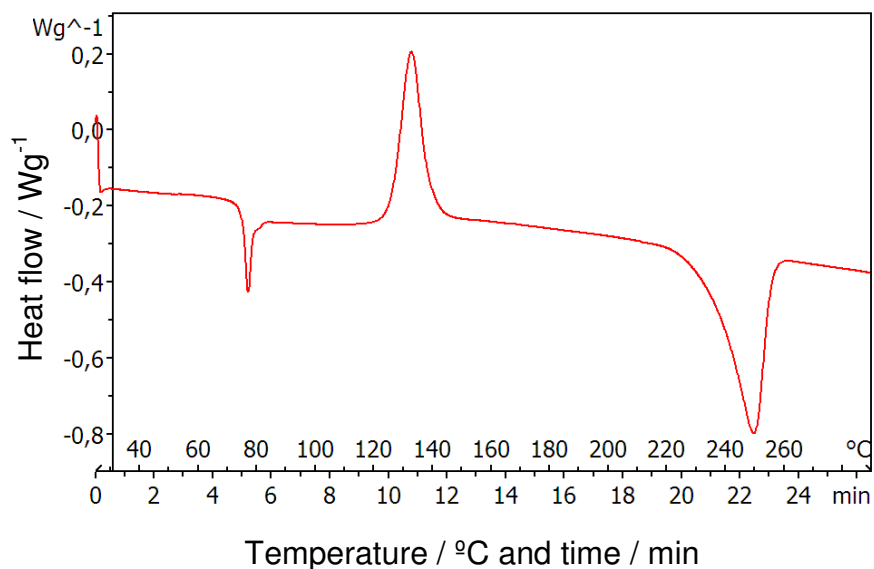


Figure 2.3. DSC curve obtained for a PET sample heated at 10 K/min from ambient temperature to 290 ºC. Black curve shows the heat flow released during the experiment, red curve is the heat flow per gram of substance.

As was presented in the previous chapter, DSC is a widely used technique with a wide variety of application areas. Its main advantages are that it is easy to use, fast, and sensitive and that only a small amount (mg) of sample is needed. It is important to remark also that the sample can be in either the solid or the liquid state. This advantage also implies some difficulties, as for example, ensure a good thermal contact in the case of powders.

12

However, it also has some drawbacks, such as not being able to separate different overlapping transitions that happen in the same temperature range, the difficulty of detecting very weak transitions, or the requirement for multiple experiments to determine heat capacities that increases the experimental time needed.

## 2.3. Modulated Temperature DSC

As was pointed out in the previous chapter, TMDSC techniques were introduced in the market in 1993 [4, 5]. In this technique a periodic temperature modulation of small amplitude is superimposed on the underlying rate of conventional DSC. It has the same heat-flux cell design as in standard DSC, the only difference being in the temperature programme imposed on the sample and reference. A temperature programme for a Temperature Modulated DSC experiment can be described by Equation (2.2):

$$T(t) = T_0 + \beta_u \cdot t + A_T \sin (\omega t) \qquad (2.2)$$

where $T_0$ is the initial temperature, $\beta_u$ is the underlying heating rate, $A_T$ is the amplitude of temperature modulation and $\omega$ is the frequency of the modulation (period=$2\pi/\omega$).

The corresponding heating rate related to this temperature programme is:

$$\beta = \beta_u + A_T \cdot \omega \cdot \cos(\omega t) \qquad (2.3)$$

This periodic modulation leads to a phase angle $\delta$ between the heating rate and heat flow signals.

Figure 2.4 shows schematic modulated temperature programmes, analogous to those presented in Figure 2.2 for standard DSC.

13
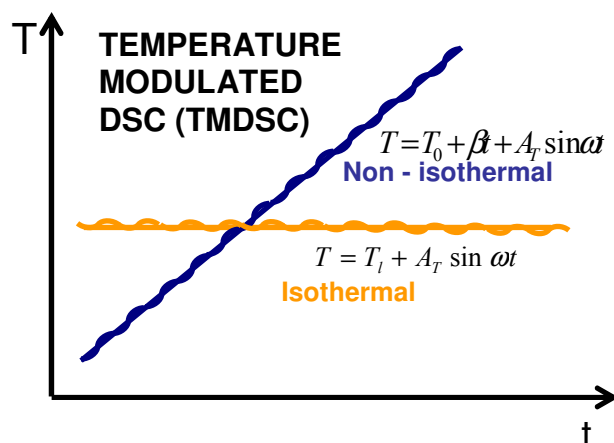
Figure 2.4. Schematic temperature programmes for isothermal and non-isothermal scans in TMDSC.

The same principle is used in all TMDSC techniques, which involves a Fourier Transformation of the modulated heating rate and heat flow signals, from which additional information can be obtained compared with that available from conventional DSC. In particular, TMDSC permits the evaluation of two different kinds of heat capacity: (i) the "thermal" heat capacity from the underlying heating or cooling rate, which is identical to that available from conventional DSC at the same rate, and (ii) the "dynamic" heat capacity from the amplitudes of the heating rate and heat flow modulations, which is dependent on the frequency of the modulations. Thus, in a single experiment it is possible to determine the response of the polymer on two different time/frequency/rate scales. The net effect of imposing this more complex heating profile on the sample is the same as if two experiments were run simultaneously on the material – one experiment at the traditional lineal (average) heating rate and one at a sinusoidal (instantaneous) heating rate [6].

The general equation which describes the resultant heat flow at any point in a DSC or TMDSC experiment is described as:

$$dQ/dt = C_p \cdot \beta + f(T,t) \tag{2.4}$$

where $C_p$ is the heat capacity, $\beta$ the underlying heating rate and f is the heat flow due to kinetic processes.

14

DSC measures only the total heat flow releases, while TMDSC is able to determine not only the total heat flow but also these two individual components presented in Equation 2.4, due to the two different heating rates imposed on the sample: the average and the sinusoidal. These individual heat flow components are usually referred to as "reversing" and "non-reversing". TMDSC calculates the total heat flow and the reversing component. The non-reversing component is calculated as the arithmetic difference between the total heat flow and the reversing heat flow. The Fourier transformation also determines the phase angle between heating rate and heat flow signals.

An average or total specific heat capacity $<C_p>$ is found from the average values of the heating rate and heat flow:

$$<C_p> = <HF>/<\beta> \tag{2.5}$$

Also, a complex heat capacity $C_p^*$ can be obtained, with two separate components, namely the real $C_p'$ (in-phase) and imaginary $C_p''$ (out-of-phase), and calculated from the amplitudes of the heating rate and the heat flow:

$$C_p^* = A_{HF}/ A_\beta \tag{2.6}$$

$$C_p' = C_p^* \cos \delta \tag{2.7}$$

$$C_p'' = C_p^* \sin \delta \tag{2.8}$$

More detailed descriptions of TMDSC can be found in the bibliography [7, 8, 9].

Figure 2.5 shows two typical curves obtained from ADSC experiments, one for heating the sample of PET and the other being the corresponding blank run, from ambient temperature to 250 ºC at 10K/min; the temperature amplitude is 0.5 K and the period is 60 s. Figure 2.6 shows the result of the Fourier transformation of the signals in Figure 2.5.

15
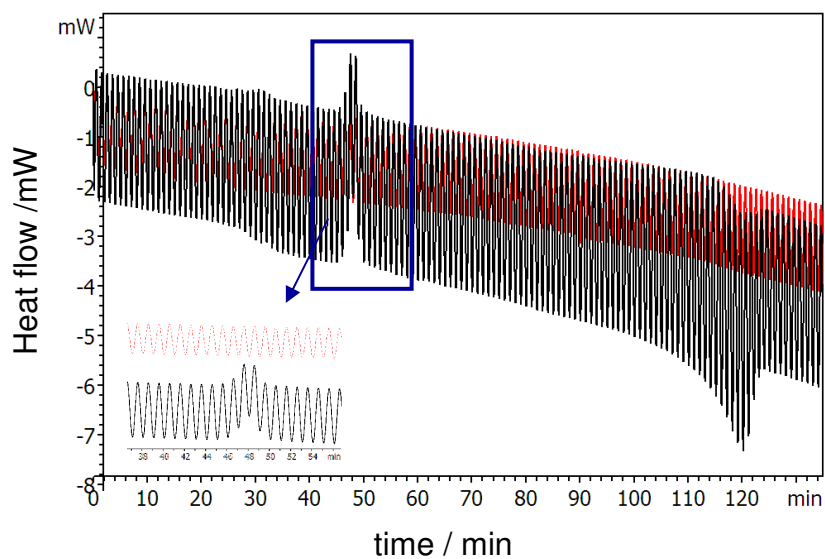
Figure 2.5. Modulated heat flow curves obtained for a PET sample and the corresponding blank run, heated at 10 K/min from ambient temperature to 250 ºC with ADSC mode
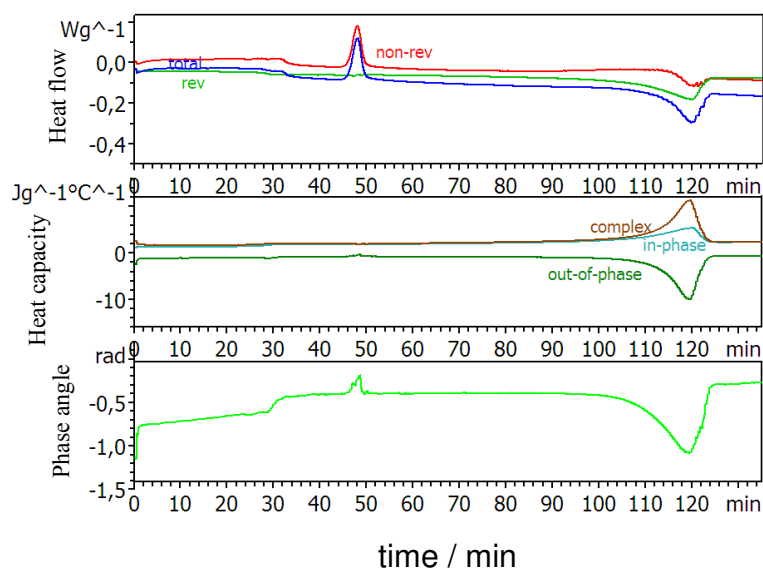


Figure 2.6. Heat flows (upper curves), heat capacities (middle curves) and phase angle (lower curves) obtained from the Fourier transformation applied to the signals shown in Figure 2.5

16

Nevertheless, despite the advantages afforded by TMDSC in various areas, particularly in those specifically mentioned above, it is not a particularly convenient technique to use. The first important point is that although the use of two different heating rates permits a better resolution and sensitivity, the use of lower underlying heating rates than in conventional DSC leads to longer experiments. But perhaps of greater importance in the case of ADSC is the fact that it requires a minimum of two separate scans a "blank" and a "sample", for any given set of experimental parameters, which results in a very time-consuming procedure if one wishes to study, for example, the frequency dependence of a certain phenomenon. Thus any technique that could overcome this drawback would be welcome, and this is just what TOPEM can offer.

## 2.4. TOPEM principles

Instead of being based upon a periodic modulation of the heating rate, as is the situation with TMDSC techniques, TOPEM uses a stochastic modulation of the heating or cooling rate by means of random pulses of temperature [12]. A temperature program for a TOPEM experiment can be described by the equation:

$$T(t) = T_0 + \beta_u \cdot t + \delta T(t) \tag{2.9}$$

where $\delta T(t)$ is the pulse amplitude, fixed by the user, with alternating sign and random duration.

The heating rate related with this type of temperature program is given by:

$$\beta(t) = dT/dt = \beta_u + d/dt\,(\delta T(t)) \tag{2.10}$$

In Figure 2.7 are shown schematic isothermal and non-isothermal TOPEM scans.

17
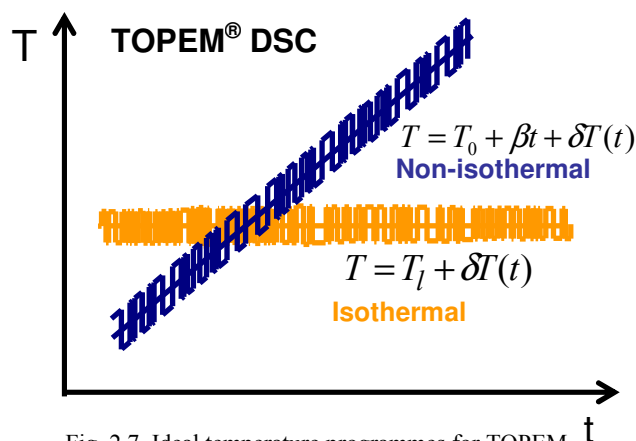
Fig. 2.7. Ideal temperature programmes for TOPEM

This stochastic perturbation introduces a broad frequency spectrum in the response, while a novel data analysis procedure, based upon a "parameter estimation method" (PEM) widely used in other technologies [13-16], allows the evaluation of a so-called "quasi-static" heat capacity and the separation of correlated and non-correlated components of the heat flow with respect to the heating rate, which are related to the reversing and non-reversing heat flows in the usual TMDSC terminology. In particular, the broad frequency response implies that TOPEM is apparently able to determine the complex heat capacity over a range of frequencies in a single scan.

### 2.4.1. Experimental parameters to define an experiment

For each TOPEM experiment, the parameters that define an experiment have to be chosen [17]; these parameters and their limits are:

- Temperature Interval [min:-30 ºC, max: 300 ºC]: defines the initial and final temperatures of the experiment for a non-isothermal run or the fixed temperature for an isothermal experiment. The minimum temperature available is due to the intracooler used, not the calorimeter.

- Heating (cooling) rate ± [1mK/min – 2K/min]: for a non-isothermal experiment, velocity of the scan between the selected temperatures.

- Time: for an isothermal experiment, the total duration of the isothermal run.

- Pulse height [1 mK-500 mK]: defines the temperature amplitude of the pulses with alternating sign; for example, if 0.5 K is selected, the pulses will superpose as +0.5 K and -0.5 K, the total height of pulses being 1 K.

- Pulse width [15 s – 1000 s] called the switching time range: time interval defined by a minim and a maxim value for the duration of the pulses. The software generates the stochastic programme with random pulses between these minimum and maximum values.

As in the case of TMDSC, different segments isothermal and non-isothermal on heating and/or cooling can be combined in the same experiment.
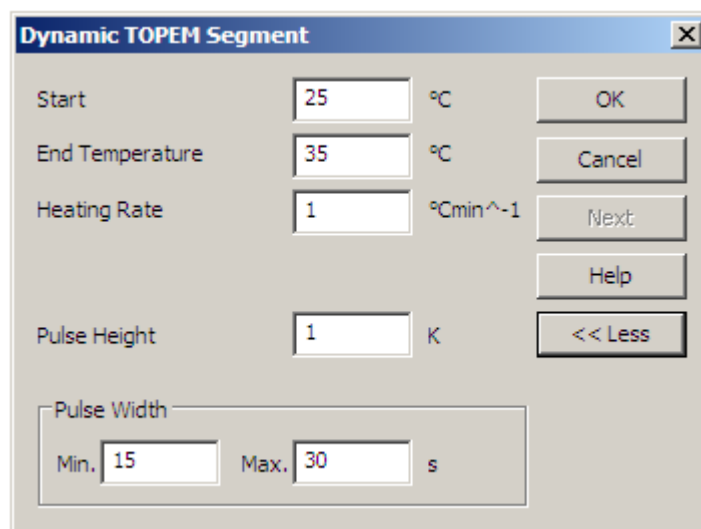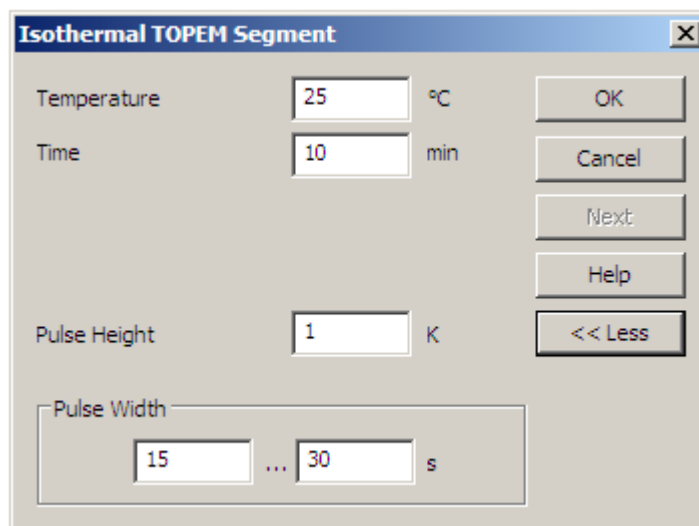


Figure 2.8. Menu for creating a non-isothermal method with TOPEM

19

Figures 2.8 and 2.9 show the menu of the software for the user to select the experimental parameters described above for the case of a non-isothermal (Fig 2.8) and an isothermal (Fig 2.9) experiment or segment.



Figure 2.9. Menu for creating an isothermal method with TOPEM

Once these experimental parameters have been defined, the temperature programme for the experiment is generated. The stochastic programmes generated are discussed in the Appendix 1.

### 2.4.2. Calculation parameters to analyze the experimental data

When an experiment is performed with the temperature program corresponding to the selected parameters, the cell temperature and the heat flow absorbed and/or released by the sample are measured. As in the case of temperature modulated DSC, an evaluation of the modulated heat flow and the heating rate is made. For each TOPEM experiment and with the "Parameter estimation method" (PEM), the evaluation is performed in a so-called calculation window width, which covers a certain time interval, and this calculation window is shifted through the

20

measurement data [17]. The PEM first estimates a model to characterize the system, supposing that in a calculation window the non-reversing heat flow and the heat capacity do not vary significantly. Then, a Laplace transformation is made to calculate the quasi-static heat capacity and the frequency dependence, as explained later.

The parameters for the evaluation have to be selected by the user:

- Width of calculation window [default value: 120 s]: in this window, the model for the characterization of the sample is evaluated. It is assumed that the sample displays a constant behaviour with time in this interval. Consequently, it is essential to ensure that there are no variations in the sample in this interval.

- Shift of calculation window [default value: 10 s]: this defines the step-by step displacement of the calculation window through the measured data; the programme will calculate the response of the sample in windows with a width defined as indicated immediately above, each successive window being displaced in time by an amount defined by this shift.

- Width of smoothing window [default value: 90 s]: this defines the width of the window used to smooth the signal; it works as a filter of the response function obtained after the evaluation, this means that first the response is obtained, and just after, the smooth of this response will be made. A window width of 0 s (no smooth) is possible and its recommended value is always narrower than the calculation window.

Figure 2.10 shows the menu where the user defines the parameters for an evaluation described above.

21
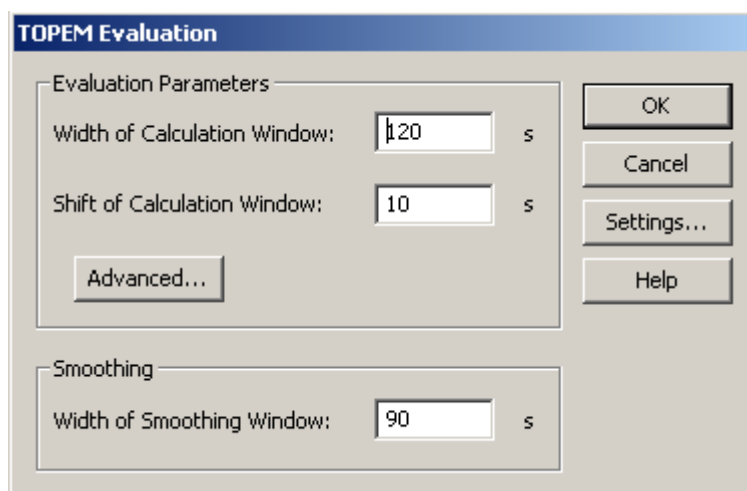
Fig 2.10 Evaluation window menu for a performed TOPEM experiment

There are also a number of advanced parameters that will be discussed in Appendix 1 together with additional observations, such as the selection of these parameters and their relation with the experimental parameters, as well as procedures for the optimization of an evaluation. However, some general rules for a good evaluation can be stated: it is necessary that at least one pulse be contained in the calculation window, and also it is advisable that the window width should be less than a third part of the total duration of the transition [18].

The mathematical theory, on which the TOPEM calculation is based that is presented below, has been extracted from the reference [19] from Mettler-Toledo. A complete explanation about the mathematical basis used by the TOPEM software can be found in reference [12].

Figure 2.11 shows a schematic temperature programme (in blue) with its corresponding heat flow response (in red) with a detail of two calculation windows, one (in green) being the initial window and the other representing the subsequent window (also in green) after its displacement (in lilac) along the curve.

22
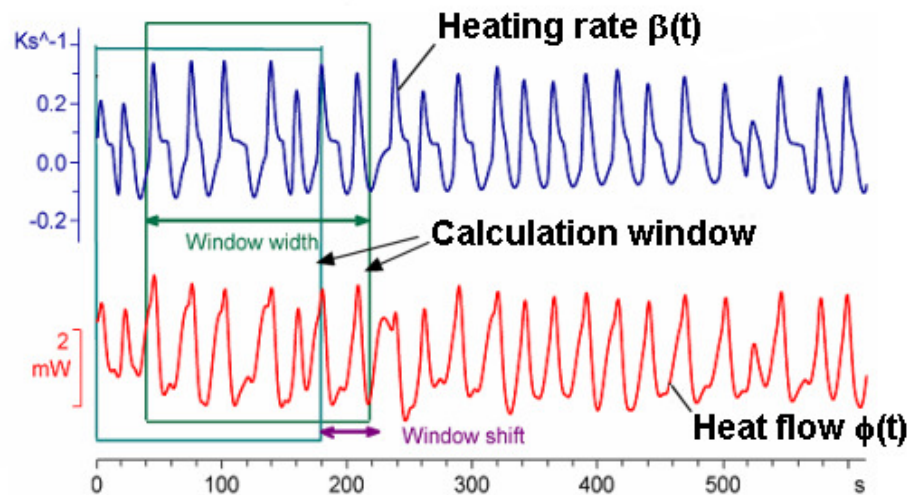
Fig 2.11. Temperature program (blue) and heat flow response (red). Also included are two calculations windows of width 180 s, the second with a shift of 40 s (in lilac) of the calculation window with respect to the first one [17]. From Mettler-Toledo.

Once the parameters for the evaluation have been defined, the programme obtains the curve of $C_{p0}$ from the modulated heat flow curve [12], together with the total heat flow and its components, namely the reversing and non-reversing heat flows. Figure 2.12 shows a schematic illustration of the input and output signals in the calorimeter cell and the relationship with the transfer function g(t) that characterizes the system which is obtained through the PEM evaluation.
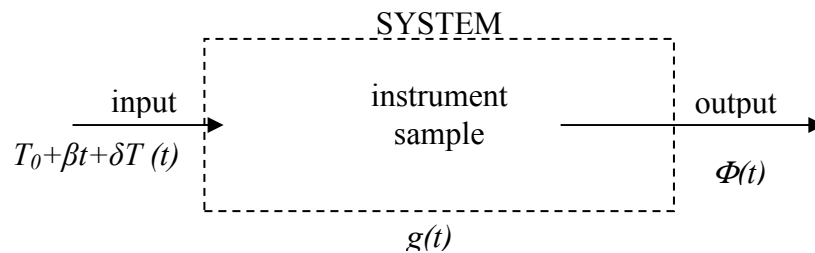


Fig 2.12. Schematic illustration of the input signal, the stochastic temperature programme, and the output signal, $\Phi$, the average heat flow. The PEM evaluation relates the input and output signals through the transfer function, g(t).

23

If the temperature modulation is sufficiently small and the sample is in an equilibrium state, it is possible to describe the system in a delimited range of temperatures as a linear system. Under these conditions, the Convolution Theorem [20] can be used, which associates the response at time $t$ with the superposition of input signals at previous times $\tau$ in order to obtain the time response. For a linear time-invariant system, the output signal is given as an integral of the input signal with the pulse response g(t) of the system:

$$\Phi(t) = g(t) \otimes \beta(t) = \int g(\tau)\beta(t-\tau)d\tau \qquad 0 < \tau < \infty \qquad (2.11)$$

where g is the transfer function which characterizes the system, $\Phi$ is the output modulated heat flow response and $\beta$ is the modulated heating rate derived from the input temperature program. The technical problem consist in determining g(t) ($0 \leq t \leq \infty$) from discrete data in a sufficiently long time frame in which the assumption of time invariance is a good approximation. The use of a discrete Laplace transformation in the z-plane is a commonly used method to solve it. Thus, the z-transformed Equation 2.11 is:

$$\tilde{\Phi}(z) = H(z) \cdot \tilde{\beta}(z)$$

$$(2.12)$$

where $\tilde{\Phi}(z), H(z) \ and \ \tilde{\beta}(z)$ denote the z-transforms of $\Phi$(t), g(t) and $\beta$(t), respectively.

The z-transformation being:

$$f(z) = \sum_{k=0}^{\infty} f_k \cdot z^{-k} \qquad with \quad f_k = f(kP) \qquad (2.13)$$

where $f_k$ are the data points of a certain sampling period P.

An often used way to solve equation 2.12 is to describe the function H(z) as a rational function:

24

$$H(z) = B(z) / A(z) \qquad\qquad (2.14)$$

where $A(z)$ and $B(z)$ are polynomials of degree q and p, respectively. Inserting Equation 2.14 into Equation 2.12 and applying the inverse z-transformation the recorded data lead to:

$$\sum_{l=0}^{p} a_l \Phi(t - l\Delta t) = \sum_{k=0}^{q} b_k \beta(t - k\Delta t) \qquad (2.15)$$

where $\Delta t$ corresponds to the sampling time interval (its default value is 0.1s) and $a_l$ and $b_k$ are the unknown coefficients of the polynomials $A(z)$ and $B(z)$. Making use of the time invariance of the system in a sufficient long time interval, this equation can be numerically solved by a least square fitting procedure in the considered time interval.

The quasi-static heat capacity, $C_{p0}$, is calculated from the integral of the transfer function:

$$mc_{p0} = \int g(t)dt \qquad 0 < t < \infty \qquad (2.16)$$

where m is the sample mass.

The frequency response is obtained by inserting $j\omega_i$ where $\omega$ is the angular frequency related to the linear frequency as $\omega_i = 2\pi f_i$, together with the calculated parameters $a_l$ and $b_k$ into the function $H(z)$. Thus, it is possible to obtain a complex quantity of the pulse response from which the phase $\varphi_{fi}$ and the complex heat capacities at frequencies $f_i$, $C_{p,fi}$ can be determined. Thanks to the previously calculated quasi-static heat capacity $c_{p0}$, the frequency dependent heat capacities $c_{p,fi}$ can be correctly adjusted by the software.

As an example of the input imposed and the heat flow response obtained in a TOPEM experiment, two real temperature programmes, together with their corresponding modulated heat flow responses measured, are illustrated in Figures 2.13 and 2.14.
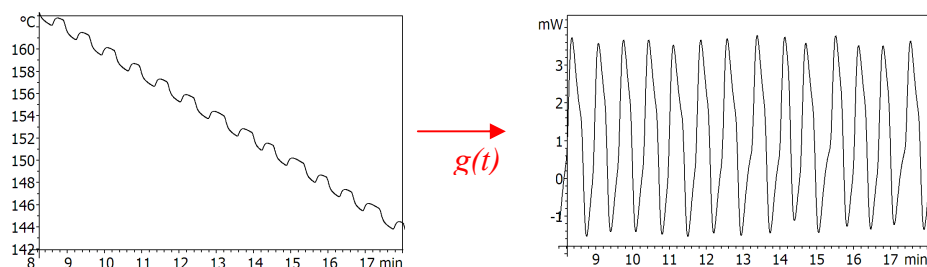


Fig 2.13. Left-hand diagram: temperature program (input) with a cooling rate of - 2K/min, temperature amplitude of 0.5 K and switching time range of 15-30 s. Right-hand diagram: corresponding heat flow response (output). The relation between the input and the output signals can be described by the transfer function, g(t), calculated through the PEM.

Figure 2.13 shows a temperature program with a short switching time range, while Figure 2.14 shows a temperature program with longer switching time ranges, in both cases the other experimental parameters are the same and the sample employed is Polycarbonate. Although the heat flow responses look to be quite different, the evaluation of both curves gives the same result for the heat capacity calculated.
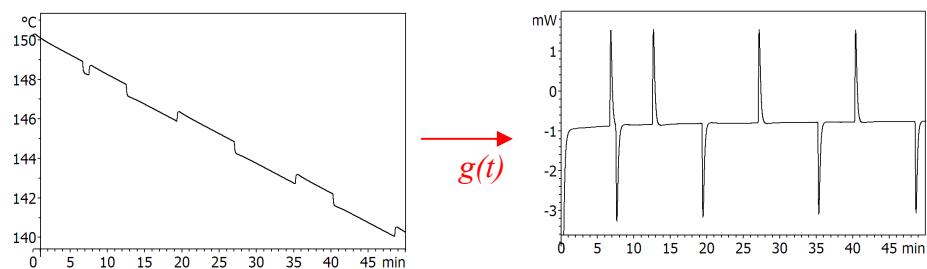


Fig 2.14. Left-hand diagram: temperature program (input) with a cooling rate of - 0.2K/min, temperature amplitude of 0.5 K and switching time range of 15-900 s. Right-hand diagram: corresponding heat flow response (output). The relation between the input and the output signal can be described by the transfer function, g(t), calculated through the PEM.

Once the $c_{p0}$ curve is calculated, the frequency dependence can be obtained. The zone of interest is selected by the user and two asymptotes appear delimiting the transition. In the case for example of a glass transition they mark the vitreous and the liquid states. Once they are adjusted, the desired frequencies can be selected and the software gives the frequency response of the sample.

Figure 2.15 shows a TOPEM experiment for the case of heating PET from ambient to 290 ºC, at 2K/min. In this case the amplitude of the pulses is 0.1 K and the switching time range is from 15 to 30 s. The upper part of this figure shows the modulated heat flow that is obtained (normalized to the sample mass) directly from the experimental measurements.
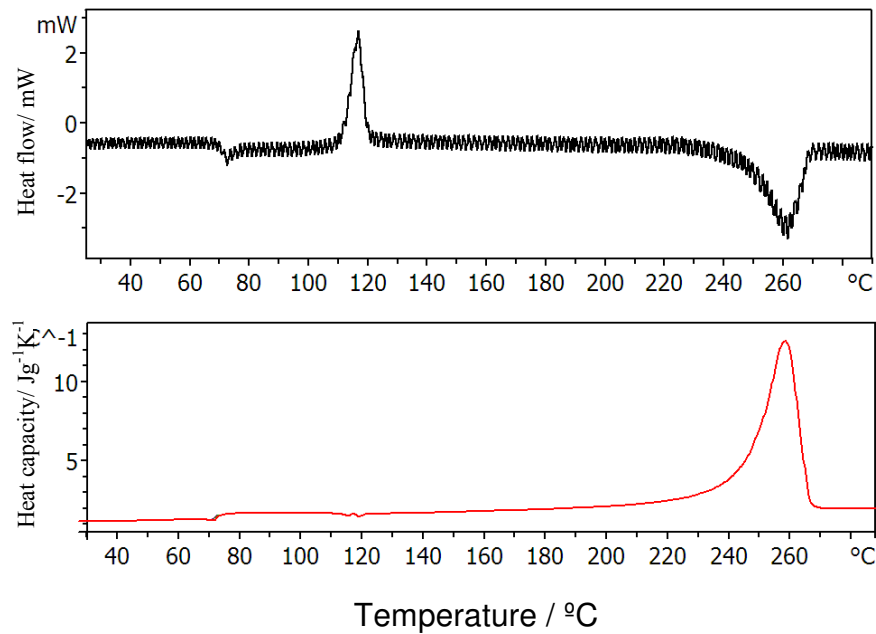


Figure 2.15. TOPEM experiment obtained heating PET from ambient to 290 ºC at 2K/min, pulse amplitude 0.1K and switching time range 15-30 s. Red curve shows the modulated heat flow response, blue curve the quasi-static specific heat capacity calculated from the red curve, and the lower curves show the frequency response in the glass transition region for 10 mHz (pink), 20 mHz (brown) and 30 mHz (cyan); the green curve corresponds to the $c_{p0}$.

27

From this response, the total heat flow together with its reversing and non-reversing components can be calculated. The central part of the figure shows the specific quasi-static heat capacity, $c_{p0}$, obtained by selecting a calculation window of 120 s, a shift of 10s and a smoothing window of 90 s, which correspond to the default values. The lower part of the figure shows the frequency response of the sample in the glass transition region for the selected frequencies of 10, 30 and 40 mHz, as indicated. The green curve corresponds again to the $c_{p0}$. Also shown are the asymptotes used for the frequency evaluation.

Normally, TOPEM experiments are made with greater pulses amplitude as those used in the experiment corresponding to Figure 2.15, and thus it is not so easy to see the transition in the heat flow response as it is in Figure 2.15. Figure 2.16 shows a typical TOPEM curve obtained from an experiment in which polycarbonate is cooled from 180 to 80 ºC at -0.5K/min, with a pulse amplitude 0.5 K and a switching time range from 15 to 30s.
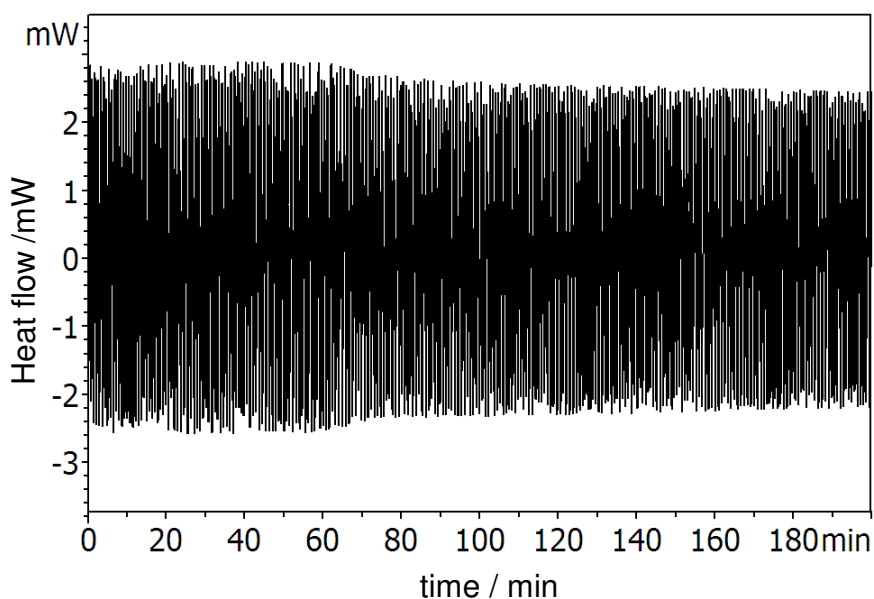


Figure 2.16. Typical heat flow response to a TOPEM experiment of polycarbonate cooled from 180 to 80 ºC at -0.5K/min, with a pulse amplitude 0.5 and a switching time range from 15 to 30s.

A more detailed description of the principles of TOPEM measurement can be found in reference 12. Some additional description and discussion are given in Appendix 1.

All the foregoing description related to the operation of TOPEM and the evaluation of the various quantities of interest can be summarized in the following three points:

-   A Temperature Programme consists of temperature pulses of fixed amplitude and random duration superimposed on a typical underlying DSC scan. The parameters that define an experiment are the temperatures (initial and final), the underlying heating (cooling) rate, the amplitude of the pulses ($A_T$) and the switching time range (min – max duration of the pulses).

-   A Parameter Estimation Method (PEM) determines the correlation between the heating rate imposed and the modulated heat flow response. The quasi-static heat capacity and the total heat flow with its reversing and non-reversing components are calculated. The parameters for the evaluation are the width of the calculation window, its shift through the curves, and the width of the smoothing window used on the calculated curves.

-   With the calculated $c_{p0}$, the heat capacity curves corresponding to the frequency response can be obtained, namely the complex heat capacity and its components in-phase and out-of-phase together with the phase angle. It is only necessary to select the limits of the transition, its asymptotes and the desired frequencies (in the range of mHz).

The main advantage of TOPEM is that, with only a single experiment, the sample properties are obtained as a function of temperature and time in a wide frequency range. This is not only time-saving with respect to other techniques, but also it avoids the experimental errors which, in the case of reactive samples, would

otherwise result from the need to change of the sample for each experiment. As the reversing and non-reversing components of the heat flow are calculated directly and separately from the measured data, the results obtained by TOPEM contain, in principle, more information than is available from other TMDSC techniques in which a periodic modulation is used.

# References

1. IUPAC. *Pure and Applied Chem. 57*, **1985**, 1737.

2. Dr. Gosse van der Plaats. "The practice of Thermal Analysis". Edited by Mettler-Toledo Switzerland ME – 724 412.

3. Mettler- Toledo AG, Analytical. MarCom Analytical. ME-51724556, 07/2007.

4. P.S. Gill, S.R. Sauerbrunn, and M. Reading; *J. Thermal. Anal. 40*, **1993**, 931.

5. M. Reading, D. Elliot, and V.L. Hill*; J.Thermal Anal. 40*, **1993**, 949.

6. Modulated DSC compendium. Basic Theory and Experimental Considerations. Edited by TA Instruments. TA-210.

7. J. M. Hutchinson and S. Montserrat*; J. Thermal Anal. 47*, **1996**,103.

8. S. Montserrat; *J. Therm. Anal. Calorim., 59*, **2000**, 289.

9. J.E.K. Schawe; *Thermoch. Acta, 260*, **1995**, 1.

10. B. Wunderlich, Y. Jin and A. Boller; *Thermoch. Acta 238*, **1994**, 277.

11. A. Boller, Y. Jin and B. Wunderlich; *J. Therm. Anal., 42*, **1994**, 307.

12. J.E.K. Schawe, T. Hütter, C. Heitz, I. Alig and D. Lellinger; *Thermochim. Acta 446*, **2006**, 147.

13. C. Y. Shih, Y. G. Tsuei, R. J. Allemang and D. L. Brown; *Mech. Sys. and signal processing, 2*, **1988**, 349.

14. C. Angeli and A. Chatzinikolaou; *Proceedings of 23rd IASTED International Conference on Modelling, Identification and Control*, **2004**, 172.

15. T.S. Koh, J.L. Zhang, C.K. Ong et al.; *Phys. In Medicine and Biology, 51*, **2006**, 2857.

16. L.G. Chen and D.R. Clarke; *Computational Mat. Sci., 45*, **2009**, 342.

17. Help Topics from Mettler-Toledo Software STARe version 9.20.

18. Mettler-Toledo internal information.

19. Mettler-Toledo software documentation, ME 51724435. It can be downloaded form the web page (www.mettlertoledo.com).

20. Sokolnikoff. "Mathematics of Physics and Modern Engineering". Edited by Mc. Graw-Hill. 2nd edition.

31

# CHAPTER 3

# APPLICATION TO THE GLASS TRANSITION OF POLYCARBONATE

## 3.1 Introduction

### *3.1.1. The glass transition*

The glass transition temperature ($T_g$) is the main characteristic temperature of the amorphous solid and liquid states. A liquid becomes a solid on cooling through the glass transition temperature. The microscopic process involved is the freezing of large-scale molecular motion without a change in structure. Since the heat capacity of the glass is always lower than that of the liquid at the same temperature and since there is no latent heat in stopping molecular motion, the glass transition takes the appearance of a thermodynamic second order transition [1].

All amorphous polymers display, at sufficiently low temperatures (below their $T_g$), the typical characteristics of glasses, including hardness, stiffness and brittleness. One property associated with the glassy state is a low coefficient of volume expansion. This low coefficient occurs as the result of a change in slope of the curve of volume versus temperature at the $T_g$. In the high-temperature region (above $T_g$) the slope of the curve (expansion coefficient) is characteristic of a rubber and the polymers offer elastic properties; below $T_g$ the expansion coefficient is characteristic
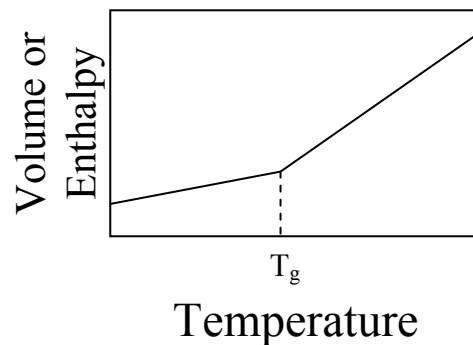


Figure 3.1. Schematic curves of Volume-Temperature or Enthalpy-Temperature showing the glass transition temperature, $T_g$.

33

of a glass. There is not an abrupt change in volume at $T_g$, but only a change in the slope of the volume-temperature curve [2].

The determination of the glass transition temperature is important in view of the different mechanical properties associated with the two different states, liquid and glassy. The range of temperatures in which a polymer can be used is related with its $T_g$. Depending on the mechanical properties and the desired use of the material, some polymers are used as glasses with a working temperature below their $T_g$, such as, for example, polystyrene or polycarbonate (with $T_g$ higher than ambient temperature) and others are used as elastomers in the rubbery state (with their $T_g$ well below ambient temperature).

### 3.1.2. Materials

The glassy polymer selected for this first study was polycarbonate, which has a glass transition temperature around $T_g \approx 145$ ºC. Polycarbonate is a well defined polymer, with all of its physical properties already well documented. Its widely extended use, alone or in blends and in many different application areas [3] (LCD screens, lenses, optical media such as CD's, electrical, communications, etc.) gives an idea of how well defined are its properties. In this respect, the objective of this study is not an investigation of the glass transition of polycarbonate itself, but rather to use polycarbonate as a model material for the purposes of investigating this new technique of TOPEM. In particular, this selection of material and of the glass transition allows an examination of the TOPEM response for a frequency dependent transition, which can then be compared with the well known response from conventional and temperature modulated DSC. The understanding of the TOPEM principles gained from this initial study will permit its later application to different materials and transitions.

34

Another reason for the selection of polycarbonate was due to its reproducibility, the easy preparation of the samples, and the possibility to repeat the measurements with the same sample. In order to obtain samples of different masses for comparison of their response, 5 mm diameter discs of different thicknesses were machined from a 40 mm diameter extruded rod of Lexan (GE Plastics) following the procedure described in detail elsewhere [4]. The surfaces of these discs were carefully polished with P#1200 silicon carbide paper to give good thermal contact with the aluminium crucibles of the calorimeter. Sample masses from about 4 mg to about 40 mg were sealed in aluminium crucibles to be used both in the TOPEM and ADSC experiments.

### 3.1.3. Experimental

The glass transition was investigated by cooling at constant rate from above to below the glass transition temperature. In all cases the temperature range selected was from 180 ºC to 80 ºC in order to cover the glass transition interval and reach an asymptotic glassy state. Experiments in heating were also made, but the analysis of the data was made always with the results obtained in cooling in order to avoid problems associated with structural relaxation.

In these TOPEM experiments, the underlying rate ranges from -2 K/min to -0.02 K/min; the amplitude of the temperature pulse was selected to take values of $\pm$ 0.5, $\pm$ 0.25 and $\pm$ 0.1 K; the switching time range (min – max) varies from the default values of 15 s – 30 s up to values of 15 s – 900 s, the particular value depending on the cooling rate (slower cooling rates allow longer switching time ranges to be used). Most TOPEM experiments were conducted with a sample mass of approximately 20 mg, the recommended value. Nevertheless, smaller sample masses were also used to investigate whether or not it had any effect, and a larger sample mass was used for the two slowest cooling rates, -0.2 K/min and -0.02 K/min.

For comparison with the TOPEM results, some ADSC experiments were also performed over the same temperature interval and for a range of frequencies between 1.04 and 33.33 mHz, corresponding to periods from 960 s to 30 s, always with an amplitude of ± 0.5 K. To accommodate this range of periods, the underlying cooling rate was decreased as the period increased, from -1 K/min for the minimum period of 30 s to -0.0625 K/min for the maximum period of 960 s. At the same time, the sample mass was increased from about 8 mg to about 40 mg in order to maintain a measurable heat flow. In some cases the sample used for both techniques was the same.

Tables 3.1 and 3.2 summarise all the experimental parameters selected for the scans performed with TOPEM and ADSC, together with the sample mass used in each case.

| TOPEM | | | |
|---|---|---|---|
| Cooling rate (K/min) | Mass (mg) | Pulse amplitude (K) | Switching time range (s) |
| -0.02 | 37.09 | 0.5 | 15-30 |
| -0.2 | 37.09 | 0.1 | 15-30 |
| | 20.93 | 0.25 | 15-30, 15-200, 15-900 |
| -0.5 | 8.04 | 0.5, 0.25, 0.1 | 15-30 |
| | 20.93 | | |
| -1 | 20.93 | | |
| -1.5 | | | |
| -2 | | | |

Table 3.1. Experimental parameters selected for the different experiments performed in TOPEM mode.

36

| ADSC | | | |
|---|---|---|---|
| Cooling rate (K/min) | Mass (mg) | Temperature amplitude (K) | period (s) |
| -0.0625 | 37.09 | | 960 |
| -0.125 | 20.93 | | 480 |
| | | | 240 |
| -0.25 | 13.76 | | 120 |
| -0.5 | 8.04 | 0.5 | 60 |
| | 13.76 | | |
| -1 | 4.08 | | 30 |
| | 8.04 | | |
| | 13.76 | | |

Table 3.2. Experimental parameters selected for the different experiments performed in ADSC mode.

### 3.1.4. Data analysis

As was explained in the previous chapter, a TOPEM experiment gives a heat flow signal which results from the stochastic temperature pulses. To calculate the response function for the system, there must be a region of the data in which there is no transition; it is for this reason that the cooling curves here start at 180 ºC, well above the nominal glass transition which is centred at about 145 ºC.

The TOPEM evaluation is made within a calculation window, the width of which is set by the user. It is recommended [5] that it be less than or equal to one third of the width of the transition interval, with larger windows giving better signals, and has a default value of 120 s. The criterion that was chosen here, on the basis of numerous previous studies, was to assign the default values of window width, shift and smooth to the fastest cooling rate, and to select, for the other velocities, values in proportion to the ratio of velocities. For example, for an experiment at -2K/min the default

37

values of a calculation window of 120 s, a shift of 10 s and a smooth of 90 s were selected, whereas for an experiment at -1K/min, the proportional parameters would be a calculation window of 240 s, shift of 20 s and smooth of 180 s, and likewise for all the cooling rates selected. This implies that in all cases the temperature range in each calculation window is 4 K.

Once the calculation window has been selected, the TOPEM evaluation yields the curve of $c_{p0}$, the "quasi-static" specific heat capacity. Figure 3.2 illustrates this, together with the original heat flow modulations from which the $c_{p0}$ curve shown has been obtained.
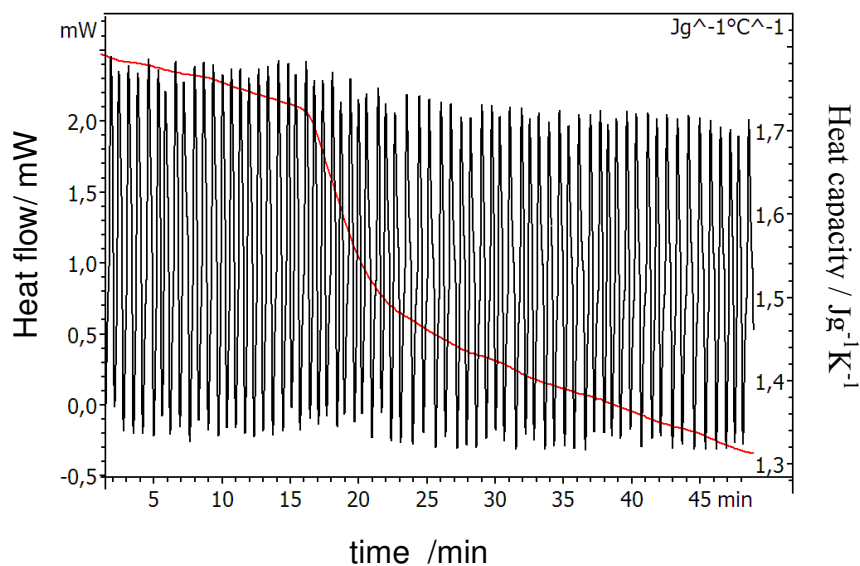


Figure 3.2. Heat flow response to stochastic temperature pulses of magnitude ±0.25 K during cooling of polycarbonate at -2 K/min from 180 ºC to 80 ºC with switching time range of 15-30 s, from which the "quasi-static" specific heat capacity curve shown is derived. Left-hand axis refers to the randomly alternating heat flow signal; right-hand axis refers to the sigmoidal-shaped specific heat capacity curve.

The next step in the procedure is to select the transition interval limits between which the frequency evaluation is to be made. Once this interval has been selected,

38

the software defines the asymptotes to the liquid-like and glassy regions of the $c_{p0}$ curve, as shown in Figure 3.3.
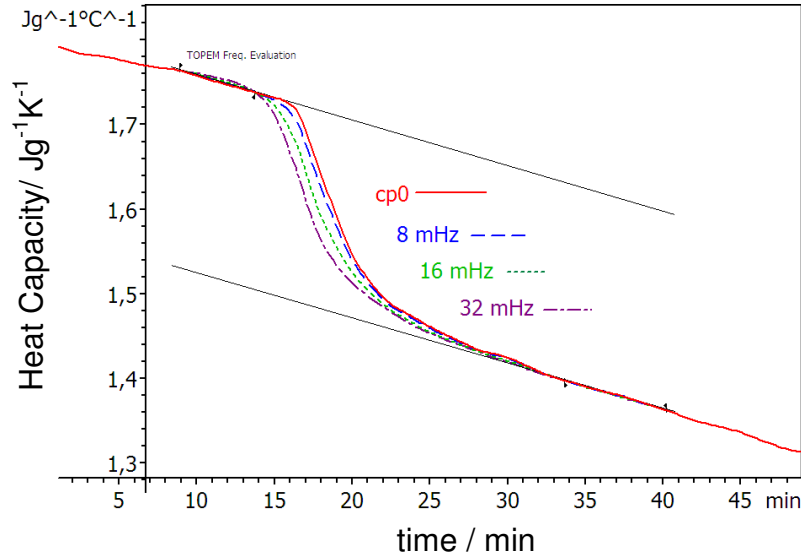


Figure 3.3. Quasi-static specific heat capacity from Figure 3.2 (full line) with asymptotes defined by transition interval selected. Short dashed, long dashed, dotted and dash-dotted lines show the frequency evaluation at selected frequencies of 32, 16, 8 and 4 mHz, respectively. The curve for 4 mHz is barely visible as it is superposed almost exactly onto the quasi-static specific heat capacity curve.

The user can adjust these asymptotes by moving the two flags in each of the liquid-like and glassy regions. Finally, the user selects the particular frequencies desired and TOPEM calculates the complex specific heat capacity corresponding to each selected frequency, also illustrated in Figure 3.3 for frequencies of 32, 16, 8 and 4 mHz. These frequencies were selected specifically for comparison with the ADSC experiments.

The ADSC experiments were analysed in the usual way in order to obtain the complex specific heat capacity curves as a function of temperature. An example of

the modulated heat flow obtained from the blank curve and the sample curve can be observed in Figure 3.4.
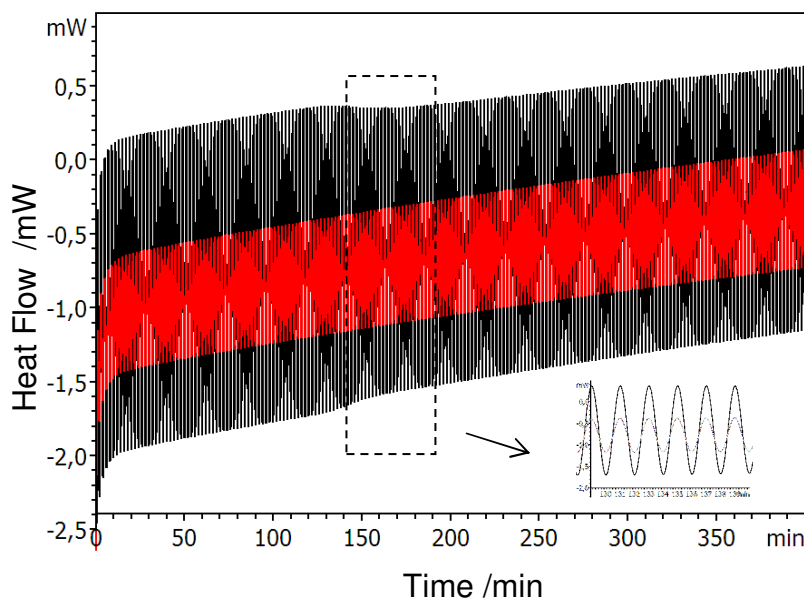


Figure 3.4. Heat flow response to modulated temperature pulses of magnitude ± 0.5 K during cooling of polycarbonate at -0.25 K/min from 180 ºC to 80 ºC with a period of 120 s. The red curve corresponds to the blank run and the black one corresponds to the sample run.

From these two curves, the software can calculate the total heat flow as well as the reversing and non-reversing components. It is also possible to obtain the heat capacities: the complex heat capacity and its in-phase and out-of-phase components, as well as the phase angle. In our case we analyse only the complex heat capacity (a single frequency for each experiment) in order to compare it with the results obtained by TOPEM. Figure 3.5 shows the complex heat capacity obtained from Figure 3.4.

The quantitative effects of the various experimental and calculation parameters for TOPEM and the comparison of TOPEM with ADSC are examined by calculating the mid-point temperature, $T_{mid}$, of the glass transition in each case, defined as the

40

temperature at which the curve passes mid-way between the liquid-like and glassy asymptotes. Since this evaluation depends to some extent on the way in which the asymptotes are drawn, unique asymptotes in the liquid-like and glassy regions were used for any given set of experiments.
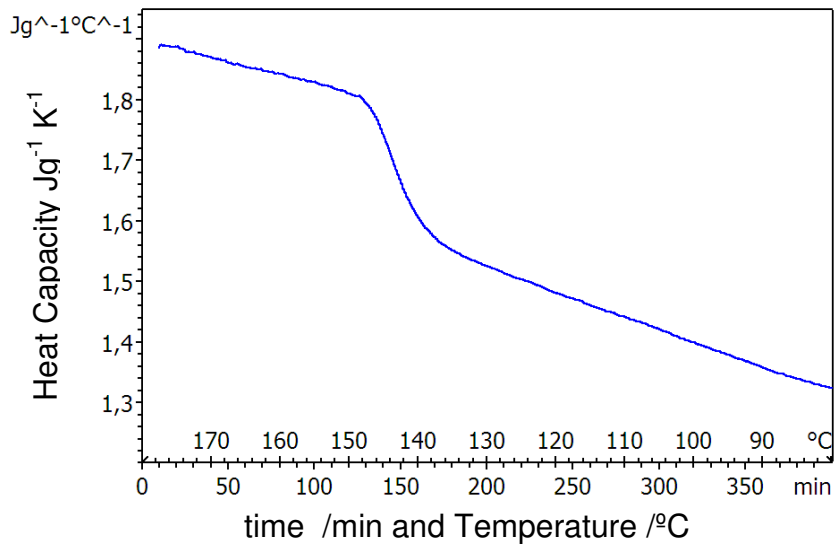


Figure 3.5. Complex heat capacity as a function of time and temperature, obtained from Figure 3.4 and corresponding to a frequency of 8.33 mHz.

## 3.2. Results

### 3.2.1. Amplitude of temperature pulses

The temperature pulse should be sufficiently small such that the sample response remains essentially linear. In ADSC the amplitude of the modulation is commonly taken to be ± 0.5 K, and so here we investigate the effect of pulse

41

magnitudes of ± 0.5, ± 0.25 and ± 0.1 K in the TOPEM results obtained. Figure 3.6 shows the results for three TOPEM experiments using an underlying cooling rate of - 0.5 K/min and with a switching time range of 15-30 s. The evaluation was made for a calculation window width of 480 s (to maintain the same width of 4 K as with 120 s for a cooling rate of -2 K/min, as explained previously) and the frequencies selected were 32, 16, 8, 4, 2 and 1 mHz to be the same as the corresponding ADSC periods selected.



Figure 3.6. Log(frequency) versus reciprocal mid-point temperature for TOPEM experiments with underlying rate -0.5 K/min, switching time range 15-30 s and pulse amplitudes of ±0.5, ±0.25 and ±0.1 K, as shown in the inset.

When the results are plotted in the form of log(frequency) versus reciprocal $T_{mid}$, as in Figure 3.6, the data should fall on a straight line if the temperature dependence of the relaxation times is Arrhenius, or on a curve with slight downward curvature for a

42

Vogel-Tammann-Fulcher (VTF) type of temperature dependence. In fact, for the rather small interval of $T_{mid}$ (about 5 K) involved in these experiments covering a range of frequencies from 32 to 1 mHz, it would be difficult to distinguish a linear dependence from a curvature of a VTF dependence, and hence an essentially linear variation in Figure 3.6 would be anticipated. The very marked curvature that is seen instead should not be confused with a VTF temperature dependence, but results from an aspect of the TOPEM analysis that is discussed later.

On the other hand, it can be seen, as would be expected for pulses small enough that the sample response remains linear, that over the whole range of frequencies there is no systematic effect of the magnitude of the pulse on $T_{mid}$. The same result has been obtained for other cooling rates of -1.0, -1.5 and -2.0 K/min, from which it can be concluded that, at least for investigating the glass transition, it is acceptable to use pulse amplitudes of up to $\pm$ 0.5 K.

### 3.2.2. Underlying cooling rate

TOPEM experiments were made with cooling rates from -2.0 to -0.02 K/min, an amplitude of $\pm$ 0.5 K and a switching time range from 15 to 30 s. As was detailed in Table 3.1, while a sample mass of approximately 21 mg was used for the majority of TOPEM experiments, a larger sample mass of approximately 37 mg was used for experiments with cooling rates of -0.2 K/min and -0.02 K/min. When the curves are evaluated with a calculation window width of 4 K and for frequencies from 32 to 1 mHz, the relationship between logarithm of frequency and reciprocal $T_{mid}$ is as shown by the filled points in Figure 3.7.

Here it can be seen that there is no obvious systematic effect of the cooling rate on the frequency dependence of $T_{mid}$, though there is rather more scatter in the data than

is seen in Figure 3.6, and resulting particularly from the data for the underlying cooling rate of -0.02 K/min. This result, that there is no effect of cooling rate on the frequency dependence of $T_{mid}$, is as would be expected by analogy with the frequency dependence of the complex heat capacity obtained from ADSC. In that case, provided that the thermal and dynamic glass transitions are sufficiently separated on the temperature scale, then the dynamic glass transition is not influenced by the underlying cooling rate [6-8]. However, there is again a very marked downward curvature of the TOPEM data noticeable in Figure 3.7, which in fact leads to a region, for frequencies less than about 4 mHz, where $T_{mid}$ is virtually independent of the frequency.



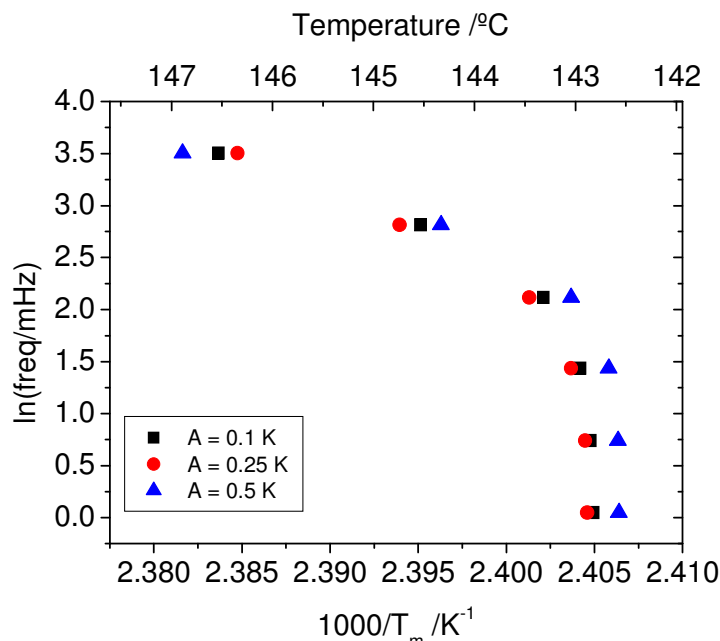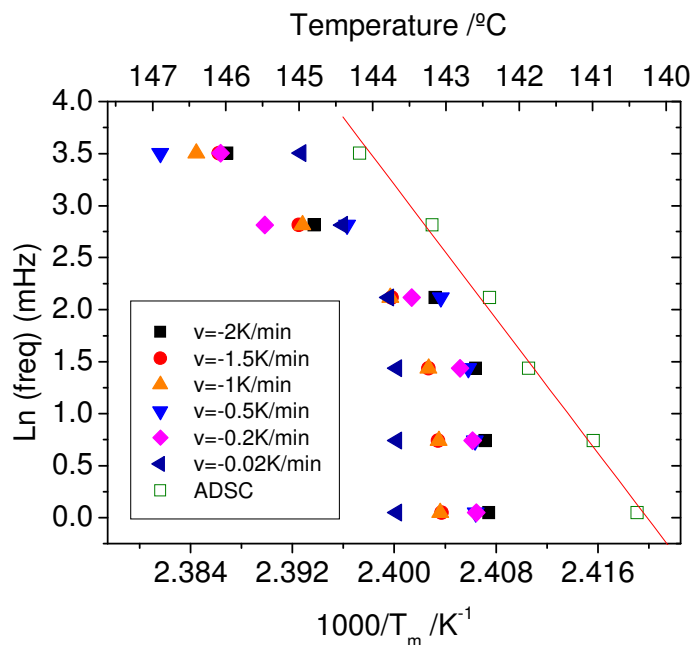Figure 3.7. Filled points: log(frequency) versus reciprocal mid-point temperature for TOPEM experiments with amplitude ±0.5 K, switching time range 15-30 s, calculation window width of 4 K, and underlying rates from -2.0 to -0.02 K/min, as shown in the inset. Open squares: ADSC results for periods from 30 s to 960 s.

### *3.2.3. Width of calculation window*

For any given TOPEM experiment it is possible to evaluate the data using different calculation window widths. For example, Figure 3.8 shows the effect of increasing the window width from 60 s to 240 s for an experiment with the parameters defined in the Figure caption.
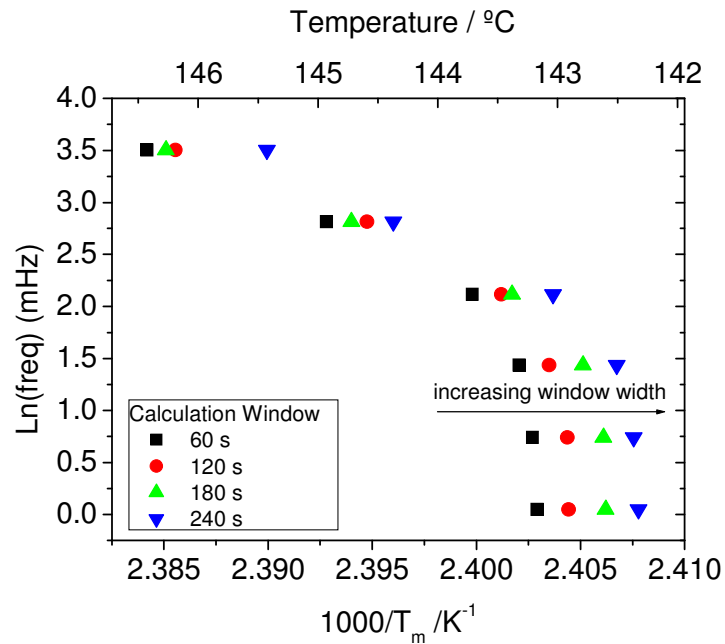


Figure 3.8. Effect of width of calculation window on plot of log(frequency) versus reciprocal mid-point temperature. The experimental parameters are: underlying cooling rate -1.0 K/min, amplitude of pulse ±0.5 K, switching time range 15-30 s.

It can be seen that there is a small but systematic decrease in $T_{mid}$ as the window width increases. It should be remembered that the recommendation is that the window width be less than one third of the transition interval, which in the present case can be estimated from Figure 3.2 to be about 15 minutes time interval at a cooling rate of -2 K/min, which equates to a temperature interval of 30 K. The

maximum window width in Figure 3.8 is 240 s for a cooling rate of -1 K/min, which equates to 4 K, or less than one sixth of the transition interval. Thus, even though the window widths fall within the limits recommended, there is a clear effect of this on the mid-point temperature.

The converse of this can be seen if a much slower cooling rate is used, -0.02 K/min, for which a wide range of window widths can be investigated while maintaining a small value for the maximum window width. The results are shown in Figure 3.9.
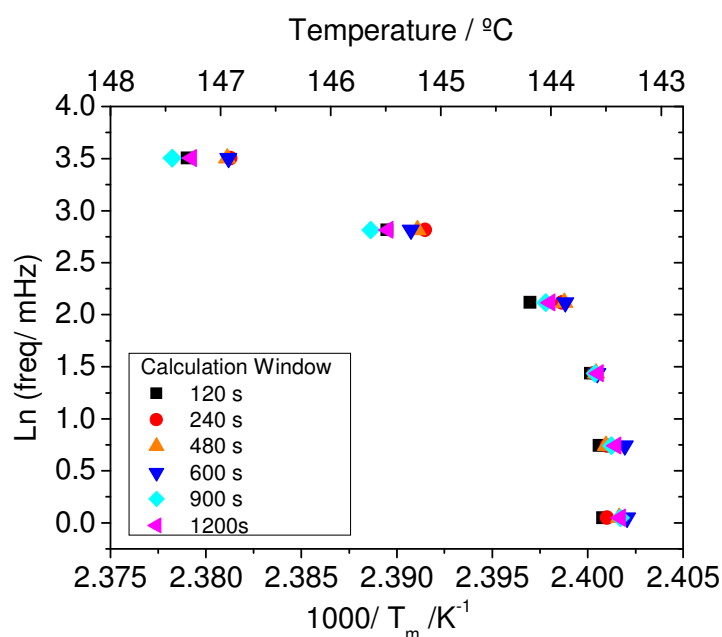


Figure 3.9. Effect of width of calculation window on plot of log(frequency) versus reciprocal mid-point temperature. Underlying cooling rate -0.02 K/min, amplitude of pulse ±0.5K, switching time range 15-30 s.

Here, the window widths from 120 s to 1200 s correspond to temperature intervals of only 0.04 K to 0.4 K, much smaller than those in Figure 3.8, and the effect is that the window width now has no influence on $T_{mid}$. Similar results were obtained for a cooling rate of -0.2 K/min, for which $T_{mid}$ was independent of window width except

46

for a width of 1200 s, equivalent to a temperature interval of 4 K, for which the mid-point temperature was displaced significantly to lower temperatures. It is concluded from this that the recommended restriction on the window width is not strict enough, and that it should be equivalent to less than about one tenth, rather than a third, of the transition interval.

### 3.2.4. Sample mass

The recommended sample mass for use in TOPEM is 20 mg. However, for the two slowest cooling rates used here, namely -0.2 K/min and -0.02 K/min, and by analogy with the experimental procedure adopted for the ADSC measurements as a function of increasing period (and hence decreasing underlying cooling rate), a larger sample mass of 37 mg was used. In order to check that the sample mass does not have an effect on the TOPEM results, though, the same experiment involving
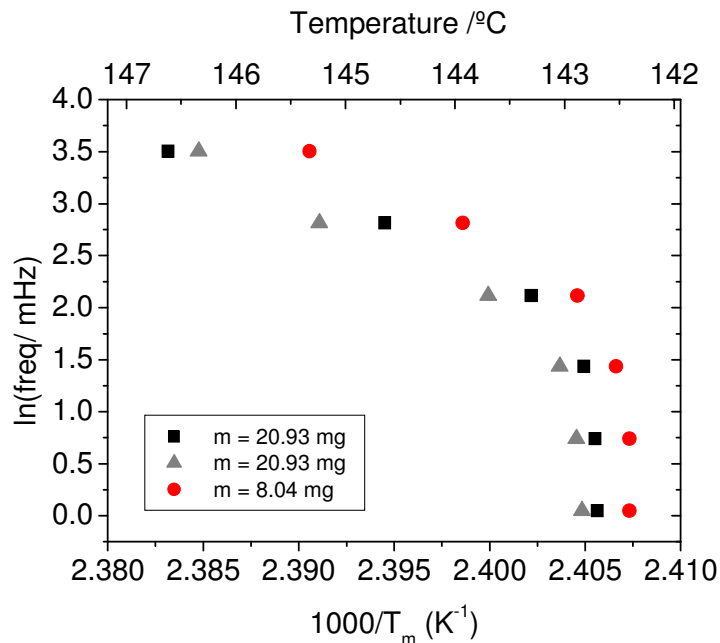


Figure 3.10. Effect of the sample mass on the dependence of log(freq) on the reciprocal of the mid-point temperature. Cooling rate of -0.5 K/min, pulse amplitude ± 0.5 K, and switching time range of 15-30 s.

47

cooling at -0.5 K/min from 180 ºC to 80 ºC with a pulse amplitude of ±0.5 K was made with two different sample masses of 21 mg and 8 mg.

Figure 3.10 shows the results obtained for two different samples in TOPEM experiments with a cooling rate of -0.5 K/min, pulse amplitude ± 0.5 K and switching time range of 15 – 30 s.

The mid-point temperature $T_{mid}$ obtained from the $C_{p0}$, is 142.6 ºC for the lightest sample and 142.5 ºC in the heaviest one, which represents an insignificant difference. On the other hand, there is a more significant effect in the frequency evaluation, whereby the complex specific heat capacity curves at the selected frequencies are displaced further to higher temperatures the larger is the sample mass, with a difference of about 1 ºC between the $T_{mid}$ values for the sample masses of 8 and 21 mg for the highest frequency of 33 mHz. On the 1000/$T_{mid}$ scale this corresponds to a difference of about 0.006 $K^{-1}$, which is somewhat larger than the typical scatter in values such as is seen in Figure 3.6. This probably contributes to the observation that the scatter is greater in Figure 3.7, where a different sample mass was used for the slowest cooling rates, than it is in Figure 3.6, but does not detract from general trend of $T_{mid}$ reaching a limiting value at low frequencies.

### 3.2.5. Switching time range

To investigate the effect of switching time range, experiments were performed with an underlying cooling rate of -0.2 K/min, pulse amplitude of ± 0.5K, and switching time ranges of 15-30 s, 15-200 s and 15-900 s. For consistency, the same calculation window of 1200 s, equivalent to 4 K of temperature interval, was used, being necessarily greater than the longest possible switching time.

It transpires that there is no systematic variation in $T_{mid}$ with switching time range, all the results displaying the same trend such as that shown in Figures 3.6 to 3.10,

48

and having a scatter of the same order as that shown in Figure 3.6 with respect to the effect of the amplitude of the temperature pulse.
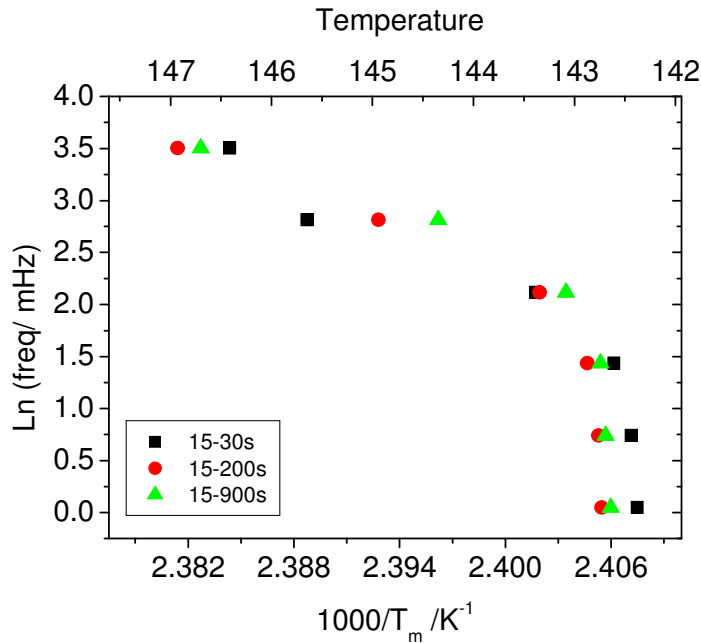


Figure 3.11. Log(freq) versus reciprocal mid-point temperature for TOPEM experiments with cooling rate of -0.2 K/min, pulse amplitude of ± 0.5 K, and switching time ranges of 15-30 s, 15-200 s and 15-900 s as indicated.

## 3.3. Discussion: frequency dependence

It is interesting to return to the observation, made above, that the plots of log(frequency) as a function of reciprocal temperature indicate that $T_{mid}$ becomes independent of frequency for frequencies less than approximately 4 mHz. This can be seen also very clearly when the individual curves of $c_p(\omega)$ for the selected frequencies are all included on the same plot as $c_{p0}$. For example, if the frequency analysis of Figure 3.3 is extended to include frequencies of 2 and 1 mHz, the $c_p(\omega)$

49

curves for these frequencies are indistinguishable from that for 4 mHz, and the curves for all frequencies less than or equal to 4 mHz are superposed onto the curve for $c_{p0}$, the quasi-static specific heat capacity, which indicates that 4 mHz appears as a kind of limiting frequency for TOPEM. The results shown in Figures 3.6 to 3.11 indicate that this limit is reached whatever are the experimental or calculation parameters, and hence that it must be intrinsic to the TOPEM experiment. One possible explanation is that it arises because $c_{p0}$ is calculated from the temperature pulses, which are applied with a certain heating or cooling rate. These rates can be estimated from the temperature programmes, as an example, for a pulse amplitude of 0.5 K and an underlying cooling rate of -0.02 K/min (parameters corresponding to Figure 3.9) they are approximately ± 8 K/min. According to the relationship between rate ($q$) and frequency ($f$) that can be derived from the temperature fluctuation model of the glass transition [9, 10]:

$$2\pi f = |q|/a\delta T \qquad (3.1)$$

where $a\delta T$ is a parameter that depends on the glassy material, it is possible to determine the frequency corresponding to the pulse heating and cooling rates. Taking values of $x$=0.46 and 0.456<$\beta$<0.6 for the non-linearity and non-exponentiality parameters, respectively, for polycarbonate [4], and using earlier theoretical results given in Table 2 of [11], we find $a\delta T$<8.32 K, and hence the frequency corresponding to 8 K/min to have a minimum value of about 2.5 mHz. This is remarkably close to the limiting value of 4 mHz found above, and suggests that this limit is determined by the way in which the pulses are imposed. A deeper discussion is presented in the Appendix 1.

This appears also to have an effect on the calculation of the frequency dependence of $T_{\text{mid}}$. The comparison of such data obtained by TOPEM with those obtained by

50

ADSC is shown in Figure 3.7. The ADSC data, shown as the open squares, display a linear dependence, from which a reduced activation energy of 160 kK is found. This compares well with the literature value of 150 kK [12]. The TOPEM data, on the other hand, not only show the marked curvature and limiting frequency mentioned above, but also yield $T_{mid}$ values significantly larger than those from ADSC. We believe that this could result from the assignment of $c_{p0}$ as a "quasi-static" specific heat capacity, equivalent to $c_p(\omega)$ as $\omega \rightarrow 0$, whereas it is in fact equivalent to $c_p(\omega)$ as $\omega \rightarrow 4$ mHz.

## 3.4. Conclusions

The effect of the experimental and evaluation parameters on the TOPEM results obtained has been studied. Different samples of polycarbonate were prepared and their glass transition has been measured. Different experiments were performed with the different parameters selected and their influence in the obtained results has been analyzed. The experimental parameters studied are the pulses amplitude, the cooling rate and the switching time range. The evaluation parameters are the calculation window width, its shift and the smoothing window. An additional parameter, the sample mass has also been analyzed. It has been observed that as it should be expected, both the experimental and the calculation parameters have no effect in the results obtained, only in the case of the calculation window width a value equal or less than 1/10 of the transition is recommended.

This first study with TOPEM shows that this temperature modulated DSC technique permits the simultaneous evaluation of the dynamic response of a sample over a range of frequencies. This has obvious advantages in respect of simplifying data acquisition and in separating frequency-dependent phenomena from those that do not depend on frequency. However, it appears that the so-called "quasi-static" specific heat capacity, $c_{p0}$, is not really equivalent to the dynamic specific heat

51

capacity $c_p(\omega)$ as $\omega \rightarrow 0$, but in fact corresponds to a limiting frequency of about 4 mHz. It is suggested that this limit is related to the heating and cooling rates of the stochastic temperature pulses. Comparison of the frequency dependence of the dynamic glass transition as determined by TOPEM with that found by ADSC indicates differences that are attributed to the same effect. The closed results obtained with TOPEM and ADSC show that TOPEM is a useful tool to investigate frequency dependent transitions with a single scan and a single sample.

52

# References

1.  "Thermal Characterization of Polymeric Materials". Edited by Edith A. Turi. Academic Press, Inc. 1981

2.  "Textbook of Polymer Science". Fred W. Billmeyer, Jr. Ed. John Wiley & Sons Inc. 1984.

3.  DOW Chemical Company web page: www.lgdow.com/products/application.htm.

4.  J. M. Hutchinson, S. Smith, B. Horne and G. M. Gourlay; *Macromolecules, 32*, **1999**, 5046.

5.  Private communication Juergen Schawe, Mettler Toledo.

6.  J. M. Hutchinson and S. Montserrat; *J. Thermal Anal., 47*, **1996**, 103.

7.  J. M. Hutchinson and S. Montserrat; *Thermochim. Acta, 305*, **1997**, 257.

8.  S. Montserrat, Y. Calventus and J. M. Hutchinson; *Polymer, 46*, **2005**, 12181.

9.  E. Donth, *Relaxation and Thermodynamics in Polymers*, Akadamie Verlag, Berlin, 1993.

10. A. Hensel and C. Schick; *J. Non-Cryst. Sol., 235-237*, **1998**, 510.

11. J. M. Hutchinson and S. Montserrat; *Thermochim. Acta, 377*, **2001**, 63.

12. I. M. Hodge; *J. Non-Cryst. Sol., 169*, **1994**, 211.

# CHAPTER 4

# VITRIFICATION DURING THE ISOTHERMAL CURE OF A THERMOSET

## 4.1. Introduction

### 4.1.1. Thermosets

Polymers can be classified, according to their properties and applications, as thermoplastics, elastomers or thermosets. The main characteristic of thermosets is that they became infusible and insoluble as a consequence of the irreversible chemical cross-linking reactions accompanying cure. Most formulations require heat or irradiation to cure; the resulting polymer, if properly formulated and processed, is a highly cross-linked, three-dimensional network [1].

In general, thermosets present good dimensional stability, thermal stability, chemical resistance, electrical and mechanical properties. Because of these properties they find widespread use in several applications such as adhesives, aircraft interiors, structural replacement for metals in automotive applications, printed circuit boards, dental materials or orthopaedic implants.

### 4.1.2. Cure of a thermoset

The cure of a thermoset is an irreversible exothermic chemical process in which a liquid prepolymer undergoes a cross-linking reaction to form a hard, rigid material with high resistance to chemical attack and thermal deformation, with high mechanical strength and a low tendency to creep.

The starting material is a substance with two or more functional groups that are capable of undergoing cross-linking. The curing process usually requires other reaction components such as hardeners (curing agents) and accelerators. These can, if necessary, be activated through temperature increase or exposure to UV light.

Thermosets can be classified according to the nature of the chemical compounds used to produce them. These include a wide range of resin materials such as acrylics, alkyds, amino resins, bismaleimides, epoxies, furanes, phenolics, polyimides, unsaturated polyesters, polyurethanes and vinyl esters.

In the case of epoxy resins, the reaction of the liquid resin to form a thermoset is carried out using hardeners as cross-linking or curing agents. Multifunctional amines or acid anhydrides are the most widely used hardeners that react stoichiometrically with the epoxy to form the final cross-linked thermoset.

### 4.1.3. Vitrification during an isothermal cure

In the isothermal curing of thermosets, the reaction initially proceeds at a rate which depends in general on the degree of cure and on the temperature dependent rate constant of the chemical reaction involved. As the degree of cure $\alpha$ increases from zero, the glass transition temperature of the curing thermoset also increases from its original value, $T_{g0}$, namely that of the unreacted mixture of the monomer and cross-linking agent. If the cure temperature is sufficiently high, the cross-linking reaction will proceed to its limit, $\alpha =1$, and the final glass transition will be that of the fully cured thermoset, $T_{g\infty}$. The relationship between the glass transition and the degree of cure at any time during the cross-linking reaction can be described by, for example, the DiBenedetto equation [2]

$$\frac{T_g - T_{g0}}{T_{g\infty} - T_{g0}} = \frac{\lambda\alpha}{1-(1-\lambda)\alpha} \tag{4.1}$$

where $\lambda$ is a parameter related to the ratio of heat capacities of the fully cured and uncured system.

On the other hand, if the cure temperature is less than $T_{g\infty}$, then there occurs a change in the overall rate of reaction from the initial chemically controlled rate to one that is controlled by the rate of diffusion of the reacting species. The change occurs roughly when the glass transition temperature of the curing thermoset reaches the isothermal cure temperature, because any further reaction implies the transition from a liquid state with high molecular mobility to a glassy state with much lower molecular mobility. This dramatic slowing down of the rate of reaction is known as vitrification and it is conventional to assign the vitrification time as that for which the glass transition of the curing thermoset is equal to the cure temperature. Knowledge of the vitrification time and its dependence on the cure temperature is important, for example, in the construction of time-temperature-transformation (TTT) diagrams [3].

The experimental determination of the vitrification time by conventional differential scanning calorimetry (DSC) for any given cure temperature is a very time-consuming process. It requires a series of separate isothermal cure experiments, at the same cure temperature but for increasing cure times, in which the system is only partially cured. Each isothermal experiment is followed immediately by a second DSC scan at constant heating rate, from which the glass transition temperature of the partially cured system is evaluated. Plotting this temperature as a function of the cure time (on a logarithmic scale) allows the determination of the vitrification time.

A good illustration of this procedure has been given by Montserrat [4]. Figure 4 of this reference of Montserrat is reproduced here as Figure 4.1. Each point in Figure 4.1 requires both an isothermal cure and a second scan, from which the time-consuming nature of obtaining these data can be inferred.
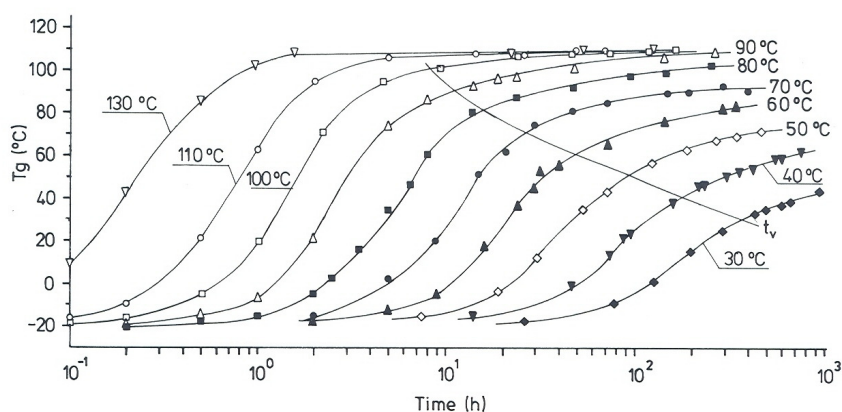
Figure 4.1. Variation of $T_g$ with time at different curing temperatures obtained by DSC [from S. Montserrat, J. Appl. Polym. Sci. 44 (1992) 545 Page 549 Fig 4].

The advent of temperature modulated DSC (TMDSC) techniques such as Modulated DSC (MDSC, TA Instruments) or Alternating DSC (ADSC, Mettler-Toledo), considerably simplified such experiments. In addition to the total heat flow given by conventional DSC, TMDSC also allows the determination, continuously throughout the reaction, of the so-called complex heat capacity, $C_p^*$, from the heat flow response to the small amplitude temperature modulations superimposed on the isotherm. When the curing system vitrifies, $C_p^*$ changes gradually from a value corresponding to the liquid state to a lower value corresponding to the glassy state. As was explained in Chapter 2, it is therefore possible, from a single TMDSC quasi-isothermal experiment, to follow both the overall heat of curing, as in conventional DSC, as well as the vitrification process in real time. In this case, the vitrification time, $t_v$, is conventionally defined as the time at which the value of $C_p^*$ is mid-way between those of the liquid and glassy states. Although this $t_v$ will not in general be exactly the same as the vitrification time defined by when the glass transition temperature is equal to the cure temperature, the correspondence is sufficiently close for the difference to be immaterial in the present context. Good illustrations of the application of TMDSC to the study of the vitrification process may be found in the

58

publications of Salvetti and co-workers [5], Van Mele and co-workers [6, 7] and Montserrat and co-workers [8, 9].

The reason why $t_v$ from TMDSC is not in general exactly the same as that from conventional DSC is related to the frequency and rate dependences of the glass transition, in other words of the $\alpha$-relaxation. In TMDSC, the vitrification time depends on the modulation frequency, whereas the glass transition temperature (or, more strictly, the fictive temperature), and hence the vitrification time, determined during the second scan in the conventional DSC process is dependent on the cooling rate prior to that second scan. Although the relationship between the frequency and rate dependences of the glass transition has been described [10, 11], the selected frequency and rate for TMDSC and conventional DSC studies, respectively, will, in general, ensure that the two vitrification times are different. For this reason, among others, the study of the frequency dependence of the vitrification time is of interest. It is in this respect that the techniques of MDSC and ADSC can exhibit some drawbacks.

In particular, ADSC experiments are conducted at a single fixed frequency. The study of the frequency dependence of the vitrification time therefore requires a series of separate ADSC experiments, together with their corresponding blank runs, at each of the frequencies to be investigated. Not only is this once again time-consuming but, in situations in which a significant, even if small, amount of cure takes place during the storage time required for the completion of the series of frequencies, it is not suitable to make a batch of the mixture of resin and cross-linking agent from which samples for curing can be taken. Instead, it requires a fresh mixture of the resin and cross-linking agent to be made for each frequency, which introduces the possibility of small variations in the ratio of resin to cross-linking agent in each mixture, which would contribute to the experimental error. To avoid this, as well as to reduce the experimental time involved, a multi-frequency

59

technique would be advantageous and this is what is provided by TOPEM [12]. The purpose of the present work is to compare the study of the vitrification process by TOPEM and ADSC for the isothermal cure of an epoxy-diamine system.

## 4.2. Calorimetric Study

### 4.2.1. Materials

The thermoset selected for this study is an epoxy resin, a diglycidyl ether of bisphenol-A (DGEBA), Epon 828 (Shell Chemicals, Resolution Performance Products), with a density of 1.16 g/cm$^3$ and an epoxide equivalent (*ee*) weight in the range 185-192 g/*ee*. The cross-linking agent was a polyoxypropylene diamine, Jeffamine D-230 (Huntsman Corporation). Stoichiometric mixtures of resin and diamine were prepared and samples of suitable mass were weighed into aluminium crucibles of 40 μl and with a hole in the lid. For TOPEM, the recommended sample mass of approximately 20 mg was used, while for ADSC the samples mass was dependent on the modulation period, increasing from about 7 mg for the shortest period (30 s) to about 26 mg for the longest one (900 s).

### 4.2.2. Experimental

The same calorimeter, Mettler-Toledo 823$^e$ with an intracooler, was used for both ADSC and TOPEM experiments, the difference being simply in the software for the temperature programme and subsequent data analysis. Also for both techniques, the same isothermal cure temperatures of 50°C and 70°C were used, the furnace in each case being preheated to the required temperature before the sample in the aluminium crucible was inserted by robot. The cure times were 14 or 15 hours for 50°C and 10 to 12 hours for 70°C, the longer cure times being used for the lower frequencies for which vitrification occurs later. For ADSC mode, a temperature

amplitude of 0.5 K was used, with modulation periods ranging from 30 s to 900 s, and a blank run being made in addition to the sample run for each period. For TOPEM, the magnitude of the temperature pulse was 0.5 K, equivalent to an amplitude of ± 0.25 K around the constant temperature baseline, and the random pulse durations, called the "switching time range", were set to be in various ranges in order to investigate this experimental parameter: 15-30 s for cure at 50 ºC, and 15-30, 15-300, 15-600 and 15-900 s for cure at 70 ºC. The difference between the temperature amplitudes for ADSC and TOPEM is immaterial, as they are considered to be sufficiently small for the response to be linear [13]. The absence of any significant effect of the temperature amplitude on the experimental results was presented earlier in section 3.2.1 of Chapter 3.

### *4.2.3. Data Analysis*

#### *ADSC experiments*

A typical result for an ADSC experiment is shown in Figure 4.2 for a modulation period of 60 s and a cure temperature of 50°C. The vitrification time, $t_v$, is found as the mid-point of this curve, as illustrated in the Figure. Similar results for other modulation periods allow the relationship between $t_v$ and period (or frequency $f$ = 1/period) to be determined. This series of experiments was repeated for a cure temperature of 70ºC, and the results for both cure temperatures are summarised in Table 4.1.

| frequency / mHz | 50ºC | 70ºC |
|:---:|:---:|:---:|
|  | $t_v$ / min | $t_v$ / min |
| 33.3 | 406.7 | 223.1 |
| 16.7 | 418.8 | 237.3 |
| 8.3 | 425.1 | 255.3 |
| 3.3 | 447.5 | 279.9 |
| 1.7 | - | 319.7 |
| 1.1 | - | 322.6 |

Table 4.1. Vitrification times, obtained from the mid-point of the $C_p^*$ curves, as a function of frequency for quasi-isothermal ADSC experiments at 50ºC and 70ºC with an amplitude of 0.5 K.
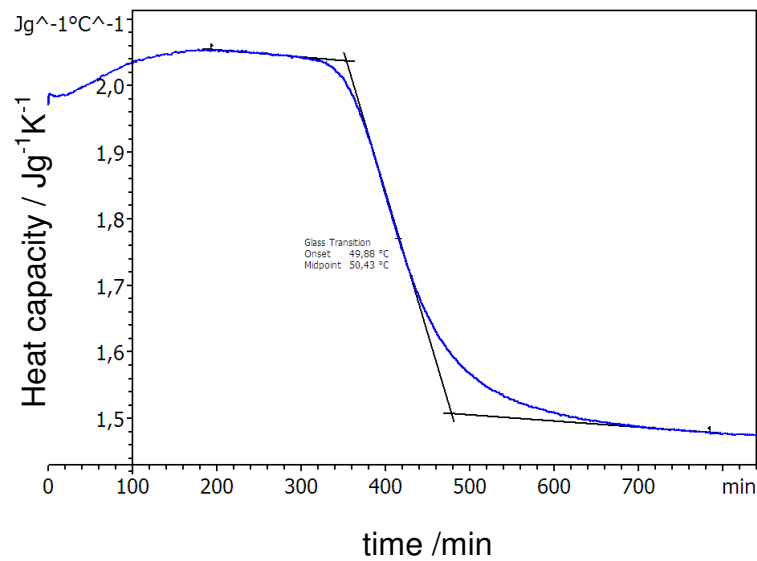
Figure 4.2. Complex heat capacity, $c_p^*$, as a function of time for ADSC experiment with a modulation period of 60 s, a temperature amplitude of 0.5 K and a cure temperature of 50ºC, showing the construction used to determine the vitrification time, $t_v$.

From the original modulated heat flow curves of the ADSC experiment it is, of course, also possible to determine the total heat flow due to the quasi-isothermal curing process, equivalent to the heat flow that would be measured in a conventional DSC experiment. This is shown in Figure 4.3 for the cure temperature of 50ºC.

In fact, although it cannot be seen on the scale of this Figure, the data start from 30 s rather than zero time, which results from the analysis procedure involving a window of width equal to one modulation period, the heat flow corresponding to this evaluation being associated with the time at the mid-point of this window. However, in this case, for which the period is 60 s, the heat of cure associated with this initial region is sufficiently small as to have a negligible effect. For much longer periods, this is not necessarily the case, for which reason the calculation of the heat flow is made only for the ADSC experiment with a period of 60 s.

62
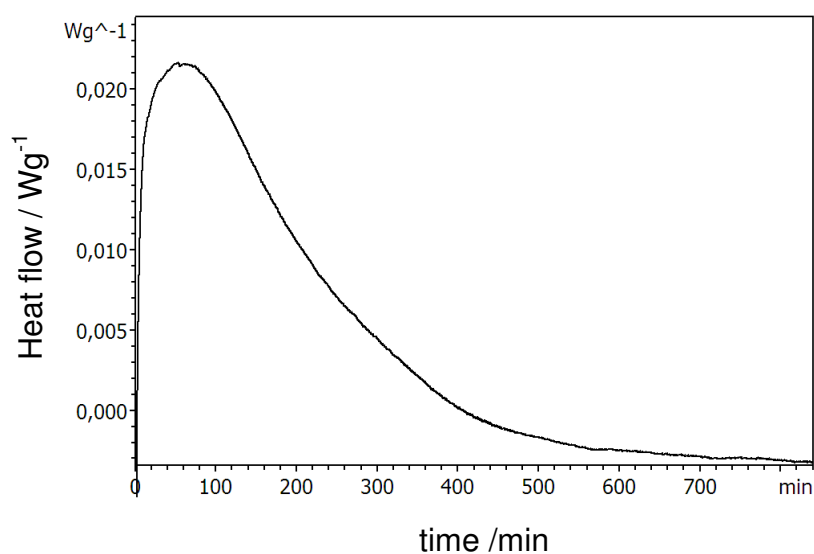
Figure 4.3. Total heat flow from ADSC quasi-isothermal experiment at 50ºC
with modulation period of 60 s and temperature amplitude of 0.5 K.

After each quasi-isothermal cure, the sample was heated in a conventional DSC scan
at 10 K/min from 10 to 270ºC to determine the residual heat of cure, and then a
further scan was made to determine the glass transition temperature, $T_g$, of the fully
cured sample.


*TOPEM experiments*

The TOPEM experiment measures the heat flow response to the
stochastic temperature programme. The heat flow for quasi-isothermal cure at 70ºC
is illustrated in Figure 4.4, with an enlarged view of the response to just a few
temperature pulses shown in the inset.

Here, the stochastic nature of the pulses can be seen in the random pulse durations
(illustrated in the inset to Figure 4.4) within the limits set by the switching time
range (15 to 30 s in the present case). Similar to ADSC, following the quasi-

isothermal cure, second and third conventional DSC scans were performed to determine the residual heat of cure and the $T_g$ of the fully cured sample, respectively.

The TOPEM evaluation procedure uses a parameter estimation method to determine the so-called quasi-static heat capacity, $C_{p0}$, from the relationship between the temperature programme and the heat flow response [12].
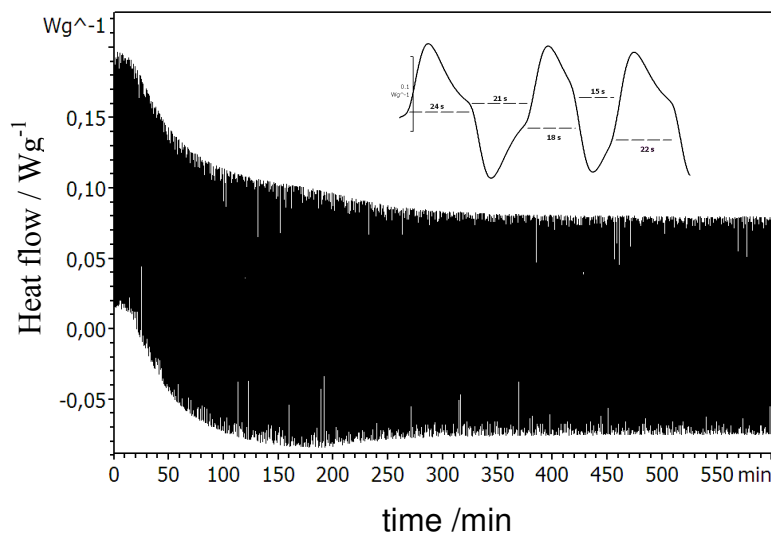


Figure 4.4. Heat flow response of TOPEM to stochastic temperature pulses with switching time range of 15 to 30 s during quasi-isothermal cure at 70ºC. The inset shows a magnified view of five pulses, of duration 24, 21, 18, 15 and 22 s.

Figure 4.5 shows the curve for $c_{p0}$ as a function of time obtained from the heat flow data of Figure 4.4, using a calculation window width of 1200 s. Just as for ADSC, vitrification is identified by a sigmoidal change in $c_{p0}$. The next step in TOPEM is to isolate the required event for the frequency evaluation, in this case the vitrification process, as shown by the box in Figure 4.5.

64
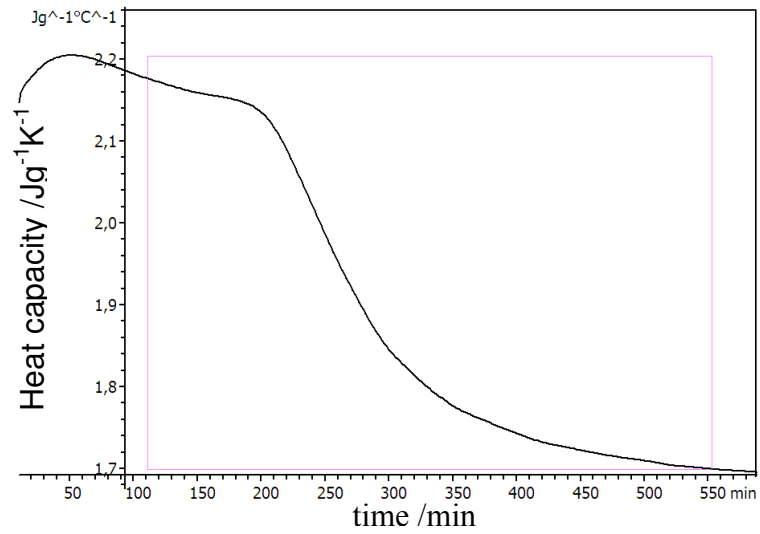
Figure 4.5. Quasi-static heat capacity, $c_{p0}$, during isothermal cure at 70ºC using TOPEM with a calculation window width of 1200 s. The box shows the isolation of the selected region (vitrification) for frequency analysis.

The user then selects the frequencies required, in the present case 3.3, 8.3, 16.7 and 33.3 mHz, chosen so as to correspond to the modulation periods used with ADSC.
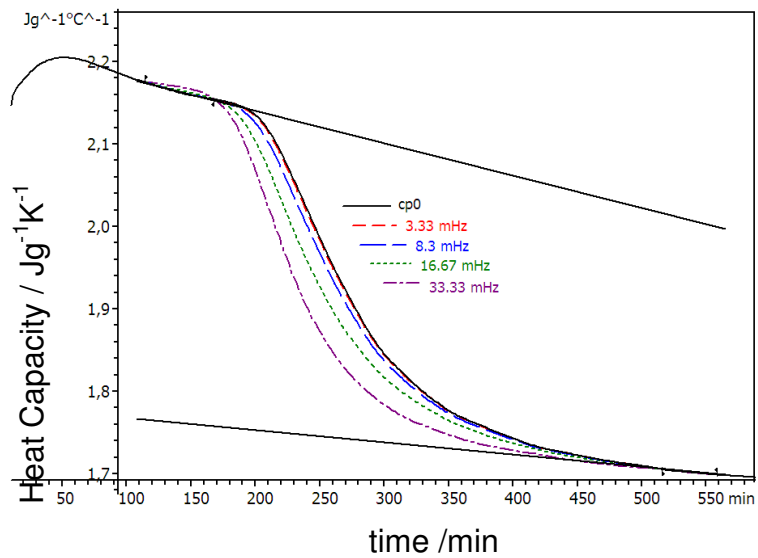


Figure 4.6. Frequency dependent $c_p(f)$ curves as a function of time obtained by the frequency evaluation of the $c_{p0}$ curve in Figure 4.5 (also reproduced here). The frequencies are: 3.3, 8.3, 16.7 and 33.3 mHz.

65

In addition, for TOPEM at 70ºC higher frequencies of 50, 66.7, 100 and 120 mHz were also selected. The software then allows TOPEM to determine the separate frequency-dependent $c_p(\omega)$ curves, analogous to $c_p{}^*$ in ADSC. The results are shown, together with $c_{p0}$, in Figure 4.6.

From this and equivalent experiments at 50ºC, the values of the vitrification time at each frequency and for each isothermal cure temperature are determined, and the results are summarised in Table 4.2.

| $f$ / mHz | Temperature | | | | | |
|---|---|---|---|---|---|---|
| | 50ºC | 70ºC | | | | |
| | 15-30 s | 15-30 s (a) | 15-30 s (b) | 15-300 s | 15-600 s | 15-900 s |
| 120 | 362.2 | 185.8 | 191.2 | 201.3 | 224.4 | 202.9 |
| 100 | 367.6 | 196.9 | 203.6 | 204.5 | 224.3 | 205.6 |
| 66.7 | 382.5 | 215.7 | 219.4 | 210.9 | 223.0 | 210.3 |
| 50 | 389.7 | 224.3 | 225.8 | 214.1 | 222.7 | 213.8 |
| 33.3 | 396.6 | 236.7 | 231.0 | 216.6 | 227.6 | 222.8 |
| 16.7 | 414.5 | 258.0 | 248.9 | 232.8 | 244.1 | 243.0 |
| 8.3 | 430.7 | 274.7 | 262.9 | 245.5 | 251.5 | 252.5 |
| 3.3 | 437.2 | 283.1 | 268.3 | 249.8 | 254.8 | 256.0 |
| 1.7 | 438.0 | 284.0 | 269.1 | 250.5 | 255.1 | 256.6 |
| 1.1 | 438.1 | 284.2 | 269.2 | 250.6 | 255.5 | 256.7 |

Table 4.2. Vitrification time (in minutes) as a function of frequency for quasi-isothermal TOPEM experiments at 50ºC and 70ºC, for the switching times indicated. Two separate experiments [(a) and (b)] with the same switching time range 15-30 s were performed at 70ºC.

The total heat flow in a TOPEM experiment can be calculated either directly from the original heat flow data of Figure 4.4 or from the sum of the reversing and non-reversing heat flow components, which may be determined independently [12] and serves as an internal check on the calculations. The result is shown in Figure 4.7. Similar to the situation for ADSC shown in Figure 4.3, the initial part of the heat flow curve is truncated up to a time equal to half the width of the evaluation window (120 s in the present case).

66
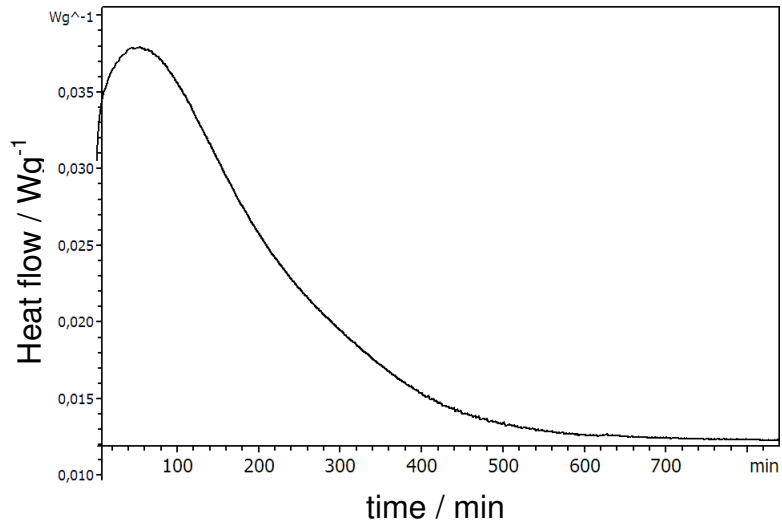
Figure 4.7. Total heat flow from TOPEM quasi-isothermal cure experiment at 50ºC with a switching time range of 15-30 s, and using the default calculation window width of 120 s.

Wider evaluation windows, therefore, have the disadvantage that an increasing amount of the heat flow curve is truncated, while the minimum width of evaluation window is the maximum value of the switching time range in order to ensure that at least one whole temperature pulse is included in any evaluation. For this reason, heat flow evaluations in TOPEM are performed with a calculation window width of a maximum of 120 s, which necessarily restricts the TOPEM experiment to have a switching time range with a maximum value less than 120 s (in the present case, only 15-30 s is suitable), while the frequency evaluations can be made for greater window widths.

### *4.2.4. Results*

The results obtained for the vitrification times with TOPEM compare well with those obtained by ADSC as can be observed in Figure 4.8, where the vitrification time $t_v$ is represented versus the logarithm of frequency for both isothermal temperatures, 50 ºC and 70 ºC.

67
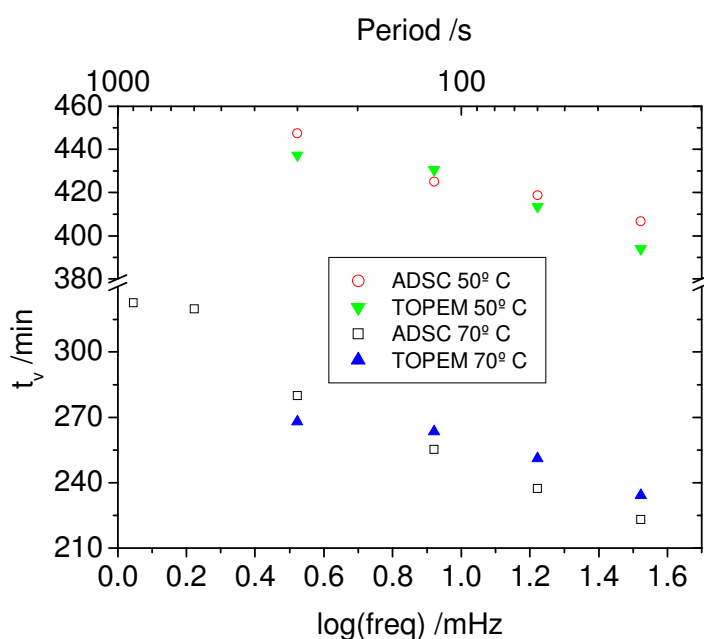
Figure 4.8. Vitrification time versus log(frequency) for ADSC and TOPEM results at 70 ºC and 50 ºC s indicated

The partial heats of curing during the quasi-isothermal ADSC and TOPEM experiments and their corresponding residual and total heats of cure from the second scans are summarised in Table 4.3.

| experiment | heats of cure / Jg$^{-1}$ | | | $T_g$ / ºC |
|---|---|---|---|---|
| | partial | residual | total | |
| ADSC 50ºC | 363.2 | 50.5 | 413.7 | 87.6 |
| ADSC 70ºC | 418.8 | 11.4 | 430.2 | 87.5 |
| TOPEM 50ºC | 364.0 | 59.4 | 423.5 | 87.8 |
| TOPEM 70ºC (a) | 386.5 | 7.0 | 393.5 | 81.6 |
| TOPEM 70ºC (b) | 395.8 | 6.5 | 402.2 | 84.8 |

Table 4.3. Partial heats of cure, residual heats of cure and total heats of cure and glass transition temperatures of fully cured samples for the ADSC and TOPEM isothermal cure experiments at 50ºC and 70ºC.

For the reasons given above, these values were obtained from ADSC experiments with a period of 60 s and from TOPEM experiments with a switching time range of 15-30 s and a calculation window width of 120 s. The rate of cure is calculated from the equation:

$$\mathrm{d}\alpha \,/\, \mathrm{d}t = \phi \,/\, \Delta H_{tot} \tag{4.2}$$

where $\phi$ is the heat flow at time $t$ and $\Delta H_{tot}$ is the total heat of cure, being the sum of the partial and residual heats of cure. The degree of cure, $\alpha$, at any time $t$ is then found simply as the area under the heat flow curve up to that time, normalised by the total heat of cure. A typical representation of the rate of cure as a function of the degree of cure is shown in Figure 4.9, for ADSC at 50ºC with a period of 60 s.
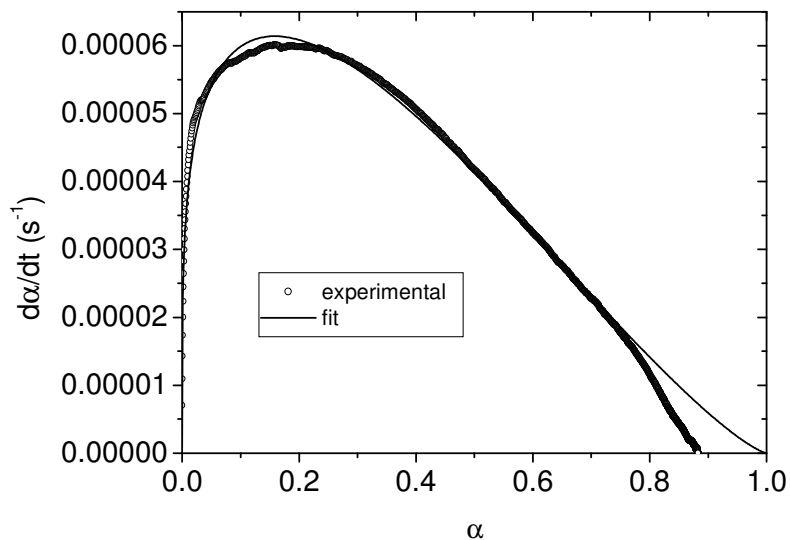


Figure 4.9. Rate of cure versus degree of cure for quasi-isothermal cure by ADSC at 50ºC with a period of 60 s and an amplitude of 0.5 K. The points represent the experimental data while the full line is the fit of Kamal equation.

The kinetic analysis of the major part of the cure process which is controlled by chemical reaction is based upon the equation of Kamal [14]:

69

$$d\alpha / dt = (k_1 + k_2\, \alpha^m)\, (1-\alpha)^n \qquad\qquad (4.3a)$$

or that of Horie [15]:

$$d\alpha / dt = (k_1 + k_2\, \alpha)\, (1-\alpha)^n \qquad\qquad (4.3b)$$

where $k_1$ and $k_2$ are rate constants with an Arrhenius temperature ($T$) dependence and the exponents $m$ and $n$ are the reaction orders. This kinetic model has been used to fit the experimental data, such as those shown in Figure 4.9, within the range in which the reaction is chemically controlled, by means of multiple regression.

An illustration of this fit is shown as the full line in Figure 4.9. It is clear that a good fit is obtained for the majority of the reaction, but that a significant deviation occurs in the region of $\alpha = 0.8$, where the experimental data decrease rather rapidly to zero at a value of $\alpha$ less than unity, while the theoretical curve continues to reach zero at $\alpha = 1$. This deviation represents the effect of vitrification.

In view of the fact that the rapid decrease in the rate of cure that occurs when vitrification intervenes is as a result of a change in the kinetics from a chemically controlled rate to one that is diffusion controlled, it is common to quantify the effect of vitrification by means of the diffusion factor (DF), defined by the equation (see, for example, reference 16):

$$(d\alpha / dt)_{exp} = DF \times (d\alpha /dt)_{chem} \qquad\qquad (4.4)$$

which relates the experimentally measured reaction rate, $(d\alpha / dt)_{exp}$, to the theoretical chemical reaction rate, $(d\alpha /dt)_{chem}$, according to the appropriate model

(Equation 3a or 3b in the present case). Thus the diffusion factor takes a value of unity in the region in which the reaction is controlled chemically, and then falls to zero when vitrification occurs. One way that has been proposed [6, 7] for modelling this effect of vitrification is by means of a mobility factor (MF) which can be determined directly from the experimental data, for any cure temperature, from the time dependence of the complex heat capacity curve for any frequency, $f$, such as that shown in Figure 4.2. The mobility factor is defined by the following equation:

$$MF(f) = [C_p^*(t,f) - C_{pg}(t,f)] \, / \, [C_{pl}(t,f) - C_{pg}(t,f)] \qquad (4.5)$$

where $C_{pl}$ and $C_{pg}$ are the (time- and frequency-dependent) heat capacities of the asymptotic liquid and glassy regions, respectively, for a given cure temperature, $T_c$, as shown in Figure 4.2. The mobility factor therefore, like the diffusion factor, decreases from unity to zero as the vitrification process occurs, and for this reason has been suggested to be an approximation to the DF. Unlike the DF, however, the MF is dependent on the frequency, since $t_v$ is frequency-dependent (see Tables 4.1 and 4.2). It is interesting, therefore, to examine the extent to which the two factors, DF and MF, are indeed comparable in any given isothermal curing experiment. To do so, the MF is calculated from the complex heat capacity $c_p^*$ data of ADSC or from the frequency-dependent $c_p(f)$ data of TOPEM according to Equation 4.5, and compared with the DF calculated from Equation 4.4 and the fit of the Kamal equation (Equation 4.3a) or the Horie equation (Equation 4.3b) to the chemically controlled part of the cure.

This approach has been applied to the TOPEM data for frequencies from 1.1 to 120 mHz. The dependence of MF on degree of cure for selected frequencies within this range at a cure temperature of 50ºC is shown in Figure 4.10, and compared with the DF for this same isothermal cure experiment. Alternatively, assuming that the MF is a good approximation to the DF, one can apply these experimentally calculated mobility factors in the place of the diffusion factor in Equation 4.4 in order to model

71

the effect of vitrification on the cure curves of $d\alpha / dt$ versus $\alpha$ for each frequency. The results are shown in Figures 4.11a and 4.11b for one selected frequency (8.33 mHz) for each of the theoretical models.
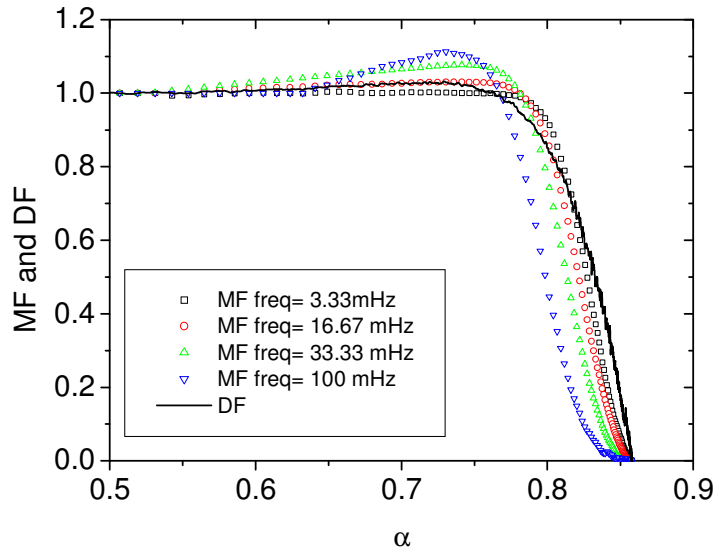


Figure 4.10. Dependence of MF, from the TOPEM quasi-isothermal cure experiment at 50ºC, on time of cure for selected frequencies, and the comparison with the DF.

Although the fit of the whole cure reaction making use of Equation 4.4 appears rather good, and with little difference between the two models (Kamal and Horie), the region of particular interest is that in which vitrification occurs. In order to examine the vitrification in more detail, an enlarged view of this region is presented in Figure 4.12 for five frequencies: 8.3, 16.7, 33.3, 50 and 100 mHz.
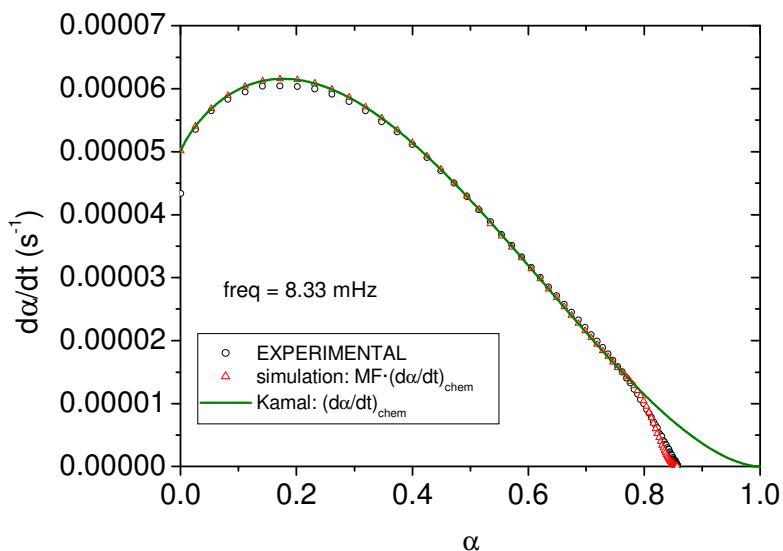
Figure 4.11a. Rate of cure as a function of $\alpha$ obtained experimentally at 50ºC (open circles), showing vitrification in the range of $\alpha \approx 0.8$. The full line is the fit of the theoretical model (Kamal, Equation 2a) to the chemically controlled region up to vitrification. The open triangles represent the fit to the whole of the reaction using Equation 3 with DF=MF.
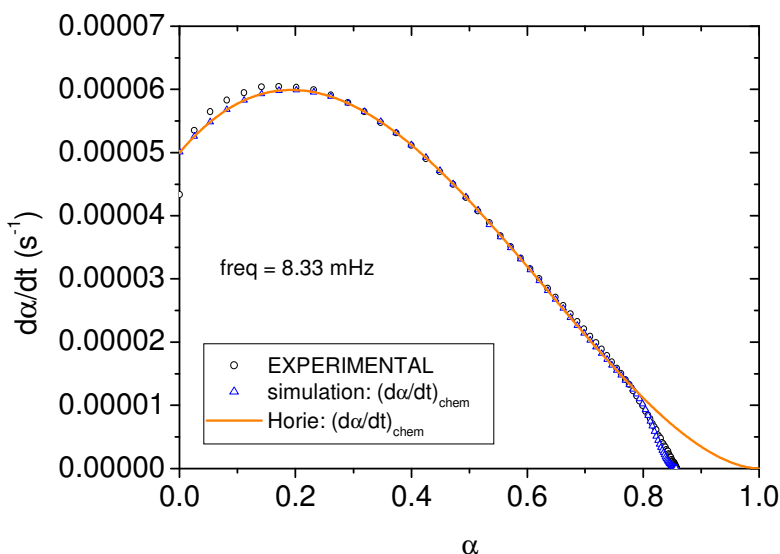


Figure 4.11b. Rate of cure as a function of $\alpha$ obtained experimentally at 50ºC (open circles), showing vitrification in the range of $\alpha \approx 0.8$. The full line is the fit of the theoretical model Horie (Equation 2b) to the chemically controlled region up to vitrification. The open triangles represent the fit to the whole of the reaction using Equation 3 with DF=MF.

73
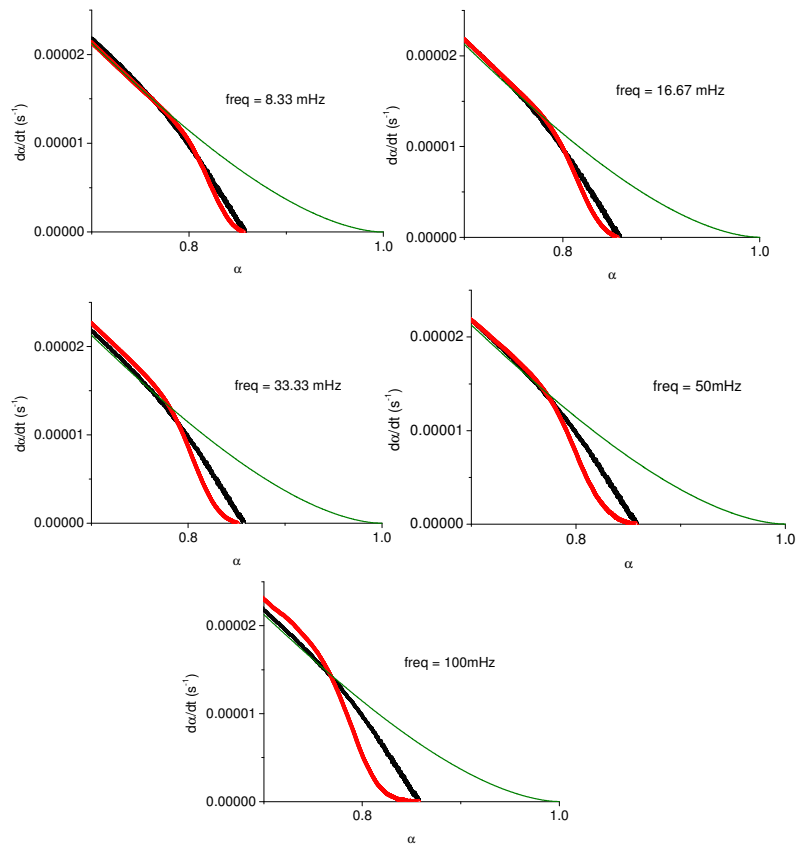
Figure 4.12. Enlarged views of the vitrification region in isothermal cure at 50ºC. The open black circles represent the experimental data. The full line is the fit if the Kamal model (Equation 2a) to the chemically controlled region up to the start of vitrification. The open red triangles are obtained by using Equation 3 in which DF=MF, with MF corresponding to the frequencies indicated.

### 4.2.5. Discussion

The use of the mobility factor to model cure in which vitrification takes place has not always been successful. Although there appears to be a good approximation between the diffusion factor and MF for a period of 60 s for epoxy-amine reactions [6-8], it has been shown to be inadequate for others, such as epoxy-

74

anhydride systems [9]. Furthermore, there is also the question of the role of the frequency of modulation. The suggestion has been made that its applicability for a period of 60 s in epoxy-amine systems is fortuitous, and that at other frequencies, and in particular at higher frequencies, significant deviations would be observed.

The use of TOPEM, in which only a single sample is required in order to obtain frequency-dependent data for the confirmation or otherwise of this suggestion, represents a useful advantage over ADSC. Examining the results shown in Figure 4.12 for the region in which vitrification occurs, it can be seen that, indeed, the quality of fit of the theoretical model applied to the whole of the reaction by means of the DF as in Equation 4.4, and using MF defined by Equation 4.5 as an approximation to DF, depends on the frequency. The differences between DF and MF are even more marked when these two factors are viewed together as a function of the degree of cure, as in Figure 4.10.

This is, in fact, what one might expect. The dependence of the rate of cure on the degree of cure, as represented for example in Figures 4.9 and 4.11, is found from the total heat flow data, which are frequency-independent. On the other hand, the mobility factor is most certainly frequency-dependent, as shown in Figure 4.10, for example, and as a consequence gives rise to the deviations seen in Figure 4.12. Nevertheless, there is in fact rather a good agreement between DF and MF in the range of the lowest frequencies used here, corresponding to modulation periods of up to 60 s, the difference between DF and MF becoming greater as the frequency increases. Why this should be so is an interesting question, particularly in view of the fact that in epoxy-anhydride systems shorter modulation periods than 60 s are necessary in order to achieve a satisfactory correspondence between DF and MF. Likewise, if the curing reaction is monitored by dielectric analysis rather than by TMDSC techniques, in other words at much higher frequencies, and if vitrification is associated with the step change in the permittivity (or the peak in the loss factor)

75

instead of the step change in the complex heat capacity, then the vitrification time would be much shorter and the degree of cure at vitrification would be smaller, thus leading to a MF which would be much more significantly different from DF. It would appear, therefore, that in the epoxy-amine system studied here the relatively good agreement between DF and MF occurs just in the range of frequencies in which TMDSC techniques are usually applied.

This is similar to the well-established relationship between the thermal and dynamic glass transitions in amorphous polymers [10, 11]. The thermal transition, as observed typically in conventional DSC for example, is dependent on the cooling rate. On the other hand, the dynamic glass transition, as observed by TMDSC techniques for example, is dependent on the frequency of modulation. It transpires that, at least for many polymers, these two transition temperatures are not very far apart for the usual ranges of cooling rates and frequencies applied in DSC and TMDSC, respectively. Indeed, this is to a certain extent a problem when it is desired to study the dynamic glass transition without any interference from the thermal transition. Furthermore, it is possible to relate the cooling rate and frequency required in order to obtain the same glass transition temperature by DSC and TMDSC, a relationship that can be interpreted in terms of fluctuation dissipation theories [17, 18] and which is significantly different for different glass-forming systems. It would seem that an analogous effect is being observed in the present studies of vitrification during isothermal cure. For epoxy-amine systems, the dynamic vitrification process appears to coincide reasonably well with the thermal vitrification for modulation periods typical of TMDSC techniques. On the other hand, for the epoxy-anhydride system a different frequency range is appropriate.

The frequency dependence of the vitrification time is in itself interesting. A plot of $t_v$ versus the frequency on a logarithmic scale for the results obtained by ADSC (Table 4.1) and TOPEM (Table 4.2) at 70 ºC is shown in Figure 4.13. The first point to note

76

is that the TOPEM data level off for frequencies less than approximately 5 mHz. An analogous observation was made in the previous chapter with the study of the frequency dependence of the dynamic glass transition in polycarbonate [13], where TOPEM data yielded dynamic glass transition values which were independent of frequency for frequencies below about 4 mHz, and this represents a current limitation in the low frequencies able to be evaluated by TOPEM.
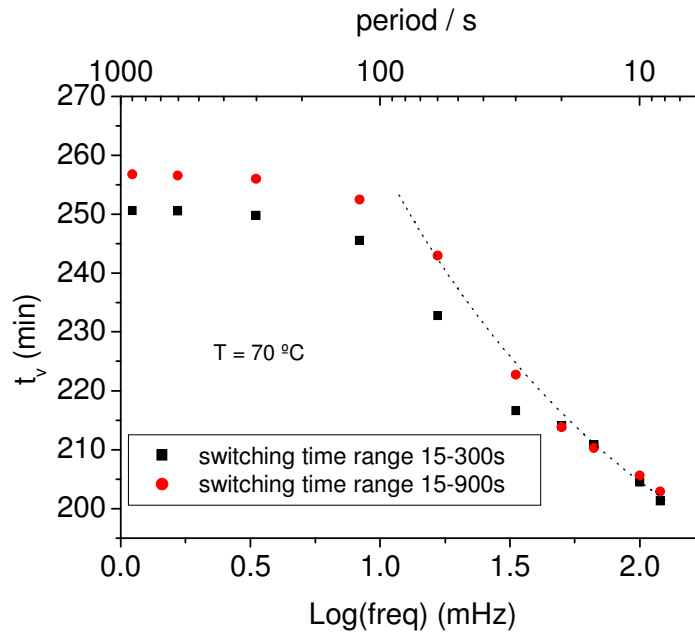


Figure 4.13. Vitrification time, $t_v$, versus log(frequency) for TOPEM experiments at 70 ºC and two different switching time ranges of 15-300 s and 15-900 s, as indicated. The line is only a guide to the eye

Leaving aside this limitation of the TOPEM data, though, it can be seen that the data for TOPEM and ADSC superpose within the errors associated with such measurements. It is particularly noticeable that the scatter of the TOPEM data is less than that for the ADSC data, which can be attributed to the elimination, in the former, of an important possible source of experimental error, namely the variation

77

in the sample due to the need to prepare a resin/diamine mixture freshly for each ADSC experiment with different modulation periods.

In fact, this reduction in scatter in the TOPEM data allows us to infer that the relationship between $t_v$ and log $f$ in the frequency range of the data in Figure 4.13 appears to have some upward curvature, as indicated by the smooth curve that is drawn to guide the eye. This is different from the situation reported at much higher frequencies and obtained by dielectric analysis (DEA) [19, 20], in which region a linear equation relating $t_v$ and log $f$ has been proposed [19], which may be written as follows:

$$t_v = -t_0 \log(f / f_0) \qquad (4.6)$$

where $t_0$ and $f_0$ are constants. Interestingly, though, in experiments in which both DEA and ADSC (with a period of 60 s) were used to study the vitrification of an epoxy-amine system [21], the linear extrapolation of the high frequency DEA data to the frequency range of ADSC did not pass through the single data point at 60 s for any cure temperature except the lowest.
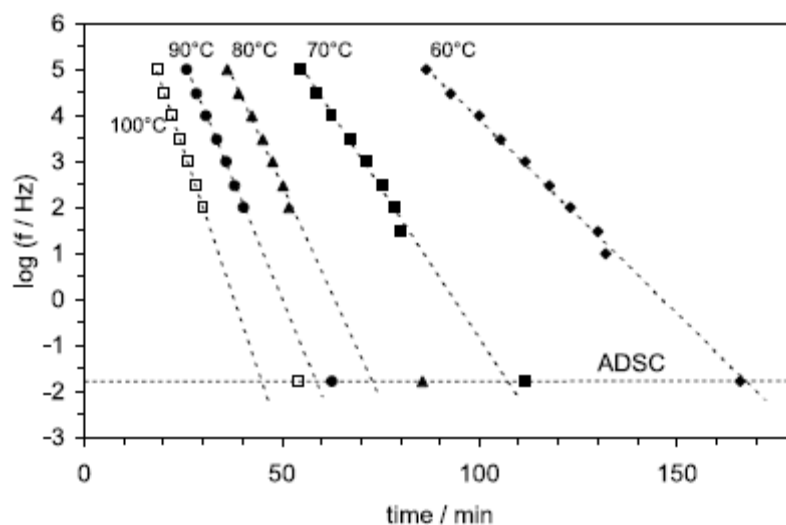


Figure 4.14. Vitrification time with frequency obtained by DEA and ADSC [from Montserrat et al; Polymer 44 (2003) Page 110, Figure 12.]

78

This suggests that in general there is an upward curvature to these plots, such as is seen in Figure 4.13, in the range of frequencies where ADSC and TOPEM are employed. In the next part of this chapter, a theoretical model is presented for the vitrification process which leads to a prediction of the frequency dependence of the vitrification time, as determined by temperature modulated DSC techniques, in which these observations are explained.

## 4.3. Simulation

### 4.3.1. Introduction.

With the aim of confirming the experimental observations in the previous TOPEM results, and in particular their relationship with data at higher frequencies, a simulation was used to determine the vitrification time as a function of frequency, considering it as the time when the (frequency dependent) glass transition temperature, $T_g$, of the curing system reaches the isothermal cure temperature. Simulations were made for different cure temperatures. Other parameters, such as the exponents (reaction orders) in the Kamal equation, $\lambda$ in the DiBenedetto equation (controlling the dependence of $T_g$ on the degree of cure), and the activation energy for the frequency dependence of $T_g$, were also considered. The results are compared with those obtained previously by TOPEM at low frequencies and by DEA at high frequencies.

### 4.3.2. Theory and simulation

MATLAB version 7.0 was used to simulate the isothermal cure reaction, taking into account the following considerations. In the absence of vitrification, the reaction is chemically controlled and the time ($t$) dependence of the degree of cure ($\alpha$, $0 \leq \alpha \leq 1$) during the reaction can be described by, for example, the equation of Kamal [14]:

$$\left(\frac{d\alpha}{dt}\right)_{chem} = (k_1 + k_2 \cdot \alpha^m) \cdot (1-\alpha)^n \tag{4.7}$$

where $k_1$ and $k_2$ are temperature dependent rate constants, and the exponents $m$ and $n$ are the reaction orders, their sum usually being approximately $m+n \approx 2$. The rate constants are considered to have an Arrhenius temperature ($T$) dependence [22]:

$$k_{c\,(1,2)} = A_{(1,2)} \cdot \exp\left[-E_{c(1,2)}/RT\right] \tag{4.8}$$

where $A$ and $E_c$ are pre-exponential parameters and activation energies, respectively, and $R$ is the universal gas constant. The subscript $c$ for $k$ and $E$ indicates that these are values for the chemically controlled reaction.

When vitrification occurs, the rate of cure becomes controlled by diffusion, and it is therefore necessary to introduce, in addition, a rate constant for diffusion, $k_d$. One possibility is to assume this rate constant to have a WLF temperature dependence [23,24]:

$$k_d = k_{dg} \cdot \exp\left[C_1(T-T_g)/(C_2+T-T_g)\right] \tag{4.9}$$

where $C_1$ and $C_2$ are constants, here assumed to take their "universal" WLF values [23] of 40.2 (= 2.303 × 17.44) and 51.6 K, respectively, $T_g$ is the glass transition temperature of the reacting system, and $k_{dg}$ is the value of $k_d$ when $T_g$ is equal to the cure temperature, i.e. at vitrification.

It should be pointed out that there are other possibilities for the temperature and $T_g$ dependence of $k_d$. Wisanrakkit and Gillham [25] and Meng and Simon [26] use a

80

modified form of Equation 4.9 in which the term $T-T_g$ is replaced by its absolute value $|T-T_g|$:

$$k_d = k_{dg} \cdot \exp\left[C_1(T - T_g)/(C_2 + |T - T_g|)\right] \quad (4.10)$$

Another approach, based upon the concept of free volume, originally suggested by Huguenin and Klein [27] and subsequently by others [28-29], uses the expression:

$$k_d = k_{d0}D_0 \exp\left[B\left(1 - \frac{1}{f_g + \alpha_f(T - T_g)}\right)\right] \quad (4.11)$$

where $k_{d0}$ is a constant related to the bonding conditions, $D_0$ is the self diffusion coefficient, $B$ is a constant that includes the critical free volume required for diffusion, $f_g$ is the fractional free volume at $T_g$ and $\alpha_f$ is the thermal expansion coefficient of the free volume. Yet another alternative expression to Equation 4.9, proposed by Havlicek and Dusek [30], is based upon the configurational entropy theory of Adam and Gibbs [31]:

$$k_d = k_{d0}D_0 \exp\left[\frac{-M}{T \ln[T/(T_g - 50)]}\right] \quad (4.12)$$

where $M$ is a parameter related to the configurational entropy of the cooperatively rearranging regions (see reference 30 for details), and is considered to be a material constant.

Finally, Chern and Poehlein [32] proposed a slightly different approach in which the overall rate constant $k$ is related to the rate constant for the chemical reaction $k_{chem}$ by the semi-empirical equation:

$$k = k_{chem} \exp[-C(\alpha - \alpha_c)] \qquad (4.13)$$

where $C$ is a constant for a given system, having an effect only on the limiting conversion, and $\alpha_c$ is the critical degree of cure at which a three dimensional network is formed, in other words at gelation.

Besides these various possibilities for the diffusion controlled rate constant, the value of $k_{dg}$ in Equation 4.9 is also open to discussion. For the present simulations, Equation 4.9 was used with a value of $k_{dg}$=0.0051 s$^{-1}$; a wider explanation can be found in section 4.3.5.

The chemical and diffusion rate constants can be combined into overall rate constants, $k_{tot(1,2)}$, by means of the Rabinowitch equation [33]:

$$\frac{1}{k_{tot(1,2)}} = \frac{1}{k_d} + \frac{1}{k_{c(1,2)}} \qquad (4.14)$$

These overall rate constants are used in place of $k_1$ and $k_2$ in the Kamal equation, Equation 4.7, in order to describe the rate of cure throughout the reaction, including that part in which vitrification occurs. As the reaction proceeds, the glass transition temperature increases from its initial value, $T_{g0}$, being that of the mixture of monomers of resin and cross-linking agent, and, in the absence of vitrification, will reach a limiting value, $T_{g\infty}$, corresponding to the fully cured system ($\alpha$=1). The relationship between the degree of cure and the glass transition temperature of the curing system can be described by the DiBenedetto equation [2, 22], see Equation 4.1 page 56. The effect of $\lambda$ is also investigated in these simulations.

Equations 4.1, 4.7, 4.8 and 4.14, together with the selected equation for the diffusion rate constant, are sufficient to define the dependence of the rate of cure, proportional

82

to the heat flow measured in a typical DSC experiment, as a function of time (or of degree of cure) during an isothermal curing reaction. In the simulation of isothermal cure in conventional DSC, for each time step $dt$ the increment in $\alpha$ $(d\alpha)$ is evaluated by Equation 4.7 using the current value of $\alpha$. For the rate constants in Equation 4.7, the overall rate constants $k_{tot(1,2)}$ are used, calculated from Equation 4.14 in which the chemical rate constants $k_c$ depend on the isothermal cure temperature, $T_c$, through Equation 4.8 and the diffusion rate constant $k_d$ is determined by both $T_c$ and the $\alpha$-dependent $T_g$ through Equation 4.9. Vitrification is considered to occur when $T_g$ reaches the cure temperature, $T_c$. The rate of cure dramatically slows down, being dominated now by the diffusion rate constant, but does not stop completely; instead, the cure continues at an ever decreasing rate, approaching a limiting value of $\alpha$, less than unity, which is determined by the cure temperature.

Although the usual experimental evaluation of the vitrification time in TMDSC is from the mid-point of the sigmoidal change in complex heat capacity, in these simulations it is evaluated as the time at which the dynamic glass transition is equal to the cure temperature, equivalent to the definition of the vitrification time determined by conventional DSC. The reason for evaluating it in this way is for simplicity, taking into consideration the following aspects. First, the complex heat capacity depends on the degree of cure, in both the liquid-like region before vitrification and in the glassy region after vitrification, in a way that depends on the curing system. Second, the sigmoidal change in complex heat capacity occurs when the average relaxation time is of the order of the modulation period. This average relaxation time is dependent on the enthalpic state of the sample, which is a function both of the degree of cure and of the non-equilibrium state of the sample with respect to its glass transition temperature, which is itself changing with the degree of cure.

For the present simulation of cure monitored by TMDSC, therefore, it is necessary to introduce the frequency dependence of the glass transition temperature. One way to do this would be to assign a frequency dependence to the initial and limiting glass transition temperatures, $T_{g0}$ and $T_{g\infty}$, respectively, such that they increase with increasing frequency. This would imply also, through Equation 4.1, a frequency-dependent glass transition temperature of the curing system. However, although this would permit the determination of the dynamic vitrification time, it would not properly represent the curing reaction since it is the *frequency-independent* calorimetric glass transition temperature which governs the vitrification process, when the change occurs from a chemically controlled reaction to one controlled by diffusion. In fact, this approach would predict that the reaction effectively stops when the dynamic vitrification time is reached, which is not what is observed experimentally.

An alternative approach, used here, for the determination of the dynamic vitrification time, is to assign a frequency dependence to the cure temperature, such that it decreases with increasing frequency, as illustrated in Figure 4.15. In this figure, the dash-dotted line represents the variation of $T_g$ with cure time that would occur in the (unrealistic) absence of vitrification during isothermal cure at $T_c$=343 K, while the dotted line indicates the variation of $T_g$ that would occur when vitrification intervenes. The horizontal lines represent the frequency-dependent cure temperatures corresponding to frequencies of 2.97 mHz (upper line), 16.7 mHz (central line) and 93.7 mHz (lower line), equivalent to periods of 337 s, 60 s and 10.7 s, respectively. These frequency-dependent cure temperatures, $T_c(f)$, are calculated according to the following equation and with a reduced activation energy of $E_f/R$=50 kK:

84

$$\ln\left(\frac{f}{f_r}\right) = \frac{E_f}{R}\left(\frac{1}{T_c(f)} - \frac{1}{T_c}\right) \tag{4.15}$$

In this equation, $E_f$ is the activation energy controlling the frequency dependence of $T_c$, and $f_r$ is a reference frequency for which the dynamic cure temperature, $T_c(f)$, is considered to be equal to the cure temperature, $T_c$. Since the vitrification time determined by conventional DSC makes use of a glass transition temperature determined on heating after, typically, previously cooling freely [4], the correspondence between cooling rate and frequency [10,34] can be used to assign a value of $1/60$ s$^{-1}$ for the reference frequency. The effect of various values of the activation energy, $E_f$, is investigated in the simulation.
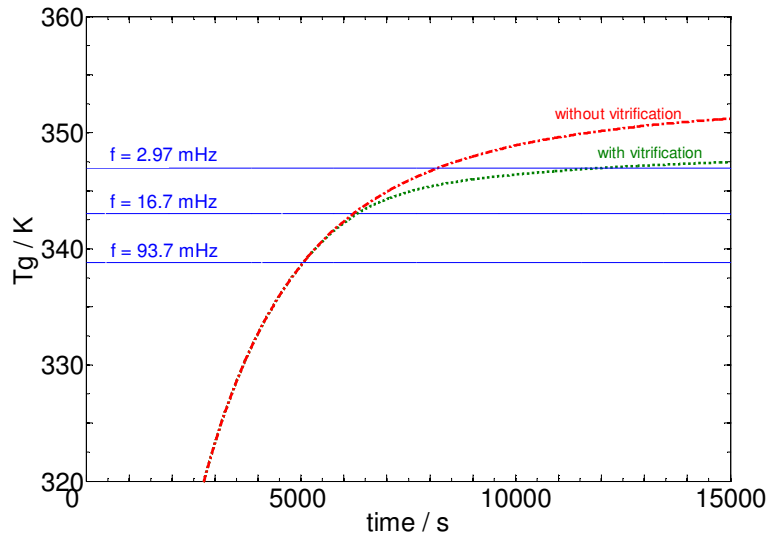


Figure 4.15. Increase of $T_g$ (from 320 K) with time during isothermal cure at 343 K for a system with $T_{g0}$=258 K and $T_{g\infty}$=353 K in the absence of vitrification (dash-dotted line) and when vitrification intervenes (dotted line). Horizontal lines indicate selected dynamic cure temperatures (see text for details).

The difference in the results obtained by DSC and TMDSC is well illustrated by this figure. The intersection of the horizontal lines with the dotted line, representing the

cure curve with vitrification, defines the dynamic vitrification times that would be obtained by TMDSC, which increase with decreasing frequency. The central horizontal line represents a frequency of 16.7 mHz, and defines a vitrification time equivalent to that which would be obtained by conventional DSC. This approach, in which a frequency dependence is assigned to the cure temperature such that it decreases with increasing frequency, maintains the same value for $T_c-T_g$ as would be obtained for a frequency-dependent $T_g$, increasing with increasing frequency, and hence will define the same dynamic vitrification time when $T_c=T_g$.

| *constant* | *value [ref] and Equation where used* | | | | | |
|---|---|---|---|---|---|---|
| $A_1$ (s$^{-1}$) | $10^{3.6}$ [24]   Equation (4.8) | | | | | |
| $E_{c1}$ (kJ mol$^{-1}$) | 51.8 [24]   Equation (4.8) | | | | | |
| $A_2$ (s$^{-1}$) | $10^{3.4}$ [24]   Equation (4.8) | | | | | |
| $E_{c2}$ (kJ mol$^{-1}$) | 41.5 [24]   Equation. (4.8) | | | | | |
| $k_{dg}$ (s$^{-1}$) | 0.0051   Equation (4.9) | | | | | |
| $C_1$ | 40.2 [23]   Equation (4.9) | | | | | |
| $C_2$ (K) | 51.6 [23]   Equation (4.9) | | | | | |
| $T_{g0}$ (°C) | -15   Equation (4.1) | | | | | |
| $T_{g\infty}$ (°C) | 80   Equation (4.1) | | | | | |
| **parameter** | **values** | | | | | |
| $T_c$ (°C) | 10    20    30    40    50    60   70 | | | | | |
| $m$ | 0    0.23   0.3   0.4   0.5    1 | | | | | |
| $n$ | 1    1.43   1.5    1.6   2 | | | | | |
| $\lambda$ | 0.1   0.18   0.2   0.22   0.33   0.66   1 | | | | | |
| $E_f/R$ (kK) | 25    50    95    100   110   120   150 | | | | | |

Table 4.4. Constants and ranges of parameter values used in the simulations

A summary of the values of the constants used in these simulations is given in Table 4.4. Also shown are the ranges of parameter values investigated here, namely the cure temperature, $T_c$, the reaction orders, *m* and *n*, in Equation 4.7, the parameter $\lambda$ of the DiBenedetto equation, Equation 4.1, and the activation energy, $E_f$, in Eq. 4.15. It should be noted that the parameters m and n have independent values, its sum being approximately $m+n \approx 2$ in many cases, but it is not a restriction, only an approximation; for this reason all the values of m and n in the simulations were used, in some cases being $m+n > 2$ as can be observed in the previous Table 4.4.

### *4.3.3. Results and discussion*

A typical result for the dependence of the dynamic vitrification time on log(frequency) for different cure temperatures is shown in Figure 4.16, for frequencies within the usual range for TMDSC experiments. In all of these plots a
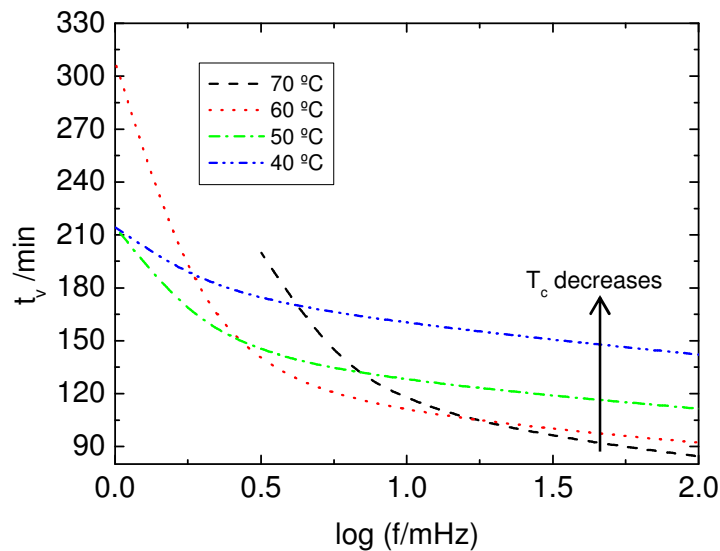


Figure 4.16. Typical plot of $t_v$ against log(*f*) for simulations with *m*=0.23, *n*=1.43, $\lambda$=0.33 and $E_f/R$=50 kK, for different cure temperatures from 70ºC to 40ºC, decreasing as indicated. The frequencies are chosen as those typical for TMDSC measurements, corresponding to periods in the range 30 to 1000 s.

similar upward curvature, rather than a linear dependence, can be observed. Such behaviour was found, not only for the combination of parameter values used in Figure 4.15, but also in all the simulations. Different values for the parameters ($T_c$, $m$, $n$, $\lambda$, $E_f$) result in a change in the curvature or displace the curves upwards or downwards, whilst maintaining the same general appearance.

### *4.3.4. Comparison with experimental results*

#### *Comparison with TOPEM measurements*

From the simulations, it is possible to obtain results very similar to those obtained previously by TOPEM [35], for a DGEBA-type epoxy resin cured with a polyoxypropylene diamine, by adjusting the parameter values appropriately.
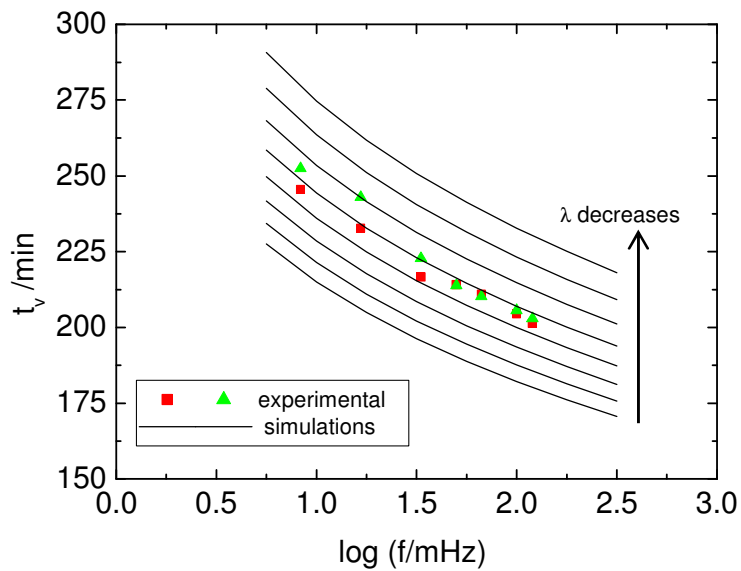


Figure 4.17. Comparison of experimental TOPEM data[16] with the simulations. The experimental points are obtained from two separate TOPEM experiments at $T_c$=70ºC. The simulations were made with $E_f/R$=120 kK, $m$=0.4, $n$=1.6 and $\lambda$ between 0.14 and 0.21.

This can be seen in Figure 4.17, where the dynamic vitrification time from the simulations is again represented as a function of the frequency, on a logarithmic scale, and is compared with the earlier experimental results. For the experimental TOPEM results, the dynamic vitrification time is taken as the time at which the frequency-dependent heat capacity is mid-way between the extrapolated asymptotic values in the glassy and liquid-like regions. The same TOPEM experiment was repeated to give two separate sets of data (squares and triangles in Figure 4.17), which provide a measure of the typical experimental uncertainty. It can be seen that there is a good correspondence between simulated and experimental data for this cure temperature of 70 ºC. The parameter values used for the simulation are $E_f/R$=120 kK, $m$=0.4, $n$=1.6, $T_c$=70 ºC, and $\lambda$ in the range 0.14 to 0.21. Not only are the simulation results very similar to the experimental data, but also the parameter values correspond closely to those obtained previously [35] from a fit of the Kamal equation, Equation 4.7, to the TOPEM data, for which values of $m$≈0.6 and $n$≈1.6 were obtained.

It is interesting to observe that a similar dependence of dynamic vitrification time on log($f$) can also be inferred from the light heating temperature modulated DSC (LMDSC) results of Van Assche *et al*. [36]. In this work, the LMDSC technique allows the frequency range to be extended to higher frequencies (up to 1 Hz), while the dynamic vitrification times fall in a different range from those in Figure 4.16 in view of the different curing agent used (methylene dianiline). In Figure 4.18 there is considerable scatter in the values of $t_v$ for each frequency, attributed by the authors to small differences in sample composition and average cure temperature, every data point resulting from a separate experiment. Nevertheless, a plot of the average value at each frequency as a function of log($f$) appears to show an upward curvature, as anticipated by the simulations presented here. These results provide an excellent illustration of the advantage afforded by TOPEM, in that a single sample suffices for the whole range of frequencies, thus eliminating the experimental error associated

with the preparation of a new sample for each frequency, as is required with TMDSC and LMDSC.
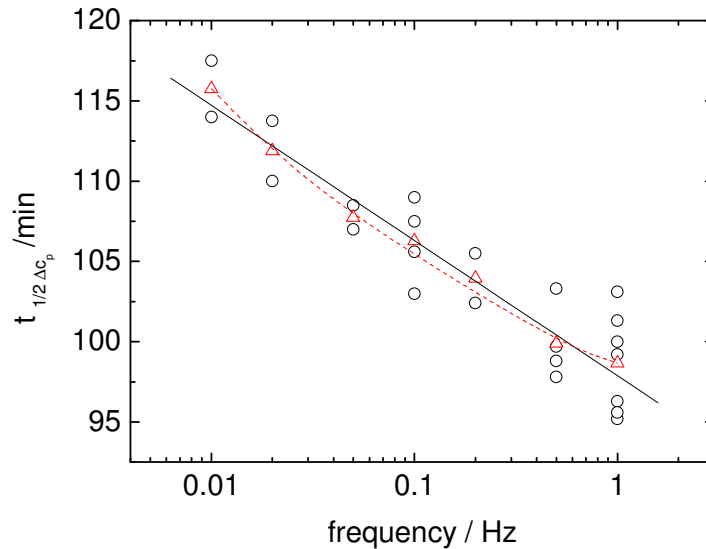


Figure 4.18. In black circles and continuous line, LMDSC Results from Van Assche et al. *Thermochim Acta* (**2001**) *377*, Page 128, Fig 5. In red triangles are represented the average values and the red dotted line is only a guide to the eye.

## *Comparison with dielectric measurements*

With these simulations it is also possible to explore higher frequencies than those attainable by temperature modulated calorimetry. Making the same simulation, but in a wider range of frequencies, the behaviour of the dynamic vitrification time at very high frequencies can be followed. Figure 4.19 shows the results for a range of frequencies between 1 and $10^8$ mHz, corresponding to periods between $10^3$ and $10^{-5}$ s. It is clear that the dependence over the whole frequency range has a non-linear behaviour, with the marked upward curvature seen in the low frequency region, corresponding to the TMDSC data.

90
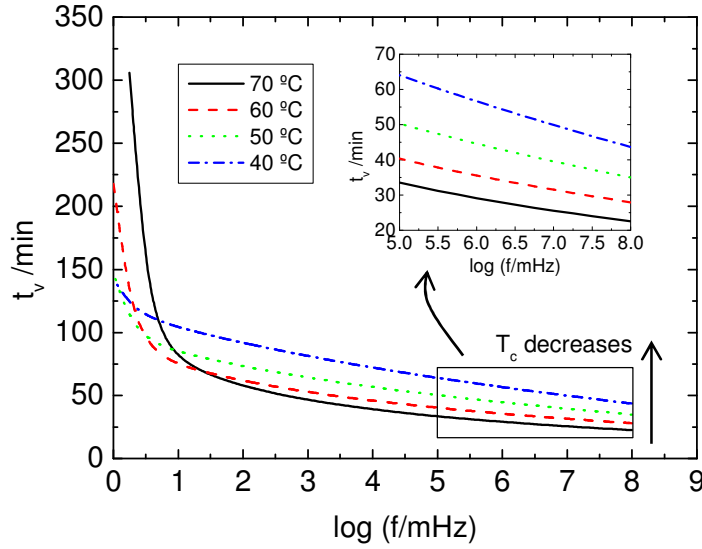
Figure 4.19. Typical dependence of dynamic vitrification time on log(frequency) for a wider range of frequencies and for cure temperatures $T_c$=70, 60, 50 and 40ºC, as indicated. The inset shows an enlarged view of the high frequency region where an approximately linear dependence is observed. Simulation parameters are *m*=0.23, *n*=1.43, $E_f/R$=50 kK and $\lambda$=0.66.

Nevertheless, in the frequency range from $10^5$ to $10^8$ mHz, corresponding to the region explored in dielectric experiments, an approximately linear dependence can be observed. This linear relationship is what is commonly reported in DEA [19, 20, 37] and can be expressed by the equation:

$$- p\left(t_v - t_{vr}\right) = \log\left(f / f_r\right) \tag{4.17}$$

where $t_{vr}$ is the extrapolated dynamic vitrification time corresponding to the reference frequency, $f_r$, here taken to be that equivalent to a period of 60 s, *i.e.* 16.7 mHz, and *p* is the reciprocal of the negative slope of the limiting high frequency region in Figure 4.19. It should be pointed out that Equation 4.17 is simply an

alternative representation of the equation originally proposed by Mangion and Johari [19]:

$$f_m = f_m(0) \exp\left[-kt_m\right] \qquad (4.18)$$

to relate the time, $t_m$, at the mid-point of the $\varepsilon'$ step to the frequency, $f_m$, in dielectric experiments. The parameter $k$ of this equation has been evaluated by various authors [19-21] for different reacting systems, and hence for comparative purposes it is useful to note that the relationship between the two corresponding parameters $p$ and $k$ is a factor of $ln(10)$, namely $k = 2.303\ p$. Do not confuse this parameter $k$ with the rate parameters presented in Equations 4.7 – 4.10.

The very different behaviours for the frequency dependence of the vitrification time in the low and high frequency ranges can be understood by making reference to the change in glass transition temperature with cure time during isothermal cure, as represented in Figure 4.15. For the high frequencies associated with DEA, the frequency-dependent cure temperature would lie at the bottom of or below the range of $T_g$ values included in Figure 4.15. For example, using the earlier value of $E_f/R$ =50 kK, the frequency-dependent cure temperature corresponding to a frequency of $5\times10^5$ mHz is about 319 K. Thus for DEA one is probing a region of Figure 4.15 in which there is a steep increase in $T_g$ with time, and which is distant from the bifurcation representative of the change in kinetics from chemical to diffusion control. This translates into the linear region of Figure 4.16 where there is a relatively small change in $t_v$ with log(frequency). On the other hand, for the much lower frequencies associated with TMDSC, the region of Figure 4.15 being probed is that which encompasses the bifurcation, and hence for which there is a strong influence of this change in kinetics on the determination of the dynamic vitrification time. In turn, this translates into the strong upward curvature seen at low frequency in Figure 4.16.

92

The simulated results presented here can be compared with experimental data from dielectric measurements for an epoxy based on DGEBA and cured with a diamine based on 4,4′-diamino-3,3′-dimethyldicyclohexyl methane (3DCM) [21]. From these data the frequency dependence of the time of the maximum loss factor can be obtained, and it is found to present an excellent linear relationship with a regression coefficient $r^2$ greater than 0.99 in most cases. Figure 4.20 shows the variation of the parameter $p$, in $\text{min}^{-1}$, as a function of the difference between the limiting glass transition temperature, $T_{g\infty}$, and the cure temperature, the difference in temperature rather than the absolute value of the cure temperature being necessary in order to compare systems with different values of $T_{g\infty}$. The filled points represent the experimental data taken from Montserrat *et al* [21] for the 3DCM system, while the different curves shown were obtained from simulations in which the values used for the parameters are given in the inset.



Figure 4.20. Comparison of the parameter *p*, calculated from Equation (11) in the high frequency range ($10^5$-$10^8$ mHz), with experimental DEA data. The results are presented as a function of the temperature difference between $T_{g\infty}$ and $T_c$. The experimental points are obtained from dielectric measurements in the epoxy-3DCM system.[21]

It can again be seen that the simulation can reproduce the trend obtained from dielectric data if appropriate parameter values are chosen. In fact, the closest approximation to the experimental data is for $m=0.4$, $n=1.6$ and $\lambda=0.2$, which compare remarkably well with values of $m=0.47$, $n=1.7$ for the isotherm at 60ºC [21] and $m=0.47$, $n=1.76$ for the isotherm at 70ºC [38], obtained from earlier kinetic analyses of the same epoxy-diamine system studied by isothermal DEA and TMDSC, respectively, and $\lambda$ in the range 0.2 to 0.5, obtained from non-isothermal TMDSC experiments on the same system [39].

Both the experimental data and the simulation results show a maximum in the value of $p$ as the temperature difference between $T_{g\infty}$ and the cure temperature decreases. This corresponds to the familiar appearance of the nose in the time-temperature-transformation (TTT) diagram for isothermal cure, which occurs some 20 K or so below $T_{g\infty}$ in this epoxy system cured with 3DCM [38]. In contrast, in the DGEBA system cured with 4,4′-diaminodicyclohexyl methane which was studied by Fournier *et al* [20], there is no evidence of such a maximum in the range of isothermal cure temperatures used, the value of $p$ increasing monotonically as the cure temperature increases. As was the case for the experimental results from reference [21] considered above, the plot of time of maximum loss versus log frequency presents an excellent linear relationship, with a regression coefficient $r^2$ greater than or equal to 0.99 for all but one of the isothermal cure temperatures. These results for $p$ are illustrated in Figure 4.21, where a value of $T_{g\infty}=365$ K has been used in order to represent the abscissa scale as the difference between $T_{g\infty}$ and the cure temperature, similar to Figure 4.20. This trend can again be modelled, the full curves showing the results of simulations using the different parameter values shown in the inset. In this respect, the parameter that has the most influence on the curve shape is the exponent $n$, which here takes a much lower value ($n=1$) than those used in the simulations of Figure 4.20. This is consistent with the effect on the cure reaction kinetics of steric

94

hindrance of the 3,3′ methyl groups in the 3DCM system, which reduces the reaction rate in the later stages of the reaction.
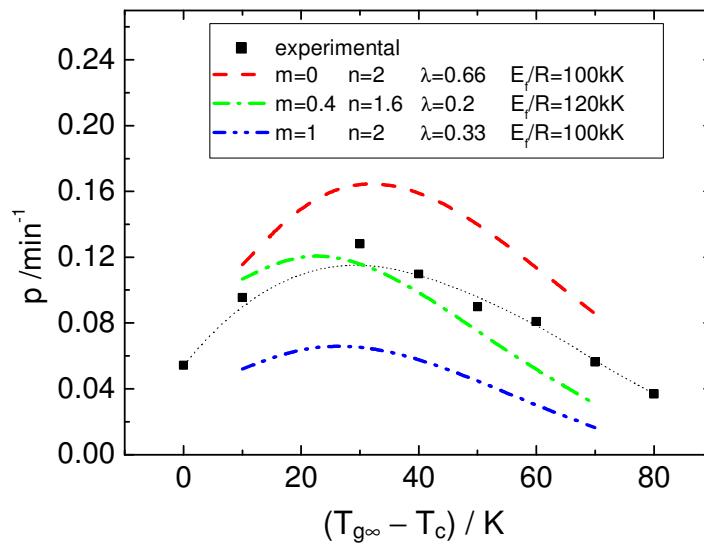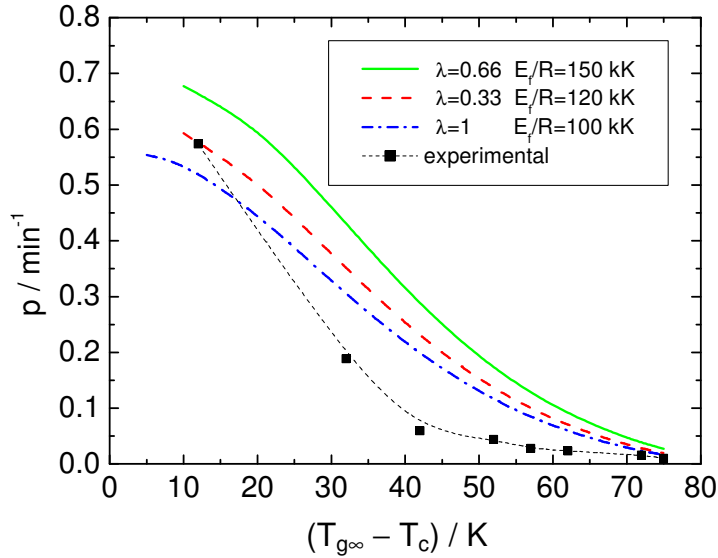


Figure 4.21. Comparison of the parameter *p*, calculated from Equation (11) in the high frequency range ($10^5$-$10^8$ mHz), with experimental data obtained from the dielectric measurements of Fournier *et al.*[20] For the simulations. *m*=1 and *n*=1

### *4.3.5. Discussion: Diffusion controlled rate constant*

The simulations discussed above were all performed using a WLF-type temperature dependence for the rate constant for diffusion [Equation 4.9], in which $k_{dg}$, the value of $k_d$ at the glass transition temperature $T_g$, is taken to have a value of 0.0051 $s^{-1}$. It is clearly important to establish to what extent this parameter value influences the results, but first this value for $k_{dg}$ is compared with some others presented in the literature, for which a surprisingly large variation is found.

Wise *et al* [24] use Equation 4.9, as is also used here, in which the diffusional rate constant at $T_g$ is obtained from an equation due to Smoluchowski [40]:

$$k_{dg} = 4\pi N_A r D_g \qquad\qquad (4.19)$$

where $N_A$ is Avogadro's number, $r$ is a collision radius defining the region of space in which the collision process occurs, taken as 0.5 nm, and $D_g$ is the diffusion coefficient at $T_g$, taken as $10^{-20}$ $m^2 s^{-1}$. This yields a value of $k_{dg}$=3.8 × $10^{-5}$ $m^3 mol^{-1} s^{-1}$, as quoted (without the units) in their Table 1. To convert this to units of $s^{-1}$, taking their average molecular weight for the epoxy monomer, 372 g $mol^{-1}$, and a density of 1.2 g $cm^3$ to obtain a molar volume of 3.1 × $10^{-4}$ $m^3 mol^{-1}$, gives a value of $k_{dg}$=0.12 $s^{-1}$.

Meng and Simon [26] use two different expressions for two different reacting systems. For an epoxy/aromatic amine system, they use the modified WLF expression of Equation 4.10 with a value of $k_{dg}$=0.51 $s^{-1}$, whereas for a dicyanate ester/polycyanurate system they use a modified Doolittle free volume equation:

$$k_{dg} = A_d \exp\left(-\frac{E_d}{RT_g}\right)\exp\left(-\frac{b}{f_g}\right) \qquad\qquad (4.20)$$

where $A_d$=1.67 × $10^{17}$ $s^{-1}$ and $b$=0.25 are adjustable parameters, $E_d$=140 kJ/mol is the activation energy for the diffusion process, and $f_g$=0.025 is the fractional free volume at $T_g$. For this latter system, Equation 4.20 gives $k_{dg}$=3.97 × $10^{-5}$ $s^{-1}$ for $T_g$=423 K, or $k_{dg}$=6.53 × $10^{-4}$ $s^{-1}$ for $T_{g\infty}$=455 K.

Havlicek and Dusek [30] use Equation 4.12, based upon the Adam-Gibbs configurational entropy theory and with parameter values of $m$=$10^3$ K and $k_{d0}D_0$=$10^{10}$ $s^{-1}$. Applying Equation 4.12 at $T$=$T_g$ yields values of $k_{dg}$ of 81.3, 94.6 and 106.7 $s^{-1}$ for vitrification ($T_g$=$T_c$) at the cure temperatures $T_c$ of 373, 337 and 313 K, respectively, used by these authors.

Summarising these calculations, the surprising result is that the rate constant for diffusion at the glass transition temperature appears to vary by more than 6 orders of magnitude, albeit for different reacting systems, whereas it might be expected to vary rather little given that $T_g$ represents the temperature at which the average timescale for molecular mobility is of the order of 100 s. More pertinently, in view of this very wide range of values for $k_{dg}$ one might ask how these various theoretical approaches can possibly model successfully the experimental vitrification behaviour. In this respect there are two important considerations. The first is that in all but one of the cases considered above [24, 26, 30] (the one exception being the dicyanate/polycyanurate system of Meng and Simon [26]), the diffusion rate constant at $T_g$ is always much greater, by two orders of magnitude or more, than the chemical rate constant at the cure temperature. This means that at the onset of vitrification, when $T_g$ reaches the cure temperature $T_c$, the reaction is still controlled chemically, the chemical rate constant being smaller than the diffusion rate constant. Hence the cross-linking reaction proceeds, with a corresponding increase in $T_g$, though at an ever decreasing rate, as is observed experimentally. The second important consideration is that the various expressions for the diffusion rate constant [Equations 4.9, 4.10 and 4.12] all involve a very strong temperature dependence, such that the two orders of magnitude or more difference between the chemical and diffusion rate constants is eliminated by the time $T_g$ has increased to only about 5 K [slightly more for Equation 4.12] above the cure temperature. Thus, even if values for the diffusion rate constant at $T_g$ are selected which differ by a factor of one hundred, this will only result in a relatively small difference in the temperature at which vitrification occurs. Consequently, our selection of the value of $k_{dg}=0.0051$ s$^{-1}$ for the diffusion rate constant at $T_g$ will only influence the actual temperature at which the dynamic vitrification is predicted to occur, and will not have a significant effect either on the overall trends or on the evaluation of the parameter *p*.

## 4.4. Conclusions

The use of TOPEM in studying the vitrification process during the isothermal cure of thermosetting resins presents a significant advantage over other temperature modulated DSC techniques, such as ADSC, in that a single experiment permits the evaluation of the vitrification time for a range of frequencies. Not only is this convenient in respect of its significant time savings, but also it reduces the experimental errors involved in that only a single sample is used.

It is shown, by both TOPEM and ADSC, that the use of the mobility factor leads only to an approximation to the experimental cure rate during vitrification. This is attributed to the fact that the mobility factor is frequency-dependent, as a result of the frequency dependence of the vitrification time, so that the predicted cure rate curve during vitrification also depends on the frequency, unlike the experimental curve which is frequency-independent.

An additional advantage of TOPEM over other TMDSC techniques is that the data analysis, which makes use of a parameter estimation method applied to the whole sample response, enables higher frequencies to be explored than is usually possible for TMDSC. From the exploration of these higher frequencies, it was observed that the dependence of vitrification time on the logarithm of frequency appears to show a slightly non-linear behaviour, with an upward curvature. A simulation has been made to model the reaction kinetics of a thermoset in which vitrification intervenes, and in particular to examine the dependence of the dynamic vitrification time on the frequency of the measurement. These simulations have shown that at low frequencies, in the range typically accessed by temperature modulated DSC, there is a non-linear dependence of $t_v$ on $\log(f)$, with an upward curvature, while at much higher frequencies, within the range accessed by dielectric analysis, a limiting linear dependence is approached. Both of these behaviours are observed experimentally,
98

and hence the simulations provide a good description of the dynamic vitrification behaviour in the isothermal curing of thermosets. Furthermore, this work shows clearly that the dynamic vitrification should not be confused with the change in cure kinetics from one controlled by the chemical reaction rate to one controlled by diffusion, which is what defines the onset of vitrification. Dynamic vitrification reflects the transition from a liquid-like response to a glassy response, which depends on the frequency in much the same way as does the glass transition of a non-reacting system. Finally, the close similarity of the results of the simulation to experimental results obtained previously shows that, for this application, TOPEM is a reliable and useful method for exploring higher frequencies and with greater precision than other TMDSC techniques.

# References

1. "Thermal Characterization of Polymeric Materials". Edited by Edith A. Turi. Academic Press, Inc. 1981.

2. A.T. DiBenedetto in L.E. Nielse; *J. Macromol. Sci. Rev. Macromol. Chem. C3*, **1969**, 69.

3. J. K. Gillham; *Polym. Eng. Sci. 26*, **1986**, 1429.

4. S. Montserrat; *J. Appl. Polym. Sci. 44*, **1992**, 545.

5. M. Cassettari, G. Salvetti, E. Tombari, S. Veronesi, and G.P. Johari; *J. Polym. Sci: Polym Phys. 31*, **1993**, 199.

6. G. Van Assche, A. Van Hemelrijck, H. Raier and B. Van Mele; *Thermochim. Acta 268*, **1995**, 121.

7. G. Van Assche, A. Van Hemelrijck, H. Raier and B. Van Mele; *Thermochim. Acta 304/305*, **1997**, 317.

8. S. Montserrat and I. Cima, *Thermochim. Acta 330*,**1999**, 189.

9. S. Montserrat and X. Pla; *Polym. Int. 53*, **2004**, 326.

10. S. Montserrat, Y. Calventus and J.M. Hutchinson; *Polymer 46*, **2005**, 12181.

11. S. Weyer, H. Huth and C. Schick; *Polymer 46*, **2005**, 12240.

12. J.E.K. Schawe, T. Hütter, C. Heitz, I. Alig and D. Lellinger; *Thermochim. Acta, 446*, **2006**, 147.

13. I. Fraga, S. Montserrat and J. M. Hutchinson; *J. Therm. Anal. Cal., 87*, **2007**, 119

14. M. R. Kamal; *Polym. Eng. Sci. 14*, **1974**, 231.

15. K. Horie, H. Hiura, M. Sawada, I. Mita and H. Kambe; *J. Polym. Sci. Part A-1, 8*, **1970**, 1357.

16. K.C. Cole, J.J. Hechler and D. Noël; *Macromolecules, 24*, **1991**, 3098.

17. E. Donth, *Relaxation and thermodynamics in polymers. Glass transition.* Akademie, 1992.

18. E. Donth, *The glass transition. Relaxation dynamics in liquids and disordered materials.* Springer, Berlin, 2001.

19. M.B.M. Mangion and G.P. Johari; *J. Polymer Sci. Polym. Phys., 28*, **1990**, 1621.

20. J. Fournier, G. Williams, C. Duch and G.A. Aldridge; *Macromolecules, 29*, **1996**, 7097.

**21.** S. Montserrat, F. Román and P. Colomer; *Polymer, 44,* **2003**, 101.

**22.** J. P. Pascault and R. J. J. Williams; *J. Polym. Sci: Polym. Phys., 28,* **1990**, 85.

**23.** M. L. Williams, R. F. Landel and J. D. Ferry; *J. Am. Chem. Soc., 77,* **1955**, 3701.

**24.** C. W. Wise, W. D. Cook, A. A. Goodwin; *Polymer, 38,* **1997**, 3251.

**25.** G. Wisanrakkit and J. K. Gillham; *J. Coatings. Tech., 62,* **1990**, 35.

**26.** Y. Meng and S. L. Simon; *Thermochim Acta, 437,* **2005**, 179.

**27.** F. C. A. E. Huguenin and M. T. Klein; *Ind. Eng. Chem. Prod. Res., 24,* **1985**, 166.

**28.** S. L. Simon and J. K. Gillham; *J. Appl. Polym. Sci., 47,* **1993**, 461.

**29.** Y. Deng and G. C. Martin, *Macromolecules, 27,* **1994**, 5141.

**30.** I. Havlicek and K. Dusek, in: "*Crosslinked epoxies*", B. Sedlacek, J. Kahovec, Eds., Walter de Gruyter, Berlin 1987, p. 417.

**31.** G. Adam and J. H. Gibbs; *J. Chem. Phys., 43,* **1965**, 139.

**32.** C-S. Chern and G. W. Poehlein ; *Polym. Eng. Sci., 27,* **1987**, 788.

**33.** E. Rabinowitch; *Trans. Faraday Soc., 33,* **1937**, 1225.

**34.** J. M. Hutchinson and S. Montserrat, *Thermochim. Acta 377,* **2001**, 63.

*35.* I. Fraga, S. Montserrat and J. M. Hutchinson; *J. Therm. Anal. Cal., 91,* **2008**, 687.

**36.** G. Van Assche, B. Van Mele and Y. Saruyama; *Thermochim Acta, 377,* **2001**, 125.

*37.* I. Alig, W. Jenninger and J. E. K. Schawe; *Thermochim. Acta, 330,* **1999**,167.

*38.* S. Montserrat and J. G. Martín ; *J. Appl. Polym. Sci., 85,* **2002**, 1263.

**39.** S. Montserrat and J. G. Martin; *Thermochim. Acta, 388,* **2002**, 343.

**40.** M. Smoluchowski; *Z. Phys. Chem., 93,* **1918**, 129.

# CHAPTER 5

# VITRIFICATION DURING THE NON-ISOTHERMAL CURE OF A THERMOSET

# 5.1. Introduction

## *5.1.1. Vitrification and devitrification*

As was explained in the previous chapter, during the cure of thermosetting resins, the glass transition temperature of the system, $T_g$, changes from its initial value, $T_{g0}$, namely that of the unreacted mixture, and increases with increasing degree of cure, $\alpha$. In a non-isothermal cure experiment, the cure temperature increases at a constant rate. If this rate is sufficiently high, the cure temperature is always higher than the $T_g$ of the reacting system, so the cross-linking reaction will proceed to its limit, $\alpha = 1$, and the final glass transition temperature will be that of the fully cured thermoset, $T_{g\infty}$. On the other hand, if the curing process takes place at a sufficiently slow heating rate, the $T_g$ of the reacting system can reach the instantaneous cure temperature, whereupon the system changes to a glassy state and vitrifies, analogous to the case of isothermal curing at sufficiently low cure temperatures [1, 2]. The subsequent process of devitrification occurs when the continually increasing cure temperature, $T_c$, again exceeds the $T_g$ of the vitrified system.

The vitrification and devitrification processes which occur during non-isothermal cure have been studied by temperature modulated differential scanning calorimetry (TMDSC) [3-6] and other dynamic techniques such as dielectric relaxation [7] and torsional braid analysis [8]. The advantage of these dynamic techniques is that they permit the observation of vitrification and devitrification in real time during the experiment, for example through the complex heat capacity in TMDSC. Nevertheless, a limitation of these TMDSC measurements is that they have until now been restricted to a single frequency in any one experiment, typically with a

period of 60 s. Since the underlying heating rate is slow, these experiments tend to be time-consuming, often requiring up to 10 hours, with the consequence that the effect of frequency has not been investigated. Accordingly, it is interesting to use TOPEM to study, by a temperature modulated calorimetric technique, the frequency dependence of the vitrification and devitrification processes during the non-isothermal cure of an epoxy-diamine system.

In the first part of this study, TOPEM is used to investigate these processes experimentally. In the second part, similar to the procedure applied in the isothermal case explained in the previous chapter, a simulation was used to obtain the vitrification and devitrification times as a function of frequency in a theoretical way, in order to compare simulated and experimental results.

## 5.2. Calorimetric Study

### 5.2.1. Materials

The system studied was the same as in the previous chapter: the epoxy resin was a diglycidyl ether of bisphenol-A (DGEBA), Epon 828 (Shell Chemicals), and the cross-linking agent was a polyoxypropylene diamine, Jeffamine D-230 (Huntsman Corporation). Stoichiometric mixtures of resin and diamine were prepared immediately prior to each experiment and samples of suitable mass, around 25 mg, were weighed and sealed into aluminium crucibles of 40 µl and with a hole in the lid.

### 5.2.2. Experimental

The same Mettler-Toledo 823$^e$ calorimeter with an intracooler was used for the experiments. Non-isothermal scans between 25 ºC and a final temperature between 100 and 125 ºC, depending on the underlying heating rate, were made. As

is shown later, the devitrification time decreases with increasing heating rate; for this reason, the final temperature for the faster heating rates can be selected to be lower. In some of the experiments, this reduction in the final temperature of the scan was made simply to save time; for example, for a heating rate of 0.05 K/min a difference of only 5 ºC corresponds to 100 min more of experimental time but without any additional information about devitrification. The underlying heating rates selected were 0.05, 0.032, 0.025, 0.019 and 0.015 K/min, which are sufficiently slow to observe the vitrification and devitrification processes clearly separated. For comparison, a velocity of 0.1 K/min was also investigated, and no vitrification was observed. For all the experiments, a temperature amplitude of the pulses of 0.1 K was selected, with the switching time range being from 15 s to 30 s.

In view of the fact that the previous studies have shown that the results obtained by ADSC and TOPEM are comparable, and since non-isothermal cure makes use of such small heating rates and  results in very long runs, no comparison was made here between ADSC and TOPEM, as was the case in the previous chapters. Consequently, only TOPEM was used for the modulated calorimetric measurements. Nevertheless, conventional non-isothermal DSC scans were also made in order to investigate the partial cure of the samples in respect of their glass transition temperature and the degree of cure reached at vitrification. The heating rates selected were the same as for the TOPEM experiments, namely between 0.05 and 0.015 K/min, and the temperature ranges for the scans were from 25ºC to the temperature of vitrification, this last being different for each heating rate and having been identified from the previous TOPEM experiments. Second scans were made in all cases in order to determine the residual heat of reaction, from which the degree of cure at vitrification is found, and the glass transition temperature of the samples at vitrification. Third scans, again using conventional DSC, were also made to determine the glass transition temperature of the fully cured samples.

105

### *5.2.3. Data Analysis*

A typical result for a non-isothermal cure using TOPEM is shown in Figure 5.1. The figure shows the on-line measured heat flow response of a sample to a scan with stochastic temperature pulses superimposed on the underlying heating rate.
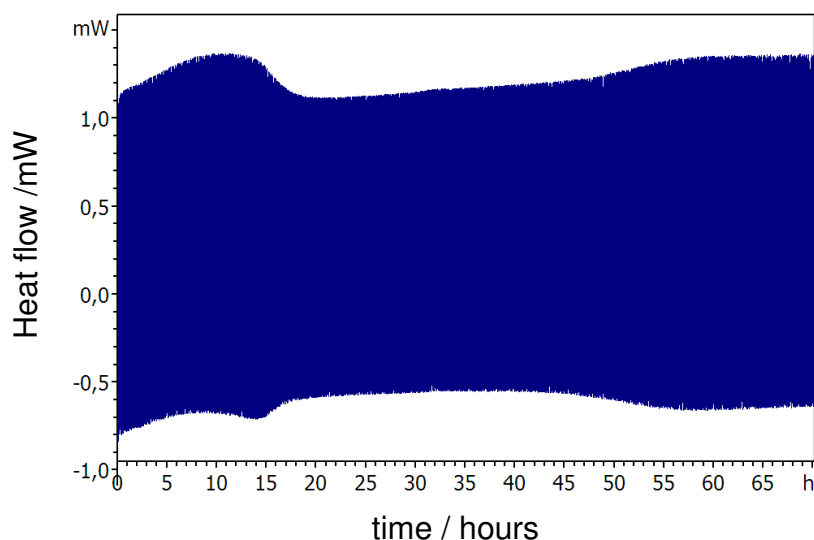


Figure 5.1. Heat flow response as a function of temperature for a TOPEM experiment from 25ºC to 100ºC at 0.019 K min$^{-1}$, with a temperature amplitude of 0.1 K and switching time range of 15 s to 30 s. The exothermic direction is upwards

Because of the very large number of pulses (more than 12000) in the total scan, the individual pulses cannot be seen in this Figure, only the envelope of the response. From this envelope one can identify the heat flow due to the exothermic reaction as the rising and then falling region in which the amplitude is rather constant, up to about 800 min, followed immediately by the vitrification process, observed as a rather abrupt reduction in the amplitude, corresponding to a reduction of the specific heat capacity. At higher temperatures, there is a much more gradual increase in the amplitude, resulting from the devitrification process, where the specific heat capacity increases again.

106

From this response, the quasi-static specific heat capacity, $c_{p0}$, can be calculated, and is shown in Figure 5.2. From the $c_{p0}$ curve, the frequency dependent specific heat capacities, $c_p(f)$, at selected frequencies ($f$) are calculated. This requires the selection, by the user, of the asymptotes to the vitrification and devitrification processes, each process being treated separately as shown in Figure 5.2, as well as of the frequencies for the determination of $c_p(f)$ [9]. The different curves for $c_p(f)$ at the selected frequencies are also shown in the same figure.
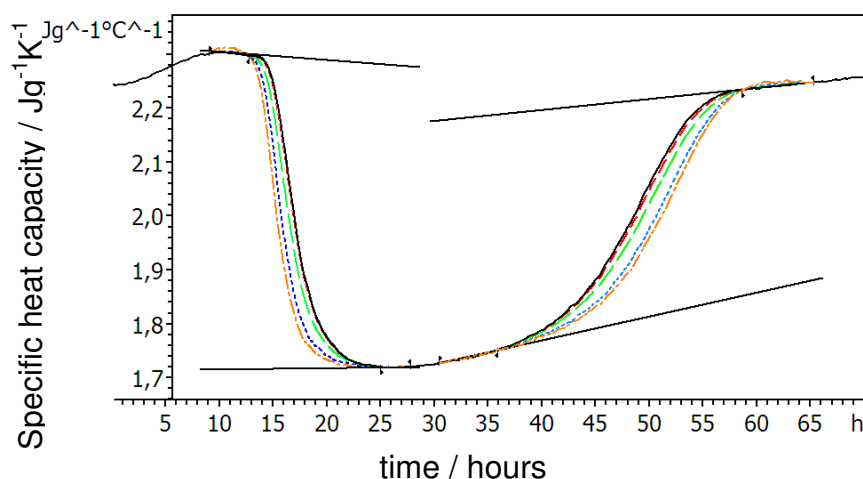


Figure 5.2. Specific heat capacity as function of temperature for selected frequencies indicated: quasi-static specific heat capacity $c_{p0}$ (black, continuous), 8 mHz (red, short dash), 16 mHz (green, long dash), 32 mHz (blue, dotted) and 64 mHz (orange, dash-dotted)

The heating rate in this experiment is 0.019 K/min, sufficiently small to identify both vitrification and devitrification processes clearly separated. The vitrification can be observed in the first rather abrupt change (reduction) of the specific heat capacity, while the devitrification is observed in the second, less abrupt, change in which the specific heat capacity increases. A similar behaviour was found for all the heating rates used. The vitrification and devitrification times are taken as the times at which the specific heat capacity has a value midway between the two relevant asymptotes. The dependence on frequency of the times for vitrification and

107

devitrification can be seen from the separation of the curves in Figure 5.2, where it is interesting to observe that the effects are opposite: with increasing frequency, the vitrification time decreases whereas the devitrification time increases. It can also be seen that such small heating rates result in very time-consuming experiments: 70 h in this case. Around 390 hours were needed to complete all the experiments for this study. By comparison, with ADSC at least 3200 hours would be necessary to include 5 frequencies and the corresponding blank runs for the same five underlying heating rates.

### *5.2.4. Results and Discussion*

Figure 5.3 shows the behaviour of the quasi-static specific heat capacity, $c_{p0}$, as a function of both time and temperature for each of the underlying heating rates. The frequency dependent heat capacities for different frequencies are not represented here for reasons of clarity, but similar results as in Figure 5.2 could be obtained.
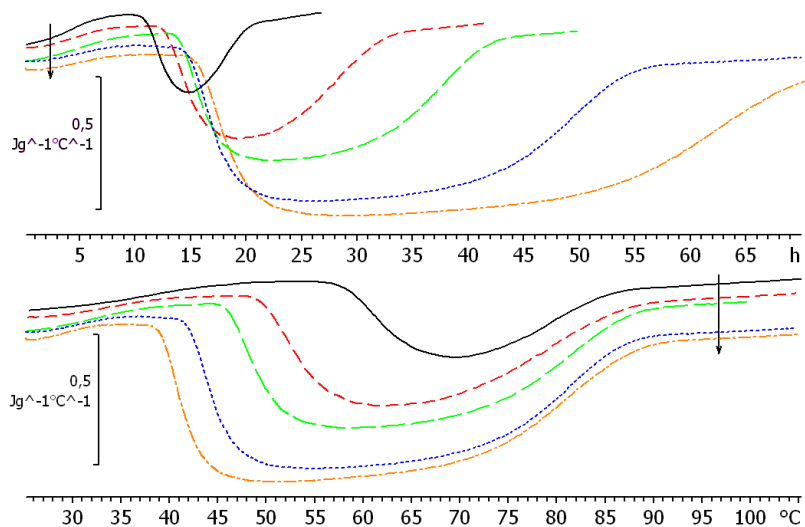


Figure 5.3. Quasi-static specific heat capacity, $c_{p0}$, as a function of time (upper) and temperature (lower) for each of the underlying heating rates used: 0.05 (black, full line), 0.032 (red, short dash), 0.025 (green, long dash), 0.019 (blue, dotted) and 0.015 K/min (orange, dash dotted). The arrows show the direction of decreasing heating rate.

It can be seen that for slower heating rates the two transitions appear more separated. It can also be clearly seen that the increment in specific heat capacity at vitrification, $\Delta c_{p,vit}$, increases as the heating rate decreases. According to the inverse relationship [10] between $\Delta c_p$ and degree of cure, $\alpha$, the effect of decreasing the underlying heating rate should be to result in a decrease in the degree of cure at vitrification, $\alpha_{vit}$. The degree of cure at vitrification for each underlying heating rate is obtained from:

$$\alpha = \frac{\Delta H_v}{\Delta H_{total}} \tag{5.1}$$

where $\Delta H_v$ is the heat of reaction evolved up to vitrification and $\Delta H_{total}$ is the total heat of reaction corresponding to the complete process of cure. These heats of reaction are determined from two conventional DSC scans: the first scan at the same heating rates as those selected for TOPEM measurements and from 25 ºC up to the temperature at which the system vitrified, this temperature previously having been obtained by TOPEM; the second DSC scan of the vitrified samples is made to measure the residual heat of curing, and is made from 25 to 250 ºC at the same heating rate of 20 K/min for all the samples, having previously cooled the sample at a controlled rate after the first scan, and without removing the sample from the furnace. $\Delta H_v$ is calculated from the first DSC scan, while $\Delta H_{total}$ is the sum of $\Delta H_v$ and the residual heat obtained in the second DSC scan.

The results obtained for both $\Delta c_{p,vit}$ and $\alpha_{vit}$ are shown in Table 5.1. Although an inverse relationship between $\Delta c_{p,vit}$ and $\alpha_{vit}$ is apparently followed here, a closer inspection reveals that the situation is more complicated. In particular, given that $\Delta c_p$ for the fully cured resin, obtained as an average following second and third scans after partial curing until vitrification at each of the underlying heating rates, is 0.484 $\pm$ 0.010 J/gK, there is an inconsistency in that several of the values of $\Delta c_{p,vit}$ in Table

109

5.1, which apply to partially cured resins, are less than this value for the fully cured resin. The explanation of this, as pointed out earlier by Van Mele and co-workers [3,4] who analysed the vitrification and devitrification processes by means of the diffusion factor concept, is that the vitrification is only partial, and particularly so for the higher heating rates. This can clearly be seen by a comparison of the $\Delta c_{p,vit}$ values from TOPEM in Table 5.1 with those obtained from the second scans by conventional DSC of the partially cured resins: for example, for heating rates of 0.05, 0.032 and 0.015 K/min, these latter values are 0.580, 0.615 and 0.624 J/gK, respectively. Thus complete vitrification does not occur, except possibly for the slowest heating rate used here (0.015 K/min), for which there is only a small difference between the $\Delta c_{p,vit}$ values obtained by TOPEM (0.601 J/gK) and by DSC (0.624 J/gK). This difference is likely to arise from the DSC value being obtained after curing only to the mid-point of the $\Delta c_p$ step (vitrification time), where the degree of cure is slightly less than at the end of the step, implying a slightly higher value of $\Delta c_p$. Furthermore, the wide separation of the vitrification and devitrification processes in Figure 5.3 for this heating rate, and the establishment of an apparently glassy baseline between them, would lead one to believe that the vitrification was complete in this case.

| underlying heating rate K/min | $\Delta c_{p,vit}$ J/gK | $\alpha_{vit}$ |
|---|---|---|
| 0.05 | 0.287 | 0.870 |
| 0.032 | 0.428 | 0.788 |
| 0.025 | 0.482 | 0.734 |
| 0.019 | 0.565 | 0.682 |
| 0.015 | 0.601 | 0.626 |

Table 5.1.  Specific heat capacity increment, $\Delta c_{p,vit}$, and degree of cure, $\alpha_{vit}$, at vitrification for each underlying heating rate.

The vitrification and devitrification times and temperatures are determined from the two sigmoidal changes observed in the curves of the specific heat capacities for each frequency. The frequency dependence of the vitrification temperature is shown in Figure 5.4, where it can be seen that it decreases with increasing frequency and that, as can also be seen in Figure 5.3, the system vitrifies at higher temperature the higher is the underlying heating rate.
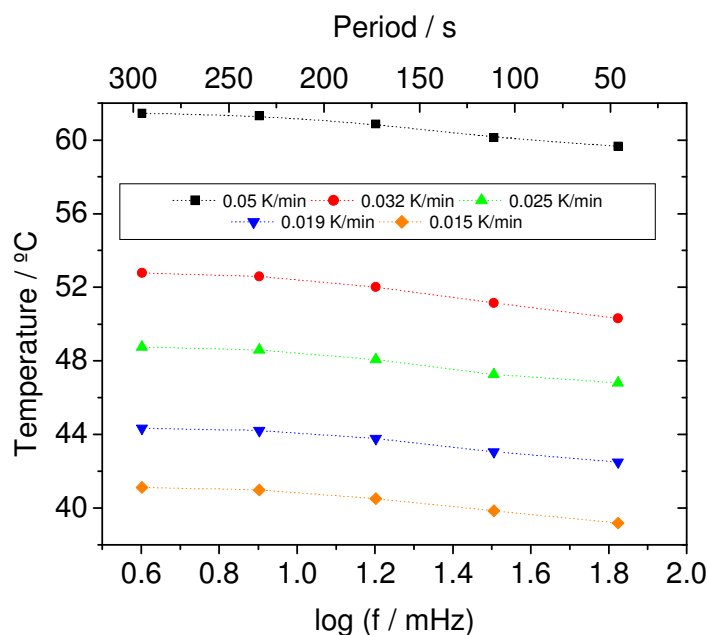


Figure 5.4. The points represent the vitrification temperature as a function of frequency, on a logarithmic scale, obtained from TOPEM experiments with underlying heating rates from 0.05 K/min to 0.015 K/min, as indicated. Dotted lines are only a guide for the eye.

In Figure 5.5, it can be observed that the vitrification time also decreases with increasing frequency and, as in the case of isothermal cure of the same system, [2] observed in the previous chapter, there is again a non-linear relationship between vitrification time and the logarithm of frequency.

111
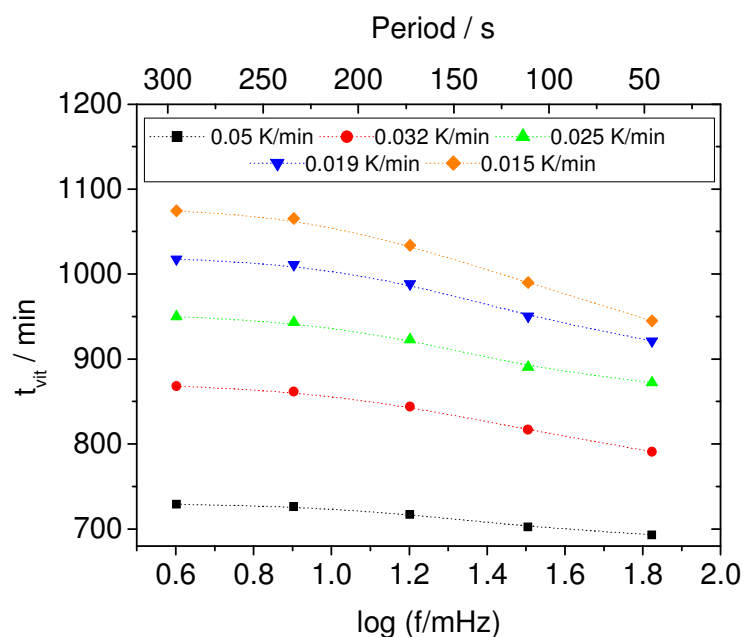
Figure 5.5. Points represent the vitrification time versus frequency, on a logarithmic scale, obtained from TOPEM experiments with underlying heating rates from 0.05 K/min to 0.015 K/min, as indicated. Dotted lines are only a guide to the eye.

In contrast to the vitrification temperature, though, the system vitrifies at shorter times the higher is the underlying heating rate, an effect seen also in Figure 5.3.

In the case of the devitrification process, as shown in Figure 5.6, the dependence of the devitrification time on frequency is the opposite of that found for vitrification, in that the devitrification time increases with increasing frequency. The dependence of the devitrification time on frequency is also less pronounced than in the case of vitrification, while, as can be seen in Figure 5.3, the devitrification temperature is almost independent of the underlying heating rate. For that reason these results are not presented here.
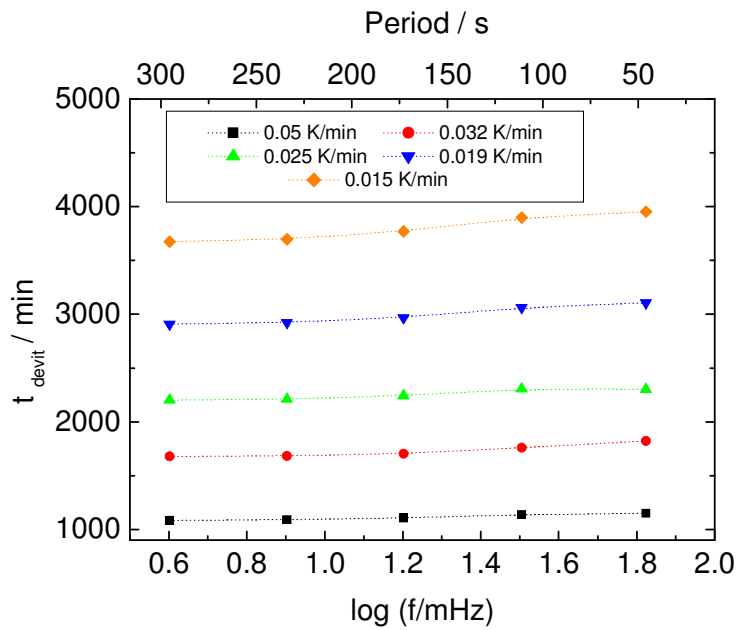
Figure 5.6. The points represent the devitrification time as a function of frequency, on a logarithmic scale, obtained from TOPEM experiments with underlying heating rates from 0.05 K/min to 0.015 K/min, as indicated. Dotted lines are only a guide for the eye.

With the results obtained from TOPEM experiments for the vitrification and devitrification times, a Continuous Heating Transformation (CHT) diagram, analogous to the TTT (Time Temperature Transformation) diagram in the isothermal case, can be constructed [5-8], and is shown in Figure 5.7. In this diagram, the vitrification and devitrification times for five selected frequencies have been included: 4.33 mHz, 8.33 mHz, 16.67mHz, 33.33mHz and 66.66 mHz. The underlying heating rates for the non-isothermal cures and the glass transition temperature of the fully cured system, obtained from second scans, are also shown. From this diagram one can obtain information about the vitrification and devitrification regions, and their dependence on time, heating rate and frequency.

113
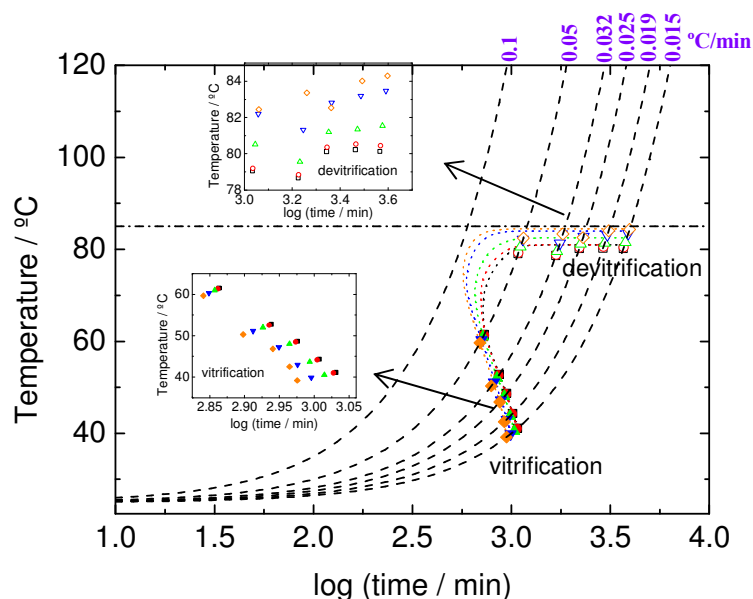
**Fi**gure 5.7. Continuous Heating Transformation (CHT) cure diagram for the system. The experimental points indicate vitrification (filled points) and devitrification (unfilled points) times, the dashed lines show the underlying heating rates as indicated, and the dash-dotted line represents the glass transition temperature of the fully cured system. The insets give an enlarged view of the vitrification and devitrification processes. Dotted lines are only a guide for the eye. The frequencies selected are: 4.33 (black squares), 8.33 (red circles), 16.67 (green triangles), 33.33 (blue inverted triangles) and 66.66 mHz (orange diamonds).

## 5.3. Simulation

### 5.3.1. Theory and Simulation

MATLAB version 7.0 was used to simulate the non-isothermal cure reaction, taking into account similar considerations as for the isothermal case [11] explained in the previous chapter. For this reason the complete theory for the simulation is not repeated here. The same equations as in the previous chapter, section 4.3.2, are used again:

- the DiBenedetto equation for the relation between the degree of cure and the glass transition temperature [13, 17];
- the Kamal equation for the reaction without vitrification [12];

114

- an Arrhenius temperature dependence for the rate constants [13];
- a WLF dependence for the rate constant for diffusion [14,15];
- the Rabinowitch equation for the combination of chemical and diffusion rate constants [16].

Vitrification is the process, characterised by a vitrification time or temperature, which occurs when the curing reaction cannot continue at the chemically controlled rate because the controlling factor becomes the rate of diffusion of the reacting species. The change from a chemically controlled rate to a diffusion controlled rate is equivalent to a transition to a glassy state, and consequently vitrification is considered to occur here when $T_g$ reaches the cure temperature, $T_c$, which is continually increasing according to the underlying heating rate. The equivalence of $T_g$ and $T_c$ was the standard method of investigating vitrification by DSC before the introduction of TMDSC [1]. The rate of cure dramatically slows down at vitrification, being dominated now by the diffusion rate constant, but does not stop completely. The cure continues, albeit rather slowly, and when $T_g$ once again reaches the continuously increasing cure temperature, devitrification takes place.

Although the usual experimental evaluation of the vitrification time in TMDSC, and of the vitrification and devitrification times by TOPEM here, is from the mid-point of the sigmoidal change in the frequency dependent heat capacity, in these simulations it is evaluated as the time at which the dynamic (frequency dependent) glass transition temperature is equal to the cure temperature, equivalent to the definition of the vitrification time determined by conventional DSC [1]. For these purposes, the same procedure is adopted here as was previously used for the earlier study of isothermal vitrification [11] in order to simplify the analysis. This procedure is based on the fact that it is the equivalence of $T_g$ and $T_c$ which is used to define vitrification, and that in reality it is $T_g$ which has the frequency dependence,

115

increasing with increasing frequency. However, the condition $T_g = T_c$ would be reached in the same way if $T_g$ were considered to be independent of frequency and a frequency dependence were instead attributed to $T_c$, but such that it decreased with increasing frequency. Hence, in the present analysis, the frequency dependence is assigned to the cure temperature which, in addition to increasing with time following the underlying heating rate, also decreases with increasing frequency. Thus the dynamic vitrification time occurs when $T_g = T_c(f)$ , where $T_c(f)$ is the frequency dependent cure temperature, given by:

$$\ln\left(\frac{f}{f_r}\right) = \frac{E_f}{R}\left(\frac{1}{T_c(f)} - \frac{1}{T_c(t)}\right)$$

(5.2)

In this equation, $E_f$ is the activation energy controlling the frequency dependence of $T_c$, and $f_r$ is a reference frequency for which the dynamic cure temperature, $T_c(f)$, is considered to be equal to the cure temperature, $T_c$, which depends on time according to the underlying heating rate. Since the vitrification time determined by conventional DSC makes use of a glass transition temperature determined on heating after, typically, previously cooling freely [1], the correspondence between cooling rate and frequency [18,19] can be used to assign a value of 1/60 s$^{-1}$ for the reference frequency. The effect of various values of the activation energy, $E_f$, is also investigated in the simulation.

Figure 5.8 shows a typical example of how the glass transition temperature varies throughout the cure process, including vitrification and devitrification, as modelled by these simulations. The dotted line represents the variation in the glass transition temperature which occurs during cure with vitrification and subsequent devitrification, whereas the dashed line shows the hypothetical variation that would occur in the absence of vitrification. The first intersection of the curve for the

116

changing glass transition temperature (dotted line) with the cure temperature (full line) for any frequency represents the vitrification point for that frequency, while the second intersection of the same curve represents the devitrification point for the same frequency. The parallel lines correspond to frequencies of 3.16, 16.7 and 100 mHz. For the reasons stated above, the intersection with the line for 16.7 mHz defines the vitrification and devitrification times equivalent to those which would be obtained by conventional DSC.
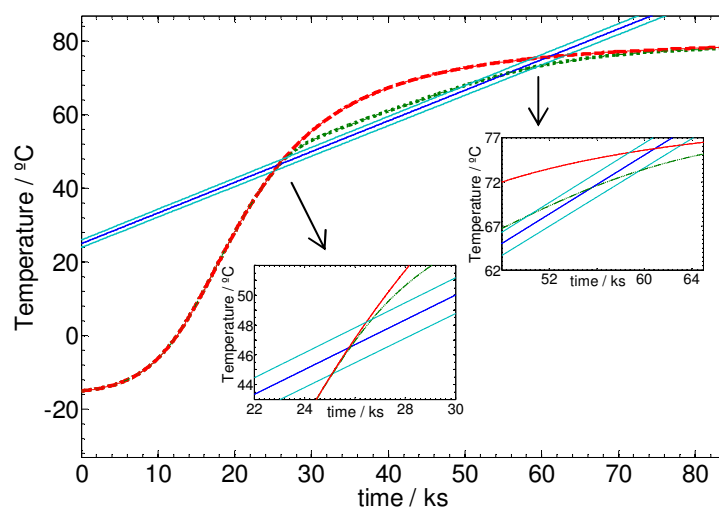


Figure 5.8. Increase of $T_g$ with time during a non-isothermal cure with an underlying heating rate of 0.05 K/min for a system with $T_{g0}$=258 K and $T_{g\infty}$=353 K in the absence of vitrification (red dashed line) and when vitrification and devitrification intervene (green dotted line). The parallel lines indicate the time dependence of the cure temperature for different frequencies: the central line for the reference frequency ($1/60$ s$^{-1}$ $\leftrightarrow$16.67 mHz), the upper line for a frequency of 3.16 mHz, the lower line for a frequency of 100 mHz. The two intersections of the cure temperature lines with the $T_g$ curve define the vitrification (first) and devitrification (second) points, which can be seen more clearly in the insets. Other parameter values for the simulation are: $m$=0.9, $n$=2, $E_f/R$=150 kK and $\lambda$=0.66.

The values of the constants used in these simulations are summarized in Table 5.2. Also shown are the ranges of parameter values investigated, namely the underlying heating rate, $q$, the reaction orders, $m$ and $n$, in the Kamal equation, the parameter $\lambda$

117

of the DiBenedetto equation, and the reduced activation energy, $E_f/R$, in Equation (1). In any one calculation, a set of parameter values is chosen. For all the results presented here, the set of values is always indicated, but in respect of trends the results shown are typical of a very large range of combinations of parameter values used in this investigation. It is only for those calculations where a fit of the model is made to the experimental data that the actual values of the parameters are important.

| Constant | Value [ref.] and equation where used |
|---|---|
| $A_1$ (s$^{-1}$) | $10^{3.6}$ [15]   Arrhenius Equation |
| $E_{c1}$ (kJ mol$^{-1}$) | 51.8 [15]   Arrhenius Equation |
| $A_2$ (s$^{-1}$) | $10^{3.4}$ [15]   Arrhenius Equation |
| $E_{c2}$ (kJ·mol$^{-1}$) | 41.5 [15]   Arrhenius Equation |
| $k_{dg}$ (s$^{-1}$) | 0.0051 [11]   WLF Equation |
| $C_1$ | 40.2 [14]   WLF Equation |
| $C_2$ (K) | 51.6 [14]   WLF Equation |
| $T_{g0}$ (ºC) | -15   DiBenedetto Equation |
| $T_{g\infty}$ (ºC) | 80   DiBenedetto Equation |
| **Parameter** | **Values** |
| $q$ (K min$^{-1}$) | 0.05  0.032  0.025  0.019  0.015 0.012 |
| $m$ | 0  0.4  0.9  0.98  1  1.24  2 |
| $n$ | 0  1  1.12  1.43  1.5  1.6  1.7  2 |
| $\lambda$ | 0.1  0.15  0.33  0.5  0.66  1 |
| $E_f/R$ (kK) | 25  50  75  110  100  120  150 |

Table 5.2. Constants and ranges of parameter values used in the simulations

118

### *5.3.2. Results of Simulation*

Typical results for the dependence of the vitrification temperatures and the devitrification times on log($f$) for different underlying heating rates are shown in Figures 5.9 and 5.10, respectively, for frequencies from 1 mHz to $10^5$ Hz. The regions of these graphs which correspond to the TOPEM experiments are at the extreme left, for log($f$/mHz) in the range 0.5 to 2.0, approximately. The region at higher frequencies would correspond to other types of dynamic experiment which operate over a higher frequency range, such as dynamic mechanical analysis (up to about $10^3$ Hz) and dielectric analysis.
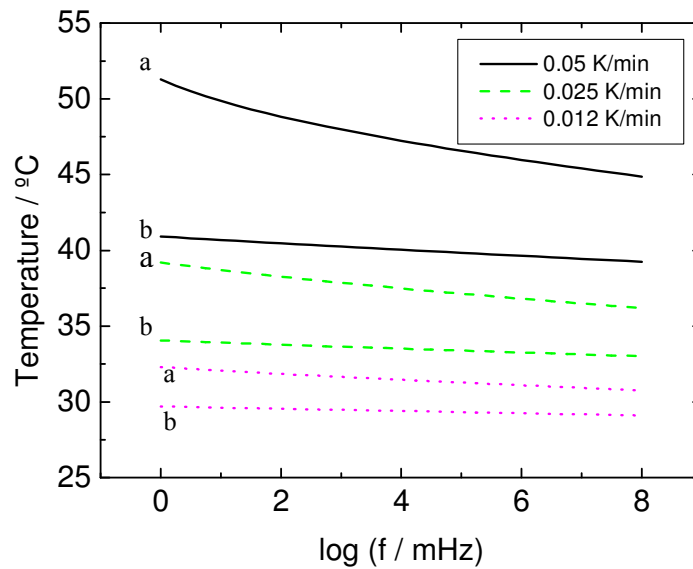


Figure 5.9. Frequency dependence of the vitrification temperature for three different underlying heating rates: 0.05 (black continuous lines), 0.025 (green dashed lines) and 0.012 (lilac dotted lines) K/min. The parameter values for the different simulations are: $m$=0.9, $n$=1.7, $E_f/R$=120 kK, $\lambda$=0.33 (upper curves, a); $m$=0.98, $n$=1.12, $E_f/R$=150 kK, $\lambda$=1 (lower curves, b).

It can be seen from Figure 5.9 that, in respect of the vitrification temperature, there is a noticeable dependence on the kinetic parameters ($m$, $n$, $\lambda$, $E_f/R$), though the general trend of a rather linear decrease of the vitrification temperature with increasing frequency is always present. In this case, the effect of changing parameter values is principally a displacement of the curves on the temperature scale, with a slight change of slope and, for the fastest underlying heating rate, the introduction of some curvature at the lowest frequencies.
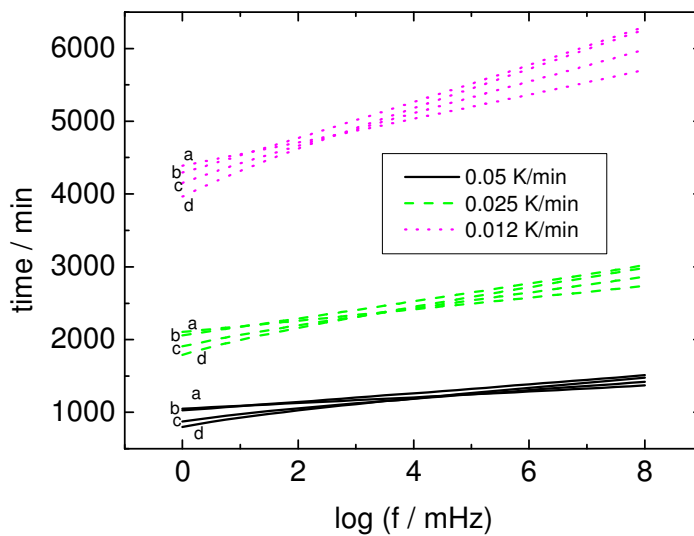


Figure 5.10. Frequency dependence of the devitrification time for three different underlying heating rates: 0.05 (black continuous lines), 0.025 (green dashed lines) and 0.012 (lilac dotted lines) K/min. The parameter values for the different simulations are: (a) $m$=0.98, $n$=1.12, $E_f/R$ =150 kK, $\lambda$=1; (b) $m$=1, $n$=1, $E_f/R$ =100 kK, $\lambda$=0.66; (c) $m$=0.9, $n$=1.7, $E_f/R$ =120 kK, $\lambda$=0.33; (d) $m$=1, $n$=2, $E_f/R$ =110 kK, $\lambda$=0.66.

In contrast, the results for the devitrification time shown in Figure 5.10 indicate that different values for the kinetic parameters have a much less significant effect on the devitrification time, which generally displays a rather linear increase with increasing frequency. The most significant deviation is the evidence of some curvature at the lowest frequencies, analogous to the deviation seen in this frequency range for the

120

vitrification temperature in Figure 5.9 for the fastest underlying heating rate. A detailed comparison of these simulations with the TOPEM experimental results is provided in the following section.

## 5.4. Comparison of Simulation with TOPEM Measurements

From the simulations, it is possible to obtain results very similar to those obtained by TOPEM by adjusting the parameter values appropriately. This can be seen in Figures 5.11 and 5.12, where the vitrification temperature and the devitrification time, respectively, are represented as a function of the frequency on a logarithmic scale, for both the simulated results and the experimental TOPEM data. It can be seen that there is a good correspondence between simulated and experimental results, in particular with the rather linear decrease in vitrification temperature and increase in devitrification time with increasing frequency being well represented.
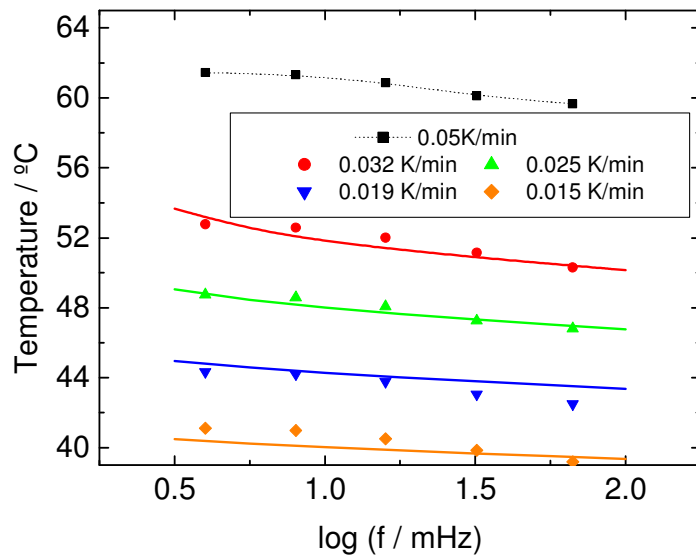


Figure 5.11. Vitrification temperature as a function of frequency, on a logarithmic scale, for underlying heating rates from 0.05 K/min to 0.015 K/min, as indicated. The full lines represent the model predictions using the following parameter values: $m$= 1.24, $n$=1.7, $\lambda$=0.15 and $E_t/R$ =150 kK. The points are the experimental results previously presented. The dotted line for the heating rate of 0.05 K/min is only a guide for the eye.

121

It will be noticed, though, that the parameter values ($m$, $n$, $\lambda$ and $E_f/R$) are different for the fit of the simulation to the experimental data in Figures 5.11 and 5.12. It has proved impossible to model precisely the vitrification and devitrification behaviours of both Figures with the same set of parameter values. In particular, the experimental data fall at longer devitrification times than are predicted by simulation making use of the parameter values obtained from the vitrification data, and the discrepancy becomes increasingly larger the slower is the underlying heating rate.
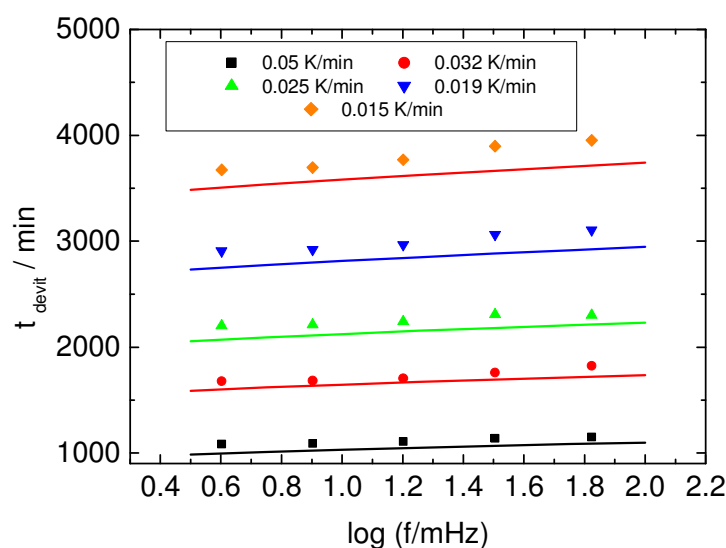


Figure 5.12. Devitrification time versus frequency, on a logarithmic scale, obtained for underlying heating rates from 0.05 K/min to 0.015 K/min, as indicated. The full lines represent the model predictions using the following parameter values: $m$=1, $n$=1.5, $\lambda$=0.5 and $E_f/R$ =150 kK. The points correspond to the experimental results previously presented.

An explanation for this may lie in a relaxation process taking place during the period between vitrification and devitrification. During this period in which the system is vitrified, it remains at a temperature just below the continuously changing $T_g$, which means that some structural relaxation will be taking place. The effect of this will be to increase the average relaxation time, with the result that the devitrification process

122

will be delayed until a higher temperature is reached. This is just the effect observed in trying to simulate the experimental results with parameter values taken from a fit to the vitrification process. Furthermore, the relaxation that takes place during the period between vitrification and devitrification will be greater the longer is this period, which occurs for slower underlying heating rates. The effect of this will be that the delay in the devitrification will be greater the slower is the underlying heating rate, which is again just what is observed in practice. As an illustration, the slowest heating rate used here experimentally was 0.015 K/min, for which this period between vitrification and devitrification lasts about 20 hours or more (see Figure 5.3), which is ample time for considerable structural relaxation to occur.

These relaxation effects could be included in a considerably more complex simulation, which would require the determination of how the average relaxation time increases during the period of vitrification. The approach would be to make use of the kind of model which describes rather well the typical glassy state relaxation behaviour of polymers, for example one which incorporates parameters to model the effects of non-exponentiality ($\beta$) and non-linearity ($x$) on the response [20-23], and to make use of the concept of fictive temperature, $T_f$, rather than $T_g$ for evaluating the changes in the relaxation time and in the rate constant for diffusion calculated by WLF Equation. Work on this aspect of the model is planned for the future.

## 5.5. Conclusions

The use of TOPEM in studying the vitrification and devitrification processes during the non-isothermal cure of thermosetting resins presents a significant advantage over other temperature modulated DSC techniques. A single experiment permits the evaluation of the dynamic vitrification and devitrification times and temperatures for a selected range of frequencies. This is an advantage compared

with other modulated calorimetric techniques, for which a similar study would not only be very time consuming but would also necessitate the preparation of a new sample for each frequency, thus introducing the possibility of additional experimental error. A simulation has been made to model the non-isothermal reaction kinetics of a thermoset in which vitrification and devitrification intervene, from which the theoretical dependence on frequency of the dynamic vitrification and devitrification times and temperatures has been established. A close correspondence between the results of the simulation and the experimental TOPEM data has been observed. Some apparent discrepancies in the devitrification times, particularly for the slowest heating rates, are attributed to relaxation effects occurring during the lengthy period during which the system remains in a vitrified state close to its glass transition temperature.

124

# References

1.  S. Montserrat ; *J. Appl. Polym. Sci. 44*, **1992**, 545.

2.  I. Fraga, S. Montserrat and J. M. Hutchinson; *J. Therm. Anal. Calorim. 91,* **2008**, 687.

3.  G. Van Assche, A. Van Hemelrijck, H. Rahier and B. Van Mele; *Thermochim. Acta 286,* **1996**, 209.

4.  G. Van Assche, A. Van Hemelrijck, H. Rahier and B. Van Mele; *Thermochim. Acta 304/305,* **1997**, 317.

5.  B. Van Mele, G. Van Assche and A. Van Hemelrijck; *J. Reinforced Plastics and Composites 18,* **1999**, 885.

6.  S. Montserrat and J. G. Martín; *Thermochim. Acta 388,* **2002**, 343.

7.  S. Montserrat, F. Roman and P. Colomer ; *J. Appl. Polym. Sci. 102,* **2006**, 558.

8.  G. Wisanrakkit and J. K. Gillham; *J. Appl. Polym. Sci. 42,* **1991**, 2453.

9.  I. Fraga, S. Montserrat and J. M. Hutchinson; *J. Therm. Anal. Calorim. 87,* **2007**, 119.

10. S. Montserrat; *Polyme*r, *36*, **1995**, 435.

11. I. Fraga. S. Montserrat and J. M. Hutchinson ; *Macromol. Chem. Phys. 209,* **2008,** 2003.

12. M. R. Kamal; *Polym. Eng. Sci. 14,* **1974**, 231.

13. J. P. Pascault and R. J. J. Williams; *J. Polym. Sci: Polym. Phys. 28,* **1990**, 85.

14. M. L. Williams, R. F. Landel and J. D. Ferry; *J. Am. Chem. Soc. 77,* **1955**, 3701.

15. C. W. Wise, W. D. Cook and A. A. Goodwin; *Polymer 38,* **1997**, 3251.

16. E. Rabinowitch; *Trans. Faraday Soc. 33,* **1937**, 1225.

17. A. T. DiBenedetto; *J. Polym. Sci: Polym. Phys. 25,* **1987**, 1949.

18. S. Montserrat, Y. Calventus and J. M. Hutchinson ; *Polymer 46,* **2005**, 12181.

19. J. M. Hutchinson and S. Montserrat; *Thermochim. Acta 377,* **2001**, 63.

20. J. M. Hutchinson ; *Prog. Polym. Sci. 20,* **1995,** 703.

21. S. Montserrat, G. Andreu, P. Cortés, Y. Calventus, P. Colomer and J. M. Hutchinson ; *J. Appl. Polym. Sci. 61,* **1996**, 1663.

22. P. Cortés, S. Montserrat and J. M. Hutchinson ; *J. Appl. Polym. Sci.63,* **1997**, 17.

23. Y. Calventus, S. Montserrat and J. M. Hutchinson; *Polymer 42,* **2001**, 7081.

# CHAPTER 6

# FUTURE STUDIES

## 6.1. Calorimetric Studies

### 6.1.1. Some preliminary results

#### 6.1.1.1. Crystallization and fusion in blends of PET/PEN

Crystallization and melting of PET, PEN and their blends have been studied by other workers by DSC [1-4] and TMDSC [5-6]. The influence of the modulation period on the values of the heat of fusion has been investigated, and the differences between the results obtained when they are analysed using the total heat flow or its reversing and non-reversing components have been examined and discussed [5].

In the study of crystallization and melting, the use of a positive instantaneous heating rate is recommended. The point is that if the modulated temperature programme includes some cooling, then the material can re-crystallise partially, forming crystals of a greater degree of order; the positive heating rate permits to avoid this extra crystallization. In the case of TOPEM, as is explained in detail in Appendix 1, the instantaneous heating rate is related with the pulse amplitude. The selection of an appropriate combination of pulse amplitude and underlying heating rate gives the desired positive instantaneous heating rate, even when the negative pulses are applied.

Some preliminary results for PET were obtained from TOPEM experiments with a heating rate of 2 K/min between temperatures of 25 and 290 ºC, an amplitude of the pulses of ± 0.05 K and a switching time range of 15-30 s, and can be observed in Figure 6.1. This combination of underlying heating rate and amplitude of the pulses ensures that the instantaneous heating rate remains positive at all times during the experiment (see Appendix 1).
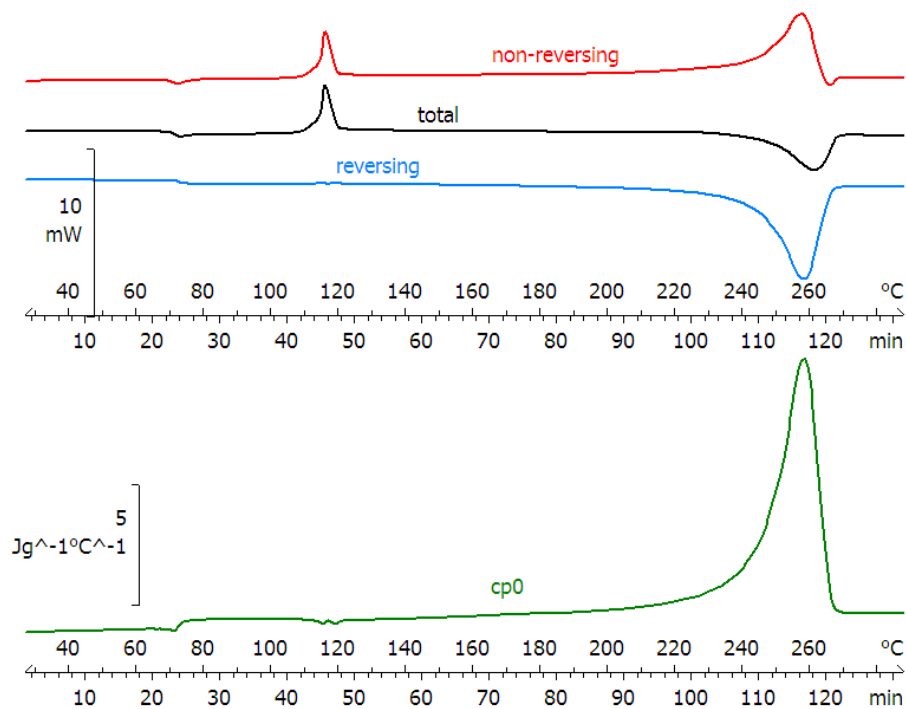
Figure 6.1. Heat flows (total, reversing and non-reversing; upper curves) and $c_{p0}$ (lower curve) that result from a TOPEM experiment with PET, from 25 to 290 ºC at 2K/min, amplitude of pulses ± 0.05 K and switching time range 15-30 s.

The total heat flow shows the glass transition around 70 ºC, followed by the cold crystallization transition at about 115ºC, which appears also in the non-reversing heat flow but not in the reversing component. This result agrees with previous ADSC results [4] in which the reversing heat flow in the cold crystallization region displays only a small oscillation, attributed to the Fourier Transform procedure and dependent on the number of modulation periods within the transition. Finally in the total heat flow trace, the melting peak appears in the temperature region around 220 to 270 ºC, also appearing in both the reversing and non-reversing components. As the melting processes depend on the heating rate, the enthalpy related depends on the modulation conditions imposed for each experiment.

In the case of a TOPEM evaluation, an in-depth study extended to PEN and the blends PET/PEN, in which the effects of changing the pulse parameters and the heating rates are investigated to see if any additional information to that obtained by ADSC [5] can be observed. The results obtained by these two techniques of ADSC and TOPEM will be compared. It is also interesting to study under what conditions (experimental and calculation parameters) the perturbation of the cold crystallization occurs in the quasi-static heat capacity and in the reversing component of the heat flow.

### *6.1.1.2. Humidity and $T_g$ in drugs*

The possible advantages of using TOPEM for the separation of two overlapping effects, such as the glass transition and the loss of humidity, can be investigated by means of a study of a hygroscopic pharmaceutical compound. For comparison, such studies on pharmaceutical compounds have previously been made by other modulated DSC techniques [7-11], while other types of materials, for example starch powders from maize, wheat and potato [12] have also been investigated.

In some preliminary experiments here, two different samples of the same drug were sealed in aluminium crucibles with initial masses of 6 and 11 mg. They were weighed before and after each experiment. Experiments in the range of temperatures from 20 to 100 ºC were run in the three different calorimetric modes available: standard DSC, ADSC and TOPEM. The loss of water that occurred during the experiments was confirmed by the difference in the weight of the samples before and after each experiment and also by thermo-gravimetric experiments.

For the case of Standard DSC, the experiments were performed with a heating rate of 10 K/min. Figure 6.2 shows the result of a Standard DSC experiment for both samples. In this figure, it is not possible to distinguish clearly either a glass

transition or a moisture peak, because both effects appear overlapped, thus making it impossible to determine the glass transition temperature.
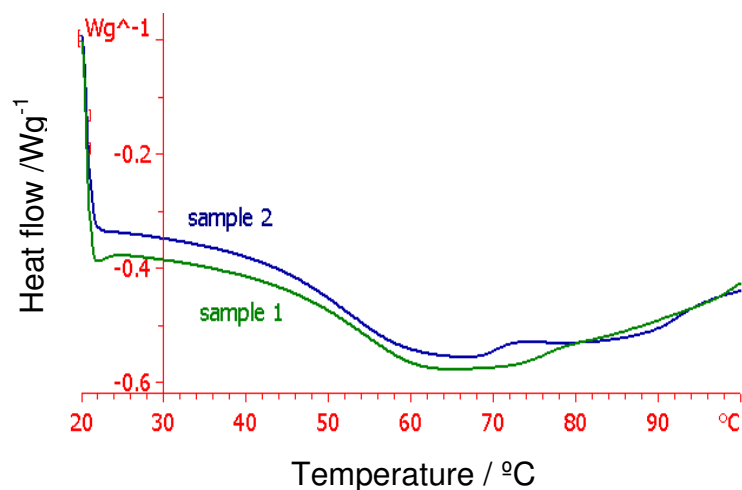


Figure 6.2 . Standard DSC scans of two different drug samples from 20 to 100 ºC at 10 K/min. The glass transition temperature does not appear clearly as it is overlapped by the moisture loss peak.

For ADSC, the velocities of scan were selected to be ± 2K/min, on heating and cooling, with a temperature amplitude of 0.5 K and a period of 60 s for the superimposed modulated signal. Figure 6.3 shows the results of an ADSC experiment for one of the samples (sample 2) after 24 h at ambient temperature: the upper graph shows the reversing and non-reversing components of the heat flow, while the lower graph shows the complex specific heat capacity. In the case of this modulated technique, it is clear that the reversing heat flow shows a glass transition around 71 ºC and the non-reversing heat flow shows a peak that can be attributed to the loss of water. The glass transition temperature was calculated from the complex specific heat capacity.

130
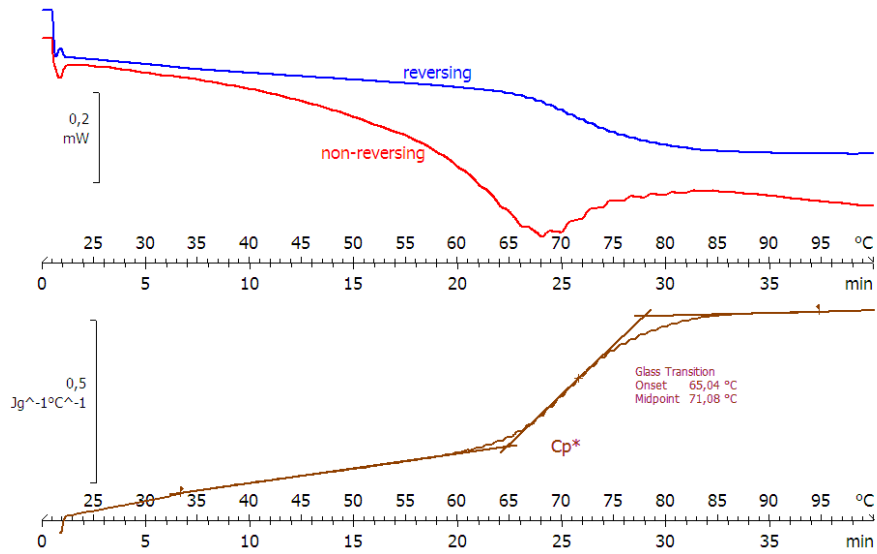
Figure 6.3. Heat flow components and complex heat capacity for an ADSC scan
from 20 to 100 ºC at 2 K/min, temperature amplitude of 0.5 K and a period of 60s.

In the case of experiments performed by TOPEM, velocities of scan of ± 0.5 K/min,
± 1 K/min and ± 2 K/min were chosen, on heating and cooling, with a temperature
amplitude of the pulses of 0.5 K and a switching time range of 15-30 s. Figure 6.4
shows the reversing and non-reversing heat flow components together with the
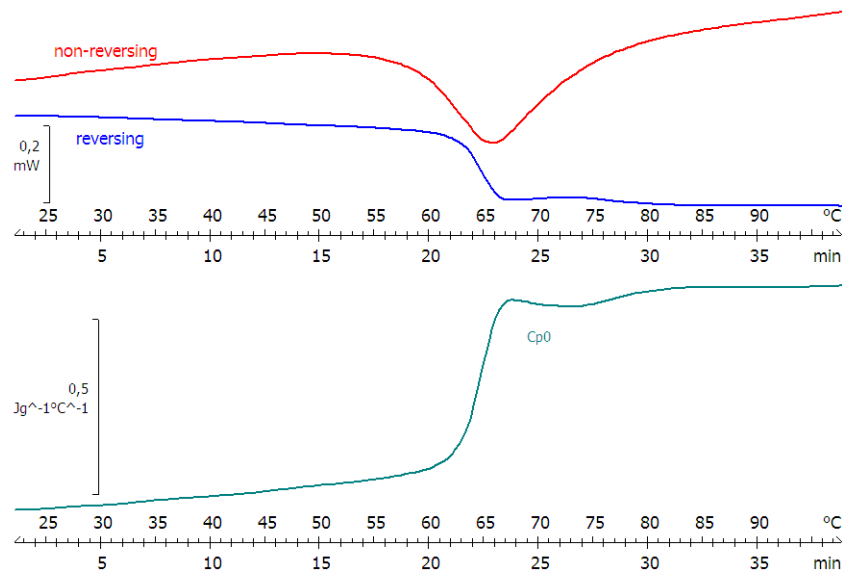


Figure 6.4. Reversing and non-reversing heat flow components (upper graph) and $c_{p0}$
(lower graph) for a TOPEM scan from 20 to 100 ºC at 2 K/min, pulse amplitude 0.5
K and switching time range 15-30 s

131

quasi-static specific heat capacity $c_{p0}$ for an experiment performed at 2 K/min, a pulse amplitude of 0.5K and a switching time range of 15-30 s. The same sample 2 was used after 2 months at ambient temperature.

In principle, as can be seen clearly, both modulated techniques (ADSC and TOPEM) present an advantage over standard DSC, in that they permit the separation of the overlapped phenomena of the glass transition and the moisture release. In this case, the advantage of TOPEM over ADSC would be that a frequency evaluation of the glass transition region could be made and also that only a single run is needed. Nevertheless, the interpretation of the results observed in these curves is not as easy as it seems. A closer examination of Figure 6.4 in the region from 72 to 85 ºC leads to the observation of an apparently weak second transition just after the glass transition. This behaviour was only observed with TOPEM, and not with ADSC, and only in the case of experiments performed on heating, not on cooling. This second weak glass transition appears only in the cases of storage at room temperature for months and it is also accompanied by a decrease in the glass transition temperature. It is not clear if this is an advantage of TOPEM over ADSC in detecting weaker transitions. There are other rather obvious differences; for example, in ADSC the glass transition appears at about 71ºC whereas in TOPEM it appears at about 65ºC. Also, the transition in TOPEM is much sharper than in ADSC, about 4ºC compared with about 15ºC. These differences can be related to the different storage times at room temperature which have a clear influence in the glass transition temperature. Posterior DSC scans show the same glass transition in both cases.

A complete study of the influence of the experimental parameters in the separation of these types of relaxations, the values of the integral of the moisture peak and the glass transition temperature under different conditions, and also the influence of the

132

storage of the samples at room temperature on the water content, will be investigated.

### 6.1.1.3. Crystallization and $T_g$ in PLA

Polylactide (PLA) is a hydrolysable aliphatic polyester that has been mainly used in surgical and biomedical applications [13-15] because of its high cost. Nowadays, new applications are investigated in order to use PLA as an economically viable biodegradable commodity polymer [16] using different ways to synthesize it.

In the present case, a preliminary study was made of a type of PLA that displays, in the same temperature range, a glass transition, an annealing peak and the beginning of the crystallization. Some other Temperature Modulated DSC studies have been made in similar materials [17].

The main problem in the use of standard DSC [18] with this material is that it is not possible to separate the three thermal events which appear overlapped, and thus is not possible to determine the initial degree of crystallinity of the samples, which is the parameter of interest.

Some preliminary experiments were performed by both ADSC and TOPEM in order to observe these overlapped phenomena and to determine the appropriate experimental parameters which permit their separation. The ADSC result for the heat flows and the complex heat capacity is shown in Figure 6.5 for an experiment from 50 to 90 ºC at 1K/min and a period of 60 s.

133
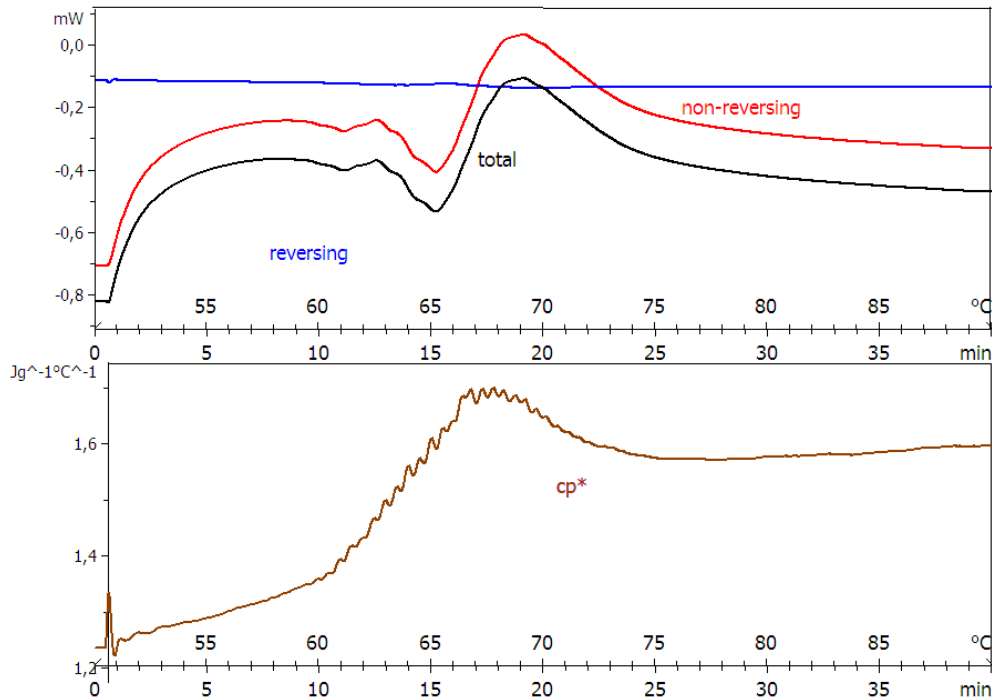
Figure 6.5. ADSC results for an experiment on PLA from 50 to 90 ºC at 1 K/min with a period of 60 s and a temperature amplitude of 0.5 K, showing the heat flow components (upper graph) and complex specific heat capacity (lower graph).

In Figure 6.5 can be observed the region of interest from 60 ºC up to approximately 75 ºC. The first endothermic peak observed around 65 ºC in the total heat flow and its non-reversing component can be associated with the annealing (due to the storage of the samples at room temperature for several months), while the exothermic peak that appears centred at 69 ºC can be related with crystallization processes. Both phenomena are overlapped to the glass transition region: in the complex heat capacity can be clearly observed the regions corresponding to the glassy (52 - 65 ºC) and the viscous (75 - 90 ºC) states. The region between these two states shows together the glass transition overlapped to the other two processes.

An additional observation from Figure 6.5 is the appearance of ripples in the complex heat capacity, which result from the Fourier Transform of periodic

modulations when the period of the heat flow is slightly different from the period of the heating rate, which occurs within a transition region. Since TOPEM does not use a periodic modulation, these ripples would not be expected to be seen.

The preliminary study using TOPEM gave similar results. The graphs for the reversing heat flow and for $c_{p0}$ obtained by TOPEM are shown in Figure 6.6 for different samples at different heating rates, as indicated. In all cases the pulse amplitude was 0.5 K and the switching time range was 15-30 s.
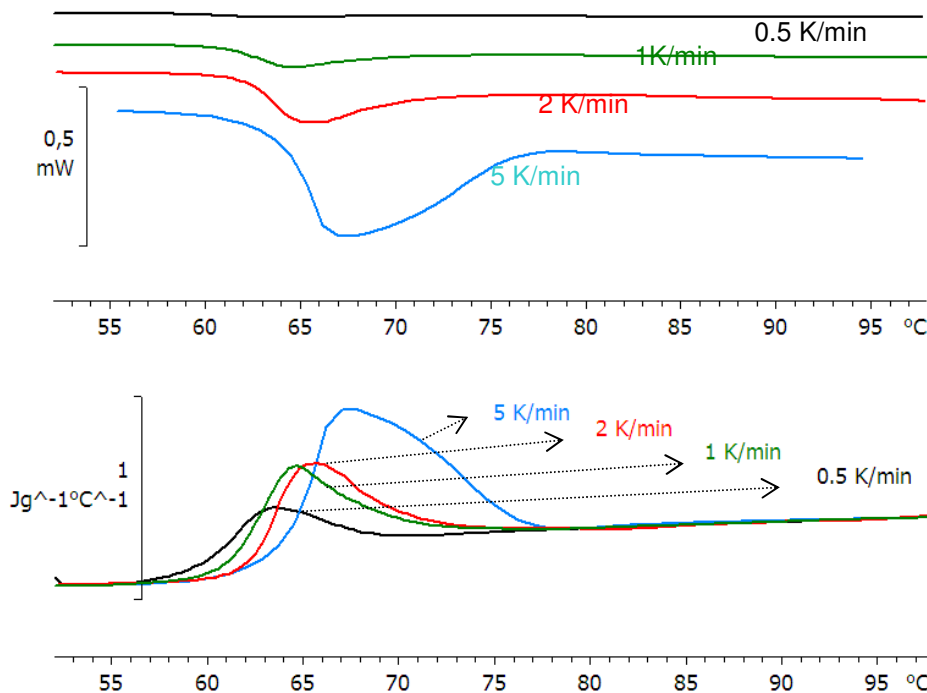


Figure 6.6 TOPEM results at different heating rates, as indicated, from 50 to 100 ºC, with a pulse amplitude of 0.5 K and a switching time range of 15-30 s. The upper graph shows the reversing heat flow components and the lower graph shows the quasi-static specific heat capacities.

It can be seen that a decrease of the heating rate results in a decrease in the peak observed in both the heat flow and $c_{P0}$, while the transition appears to be displaced to lower temperatures. Lower heating rates could lead to the separation of the

phenomena observed. Figure 6.7 show the results obtained for a TOPEM experiment in the same range of temperatures and with the same experimental parameters, the difference being in the heating rate selected to be 0.02 K/min. Although it is still not clear how to interpret the curve, a frequency evaluation of the quasi-static heat capacity leads to a displacement in the curves that is similar to those observed in other glass transitions such as, for example, the case of Polycarbonate previously shown in Chapter 3.
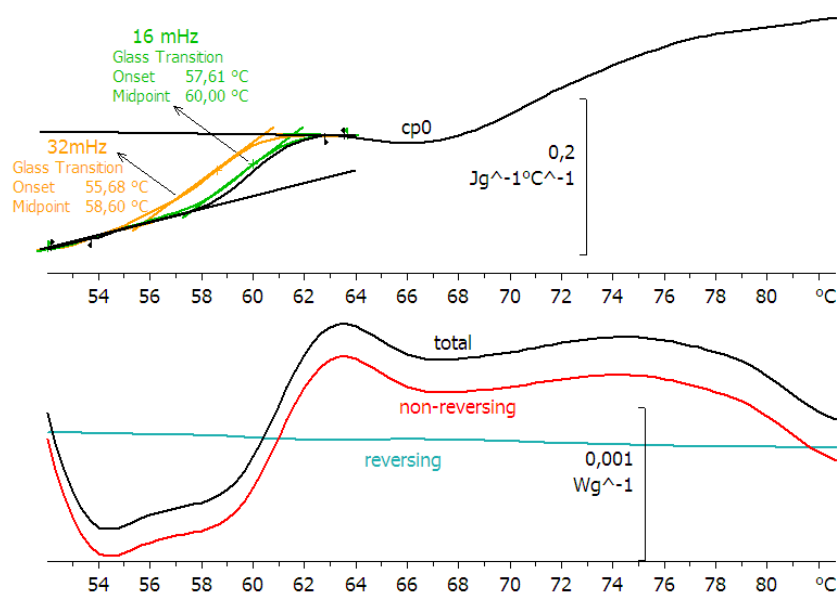


Figure 6.7. TOPEM results of PLA from 50 to 90ºC at 0.02K/min, pulses amplitude 0.5 K and switching time range 15-30 s. Frequency evaluation of the $c_{p0}$ (upper part), and heat flow components: mHz (green curve), 20 mHz (yellow curve) and heat flow curves (lower part): total (black), reversing (blue) and non-reversing (red).

With an appropriate combination of heating rates and experimental parameters it is expected to be able to separate the phenomena and to make a deeper study extended in temperatures to include the melting region with the purpose of obtaining the initial crystallinity of the samples.

The additional advantage observed by TOPEM is the possibility to study, in the same scan, the frequency dependence of the transition; if no frequency dependence is observed, it implies that it is not a glass transition and thus it can be derived that it has not been completely separated from other processes.

## 6.2. Modelling

### 6.2.1. Some questions about $C_{p0}$

Although some benefits of TOPEM have been identified through the examination of different transitions and using different materials, and its advantages over other modulated DSC techniques such as ADSC have been discussed, there are still several questions that remain unanswered with respect to the calculations made by the software, the interpretation of the heat flow components, or the reason why a limiting frequency appears in the frequency evaluation at about 4 mHz. But perhaps the most fundamental question regarding the TOPEM evaluation is what exactly does the quasi-static heat capacity, $C_{p0}$, represent. As was previously explained, theoretically it is a limiting heat capacity when the frequency is equal to zero. But, as was also explained, TOPEM shows a limit for low frequencies corresponding to approximately 4 mHz, so the theoretical limit of zero frequency is not really obtained experimentally. In practice, it is a mathematical tool which is used by the software to obtain the frequency response of the system (sample and instrument), but there remains the question of whether the theoretical assumption that $C_{p0}$ represents the zero frequency response has an adverse effect on the calculations of the frequency response.

Some preliminary results obtained for two different epoxy resins and their mixtures with a nanoclay have raised further questions about the information obtained with the software calculation and its physical interpretation. The epoxy resins selected are

a bi-functional resin based upon diglycidyl ether of bisphenol A (DGEBA), namely DER 331 (Dow Chemical Company) with a viscosity in the range 11,000 to 15,000 mPa.s and an epoxy equivalent of 182 to 192 g/eq., and a tri-functional resin based upon triglycidyl ether of para-aminophenol (TGAP), namely Araldite MY 0510 (Huntsman), with a viscosity of 550 to 850 mPa.s and an epoxy equivalent of 95 to 106 g/eq.

When the neat epoxy resins are heated through their corresponding glass transition regions (centred at about -15 ºC for the DGEBA and -45 ºC for the TGAP), a peak can be observed in the $c_{p0}$ curve and also in the reversing component of the heat flow, these peaks being independent of the heating rate and other experimental parameters. Similar results were observed for both epoxy resins, which have different density, epoxy equivalent and functionality, and which also have their glass transition temperature in different ranges. Both resins were also mixed, using various methods for the mixture (by hand, mechanically, by different ultrasonic treatments, and after prior dissolution in a solvent and subsequent removal of the solvent under vacuum) with 5 wt% of a nanoclay, an organically modified montmorillonite. The purpose of this was to investigate the response of these resin/clay mixtures in which some part of the resin is intercalated in the clay galleries, which are the nanometric separations of the clay layers, and hence experience a certain constraint which might be expected to influence the molecular mobility and hence the location and kinetics of the glass transition. However, it transpired that all the TOPEM experiments performed for these resin/clay mixtures show the same results as those obtained for the neat epoxy resins indicating that the nanometric spatial constraint did not in fact affect the molecular mobility. For this reason the complete study is not shown here. Nevertheless, some other aspects of the TOPEM results are worthy of further consideration.

A TOPEM experiment for one of the resins, the TGAP is shown in Figure 6.8. It can be seen that there is a peak in the $c_{p0}$ for the case of heating which does not appear in the case of cooling. This behaviour is not observed if other Temperature Modulated DSC techniques, such as IsoStep or ADSC, are used, and their corresponding heat capacities are obtained. Theoretically, a peak for the or complex $c_p$ or the in-phase $c_p$ is not expected in either the cooling or heating scans, whereas for standard DSC there is always a peak on heating but not on cooling.
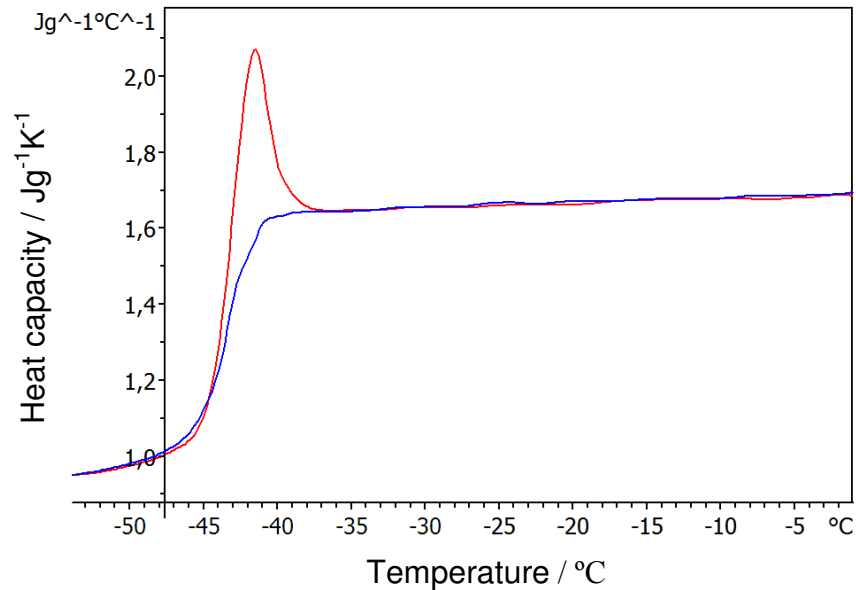


Figure 6.8. Quasi-static specific heat capacity, $c_{p0}$, for a tri-functional epoxy resin obtained during heating (red curve) from -60 to 0 ℃ at 1 K/min and cooling (blue curve) from 0 ℃ to -60 ℃ at -1 K/min. The pulse amplitude is 0.5 K and the switching time range is 15-30 s.

But this behaviour was not only observed for the trifunctional epoxy resin TGAP, and so is not a particular feature of a particular material; similar results were obtained also for DGEBA and for all of the mixtures prepared by adding the nanoclay to this resin. These results are not presented here, but the same effect of heating and cooling observed in Figure 6.8 was obtained.

Figure 6.9 shows the specific heat capacity obtained from an Isostep experiment on heating for a TGAP sample. There is no peak observed in the heating scan (as was expected) and the curve looks like the curve on cooling shown in Figure 6.8.
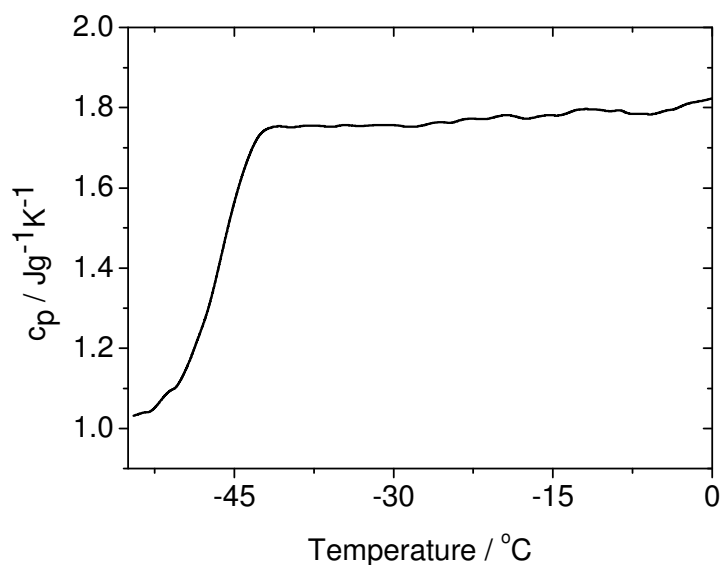


Fig 6.9. Specific heat capacity obtained from an Isostep method for a TGAP sample heated from -50 to 0 °C, the isothermal segments have a duration of 1.5min, the temperature difference between consecutive isothermal segments is 1 °C and the heating rate between them is 5 K/min.

The peak that appears on heating scans in TOPEM represents an overshoot in the heat capacity that results from relaxation effects. The problem here is that, while ADSC and IsoStep correctly separate reversing effects from relaxation (non-reversing) effects, TOPEM appears not to do so in this particular case. This unexpected peak can not be attributed to any effect of the sample; instead, it is likely to be related to the software calculations to characterize the system, and thus raises more questions about the evaluation procedure.

### *6.2.2. Simulation*

With the aim of answering at least some of these questions, a simulation is planned to be made. It is proposed to simulate how the instrument (TOPEM) analyses the data and provides as output the curves of $c_{p0}$, its frequency components, and the reversing and non-reversing heat flows.

A similar procedure was used earlier with ADSC [19-23], where the sample response in the glass transition was modelled and then analysed in the same way as the ADSC instrument does, i.e. using a Fourier Transform. The different approaches used by the model introduce different parameters related with the material, such as the relaxation time, the apparent activation energy or the non-linearity parameter. On the other hand, the experimental parameters involved in an ADSC experiment are also considered, such as the heating or cooling rate, the temperature amplitude or the period. This modelling led to the prediction of the effects of these different parameters, both material and experimental, and also their relationship with the response obtained, namely the heat flows and the heat capacities.

In the case of TOPEM, the idea is again to model the response in the glass transition region, but now to use the TOPEM analysis to determine the corresponding curves of $c_{po}$, its frequency components, and the reversing and non-reversing heat flows. It will be possible then to compare the output from the TOPEM black box with the known input from the imposed model, which is the same as that previously used for ADSC. A possible comparison will be, for example, the activation energy used in the model with that which can be obtained from the TOPEM frequency response. In the case that they were not the same, it is possible to modify the experimental and model parameters in the simulation in order to investigate under which conditions the TOPEM response is best adapted to the input from the model. It will be also interesting to study if the heating rate in the TOPEM pulses has any effect, and what is the nature of this effect. It is expected that this approach will be equally useful in

141

the understanding of TOPEM as it was in the analogous case of understanding ADSC [19-23]: for example, the separation of the frequency and cooling rate dependences of the various parameters , the effects of non-linearity and non-exponentiality in the response, the equivalence of cooling rate and frequency and the association with the temperature fluctuation model of the glass transition, and the method for allowing for heat transfer corrections to the phase angle curves, all of which resulted directly from such modelling aspects. To perform these simulations, it is necessary to know exactly how the calculations are made by the software. The experts in Mettler-Toledo Switzerland have agreed to share the detailed calculations, which are patented, in order that we may use their software to make the simulation. The results of the TOPEM analysis of the simulation will be compared with the input to the simulation. Only in certain respects will this be compared with experiment, for example to see whether any of the simulation or TOPEM parameters have an influence on the experimentally observed limit of 4 mHz.

It is anticipated that the TOPEM analysis of these simulated inputs will provide the answers to the various questions raised above: perhaps most importantly, to understand the origins of the limiting frequency, or to interpret what exactly is the meaning of the quasi-static heat capacity from which the frequency dependent components are derived.

142

# References

1. S.D. Cheng and B. Wunderlich*; Macromolecules, 21*, **1988**, 789.

2. S. Buchner, D. Wiswe, and H.G. Zachman; *Polymer, 30*, 1989, 480.

3. B.B. Sauer, W.G. Kampert, E.N. Blanchard, S.A. Threefoot and B.S. Hsiao; *Polymer, 41*, **2000**, 1099.

4. S. Montserrat, P. Colomer and J. Belana; *J. Mater. Chem., 2*, **1992**, 217.

5. S. Montserrat, F. Roman and P. Colomer; *J. Thermal Anal. Calorim., 72*, **2003**, 657.

6. J.C. Cañadas, J.A. Diego, J. Sellarès, M. Mudarra and J. Belana; *Polymer, 41,* **2000**, 8398.

7. P.G. Royal, D.Q.M. Craig and C. Doherty; *Pharma. Research, 15*, **1998**, 1117.

8. P.G. Royal, D.Q.M. Craig and C. Doherty; *International J. of Pharmaceutics, 192*, **1999**, 39.

9. K.C. Thompson; *Therm. Acta, 355*, **2000**, 83.

10. M. Schubnell and J.E.K. Schawe; *Intern. Jour. Pharmaceutics, 217*, **2001**, 173.

11. J.E.K. Schawe and U. Hess; *J. Therm. Anal. Calorim., 68*, **2002**, 741.

12. W.Louaer, A.H. Meniai and J.P.E. Grolier; *J. Therm. Anal. Calorim., 93*, **2008**, 605.

13. B. Ething, S. Gogolewski and A.J. Pennings; *Polymer, 23*, **1982**, 1587.

14. K.Kim, M. Yu, X. Zong, J. Chiu, D. Fang, Y.S. Seo et al. Biomaterials, 24, 2003, 4977.

15. J.V. Seppälä, A.O. Helminen and H. Korhonen; *Macromol. Biosci., 4*, **2004**, 208.

16. S. Jacobsen, H.G. Fritz, P. Degée, P. Dubois and R. Jérôme; *Polymer, 41*, **2000**, 3395.

17. S. Solarski, M. Ferreira and E. Devaux; *Polymer, 46*, **2005**, 11187.

18. Diana Cayuela, Institut Invest. Tèxtil i Coop. Industrial, personal information.

19. J.M. Hutchinson and S. Montserrat; *Thermoch. Acta, 286*, **1996**, 263.

20. J.M. Hutchinson and S. Montserrat; *J. Therm. Anal. Calorim., 47*, **1996**, 103.

21. J.M. Hutchinson and S. Montserrat; *Thermoch. Acta, 304/305*, **1997**, 257.

22. J.M. Hutchinson; *Thermoch. Acta, 324*, **1998**, 163.

23. J.M. Hutchinson and S. Montserrat; *Thermoch. Acta, 377*, **2001**, 63.

# CHAPTER 7

# CONCLUSIONS

# 7. Conclusions

1. TOPEM is a new temperature modulated calorimetric technique. The bases of the operation and the evaluation procedure have been described. The dependence of the results obtained on the experimental and evaluation parameters selected has been analyzed and discussed.

2. TOPEM has been applied to several different transitions in polymers: the glass transition of polycarbonate, vitrification during isothermal cure and vitrification and devitrification during non-isothermal cure of a thermoset. The results obtained have been analyzed in order to show what additional information can be derived using TOPEM rather than other temperature modulated calorimetry techniques. Some preliminary experiments related to other transitions and materials have been made and are planned to be studied in the future.

3. A lower limit to the frequency components that can be obtained from TOPEM has been found to be around 4 mHz. This limit could possibly be related to the instantaneous heating rate that occurs in the pulses. This instantaneous heating rate has been studied and a dependence only on the pulse amplitude has been found. A better understanding of the evaluation procedure made by the software in order to obtain the "quasi-static" heat capacity, the heat flow components or the frequency calculation is needed in order to verify this hypothesis or otherwise to explain this observed limit. A future simulation is planned to be made with the purpose of obtaining a better understanding of this limit and, more generally, of the TOPEM evaluation procedure so that the results can be better interpreted.

4. Simulations in MATLAB have been made to compare the experimental results obtained by TOPEM in the cure of a thermoset with the theoeretical predictions. Two different simulations were made, one for the isothermal and another for the non-isothermal case, the results for both simulations being shown to be in good agreement with the TOPEM results. In the isothermal case, the calculated results not only predict the experimental results obtained with TOPEM but also are able to describe some earlier higher frequency data, from dielectric measurements, obtained from the literature.

5. The results obtained by TOPEM have been compared with those obtained by ADSC and they are found to be in good agreement, leaving aside the limit at low frequencies. A better resolution in the signals of TOPEM has been observed.

6. The advantages of TOPEM in making a multi-frequency analysis in only one single measurement have been shown clearly: only one sample is needed to make a multi-frequency analysis, which in some cases results in a significant reduction of the experimental time needed compared with other calorimetric techniques. It provides the ability also to distinguish, in a single scan, frequency-dependent phenomena from those that are frequency independent.

7. The ability of TOPEM, as of other temperature modulated DSC techniques, in separating overlapping transitions has been demonstrated.

*APPENDIX*

### Appendix 1. Some additional information about TOPEM

#### Advanced parameters

As was explained in Chapter 2, the software relates the modulated temperature program with its corresponding heat flow response in order to calculate the transfer function, which characterises the system and which depends on both the instrument and the sample response. The advanced parameters are related to the sample and the instrument response and have to be selected in the TOPEM evaluation window (see also Figure 2.10), together with the calculation window width and the parameters for the shift of this window and the smoothing of the data. Figure A.1 shows the menu for the selection of the advanced parameters for an evaluation.



Figure A1.1. Menu for the selection of advanced parameters.

The sample and reference pan weights are normally introduced in the experiment window before running the experiment, but the possibility of changing it in this evaluation window after the experiment has been run is useful, for example if it is necessary to correct wrongly inserted or values that have been omitted, without having to repeat the experiment.

The other two parameters, the sample and instrument response parameters (in Figure A.1 the default values are presented), are related to the way the software calculates the response of the system through the transfer function. The use of a discrete Laplace transformation of the transfer function is made with two polynomials of degree p and q. These degrees for the polynomials correspond, respectively, to these two parameters, which are used to characterise the sample and instrument response.

The selection of the option for "HFnon rev" is related to the way the software calculates the non-reversing component of the heat flow response from these previously selected parameters, p and q. The best fitting for the calculation is provided by the quadratic option, while the linear option gives faster results.

In all the results previously presented in this work, the default values shown in Figure A1.1, except for the capsule masses, were used and the quadratic fit for the non-reversing heat flow was selected.

## *Optimization of an evaluation*

When an experiment is performed and the calculation window has to be selected to make an evaluation, some particular considerations should be taken into account:

- The maximum window width that can be selected is limited by the width of the transition. Mettler-Toledo recommend this maximum limit to be less or equal to 1/3 of the transition width; as was shown in Chapter 3, accurately results were obtained for calculation windows of 1/10 of the transition width in the case of the lowest heating rates employed.

148

- The more pulses are in a calculation window, the better signals are obtained because the calculation is more precise obtaining the relationship between the input and the output.
- A general rule (personal information provided by J.E.K. Schawe from Mettler-Toledo) relates the calculation window to the sampling interval s.i. (number of data points measured per second) and the advanced parameters:

$$\frac{t_{c.w.}}{s.i. \cdot (p+q)} = N$$

(A1.1)

where $t_{c.w.}$ is the width of the calculation window, s.i. is the sampling interval, with a default value of 0.1, p is the sample response parameter and q is the instrument response parameter. The selection of these parameters gives the value of this number N, which is related to the precision of the calculations:

N=10 lower limit

N=20 default value, which result from putting default values from $t_{c.w.}$, s.i., p and q in equation A1.1.

N=50 optimum value

N>> 50 evaluation of very low frequencies

It should be pointed out that the selection of these parameters is also related to the time the computer takes to make a calculation. In the case of the longest experiments presented here with the widest calculation windows, this time is of the order of several hours. The optimization of the calculations serves not only to obtain the most accurate results but also to obtain them within a reasonable period of time.

Table A1.1 gives a general summary of the optimum set of parameters needed to make a good evaluation of the data. These recommendations were taken into account in the all evaluations performed in the previous studies presented. They are only valid with aluminium crucibles and in the case of the sensor FRS5 (56 thermocouples for each crucible). With a different sensor of 120 thermocouples, the switching time ranges should be longer and the instrument response parameter should be changed.

| | METHOD | | | EVALUATION | | | | |
|---|---|---|---|---|---|---|---|---|
| | $\beta$ K/min | Pulse height K | Pulse width s | Calculation window s | Shift s | p | q | Remarks |
| High precision with frequency evaluation | ≤ 0.5 | 1 | 15-30 Low freq: 15-100 15-500 | ≥ 120 ≥ 1000 | ≥ 10 | 20-50 200 | 45 | Three Calculation windows in a thermal event |
| Fast Processes | ≤ 0.5 | ≤ 0.1 | 15-30 | 120 | ≥ 10 | 50 | | Best results: $(n_a+n_b)= 50 \cdot$ s.i. |
| Normal measurements | 0.5 - 2 | 0.002-1 | 15-30 | 120 | 1-10 | 2-20 | | Normal: $(n_a+n_b)= 20 \cdot$ s.i. |
| Fast measurements | 5 - 15 | 0.5-1 | 5-15 | 15-30 | 1 | 2-5 | | Not recommended |

Table A1.1. Summary of the recommended experimental and evaluation values to optimize the results obtained by TOPEM. From Mettler-Toledo personal communication.

### *Relationship between instantaneous heating rate and pulse amplitude*

Some calculations were made "by hand" to measure the instantaneous heating rate that occurs during the application of the pulses for a given temperature programme. These calculations were made for different heating rates, pulse amplitudes and switching time ranges, and an interesting relationship has been obtained between the instantaneous heating rate and the pulse amplitude.

150

As was explained in Chapter 2, a modulated temperature programme in TOPEM is described by:

$$T = T_0 + \beta_0\, t + \delta T \qquad\qquad (A1.2)$$

The corresponding heating rate is:

$$\beta = \beta_0\, t + d(\delta T)/dt \qquad\qquad (A1.3)$$

where $\beta_0$ is the underlying heating rate, and the second term defines the instantaneous heating rate with which the pulses are superimposed. In an ideal (unrealistic) case, this heating rate would be infinite (with square pulses, and instantaneous changes in temperature), but in the real case this instantaneous heating rate is limited. Experimentally it was found to be related with the pulse amplitude, $A_T$, according to:

$$\frac{d(\delta T)}{dt} = \pm\, 20 \cdot A_T \qquad\qquad (A1.4)$$

Figure A1.2 shows a typical temperature programme, from which this expression can be derived.
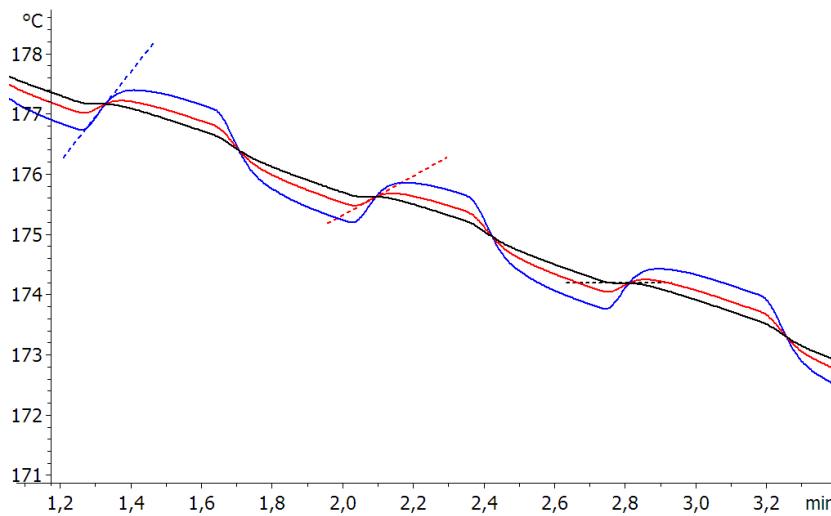


Figure A1.2. Detail of three pulses extracted from three temperature programs for three different experiments for temperatures from 180 to 80 ºC, cooling rate of -1K/min and pulses amplitude of 0.5 K (blue), 0.25 K (red) and 0.1 K (black). Also shown are the tangents to the curves in the beginning of the pulses, which correspond to the instantaneous heating rates.

151

### Stochastic programs

Some additional observations can be made with respect to Figure A.2. Although three different temperature programs are represented here, with three different pulse amplitudes, the time intervals between the pulses are the same. The same observation can be made if the complete range of the experiment is examined. Additional observations for different temperature programmes also give the same result: with the selection of the same range of temperatures, the same underlying heating (cooling) rate and the same switching time range, the software constructs a "stochastic" temperature programme which is always identical; the pulses have different duration between the minimum and the maximum values of the switching time range selected, but they are superimposed always at the same moment. This observation has two consequences:

- The stochastic perturbation is not as stochastic as it was expected to be; in contrast to a completely random application of the pulses, in these sets of supposedly "stochastic" experiments there is always the same "predictable" temperature program.
- The same combination of temperature range, underlying rate and switching time range in the method window will always give the same experiment, the only difference being in the instantaneous heating rate of the pulses for different pulse amplitudes.

Although this could seem to be a limitation of the technique, it should be remarked that the way the software calculates the frequency response is based on the different duration of the pulses superimposed on the underlying heating rate throughout the whole range of the experiment, and it would not be influenced by the way the pulses are superimposed. Therefore, this curious observation of a degree of "non-stochasticity" should not be of importance in terms of the evaluation of the frequency response of the system.

152

### *Appendix 2. Checking the calorimeter accuracy through the measurement of the heat capacity of sapphire*

The absolute heat capacity of sapphire was measured by TOPEM to check the accuracy of the results obtained. ADSC scans were also made to compare with TOPEM results. A total of 26 TOPEM scans and 2 ADSC scans were made and the values of the heat capacity obtained were compared with those of a reference curve. The temperatures selected were in the range between -70 ºC and 0 ºC, in view of a subsequent study that was planned for the investigation of the glass transition of epoxy resins, which was made in the same temperature range but is not presented here. Different heating rates and switching time ranges (s.t.r.) were selected and three different samples were prepared and studied. The error for the different experiments was calculated as:

$$error(\%) = \frac{100 \cdot |x_i - x_{ref}|}{x_{ref}} \tag{A2.1}$$

where $x_i$ is the value of each experimental result for the heat capacity and $x_{ref}$ is its corresponding reference value (the value expected and obtained from a reference curve). In all the cases, the prepared samples were little crystals of sapphire sealed in aluminium crucibles.

The results for the errors obtained for each run are summarized in tables A2.1 and A2.2, together with characteristics of the sample and the experimental parameters selected. Different heating rates (*veloc.* in Table A2.2) and switching time ranges (*s.t.r.* in Table A2.2) were selected with a constant amplitude of the pulses of 0.5 K. Three different samples were sealed in three different crucibles. The first one was sealed in a standard capsule (*Std.* in Table A2.2) which are aluminium crucibles of 40 µl, the second one was sealed in a similar capsule of 40 µl but with a pin in the base (*PIN* in Table A2.2), and the third one was sealed in a light aluminium crucible of 20 µl (*20* in table A2.2).

| Number | Date | error | veloc. | s.t.r. | capsule | Cap.mass | Mass |
|--------|------|-------|--------|--------|---------|----------|------|
|        | dd.mm.yy | % | K/min | s | | mg | mg |
| 1 | 27.03.09 | 7.21 | 2 | 15-30 | Std. | 47.214 | 26.196 |
| 2 | 27.03.09 | 7.05 | 2 | 15-30 | Std. | 47.214 | 26.196 |
| 3 | 27.03.09 | 0.23 | 5 | 15-30 | Std. | 47.214 | 26.196 |
| 4 | 30.03.09 | 1.08 | 5 | 15-30 | Std. | 47.214 | 26.196 |
| 5 | 30.03.09 | 0.41 | 3 | 15-30 | Std. | 47.214 | 26.196 |
| 6 | 30.03.09 | 4.89 | 1 | 15-120 | Std. | 47.214 | 26.196 |
| 7 | 31.03.09 | 3.92 | 1 | 15-120 | Std. | 47.214 | 26.196 |
| 8 | 31.03.09 | 3.61 | 2 | 15-120 | Std. | 47.214 | 26.196 |
| 9 | 31.03.09 | 0.43 | 2 | 15-120 | Std. | 47.214 | 26.196 |
| 10 | 03.04.09 | 4.13 | 2 | 15-120 | Std. | 47.214 | 26.196 |
| 11 | 07.04.09 | 6.51 | 2 | 15-120 | Std. | 47.214 | 26.196 |
| 12 | 07.04.09 | 1.16 | 2 | 15-120 | PIN | 48.272 | 26.248 |
| 13 | 07.04.09 | 0.93 | 2 | 15-120 | PIN | 48.272 | 26.248 |
| 14 | 07.04.09 | 32.94 | 2 | 15-120 | Std. | 47.214 | 26.196 |
| 15 | 07.04.09 | 7.26 | 2 | 15-120 | PIN | 48.272 | 26.248 |

| Number | Date | error | veloc. | s.t.r. | capsule | Cap.mass | Mass |
|--------|---------|-------|--------|--------|---------|----------|--------|
|        | dd.mm.yy | % | K/min | s | | mg | mg |
| 16 | 07.04.09 | 13.96 | 2 | 15-120 | Std. | 47.214 | 26.196 |
| 17 | 08.04.09 | 3.33 | 2 | 15-120 | Std. | 47.214 | 26.196 |
| 18 | 08.04.09 | 3.18 | 2 | 15-120 | Std. | 47.214 | 26.196 |
| 19 | 08.04.09 | 3.15 | 2 | 15-120 | Std. | 47.214 | 26.196 |
| 20 | 08.04.09 | 3.64 | 2 | 15-120 | PIN | 48.272 | 26.248 |
| 21 | 08.04.09 | 3.46 | 2 | 15-120 | PIN | 48.272 | 26.248 |
| 22 | 08.04.09 | 3.8 | 2 | 15-120 | PIN | 48.272 | 26.248 |
| 23 | 08.04.09 | 12.95 | 2 | 15-120 | 20 | 22.658 | 26.09 |
| 24 | 08.04.09 | 15.70 | 2 | 15-120 | 20 | 22.658 | 26.09 |
| 25 | 14.04.09 | 6.58 | 2 | 15-120 | Std. | 47.214 | 26.196 |
| 26 | 14.04.09 | 0.49 | 2 | 15-120 | PIN | 48.272 | 26.248 |

Table A2.1. Summary of the experiments performed by TOPEM. "Std." means standard aluminium crucibles of 40 μl, "PIN" means that it has a pin in the base to ensure a centred position in the sensor, and "20" denotes light aluminium crucibles of 20 μl. The switching time range is simplified as "s.t.r.". In all cases the pulse amplitude was selected to be 0.5 K.

| Number | Date | error | veloc. | period | Capsule | Cap.mass | Mass |
|--------|------|-------|--------|--------|---------|----------|------|
|        | dd.mm.yy | % | K/min | s |         | mg | mg |
| 1 | 27.03.09 | 14,32 | 1 | 120 | Std. | 47.214 | 26.196 |
| 2 | 27.03.09 | 10,52 | 1 | 120 | Std. | 47.214 | 26.196 |

Table A2.2. Summary of the experiments performed by ADSC. In both cases the temperature amplitude was 0.5 K as in TOPEM.

The differences in the errors obtained do not follow a systematic trend and could not be related either with the different samples or with the parameters selected. The effect of the different variables on the results has been investigated separately for each of the variables, and the results are shown in the figures below.

### DATE OF THE SCAN

Taking into account the day when the experiments were made, the different experiments performed for each day were analyzed to see if there is any influence of the day of the scan on the value of the heat capacity obtained.
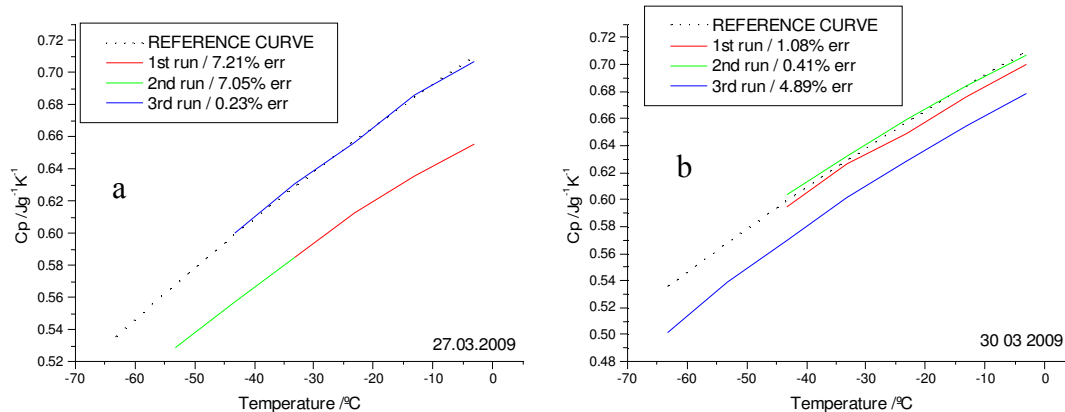


a) $2^{nd}$ scan immediately followed $1^{st}$ scan. Between $2^{nd}$ and $3^{rd}$ scans there were some resin scans
b) $2^{nd}$ scan immediately followed $1^{st}$ scan. Between $2^{nd}$ and $3^{rd}$ scans there was an ADSC scan. Standard Capsules were used in all cases.
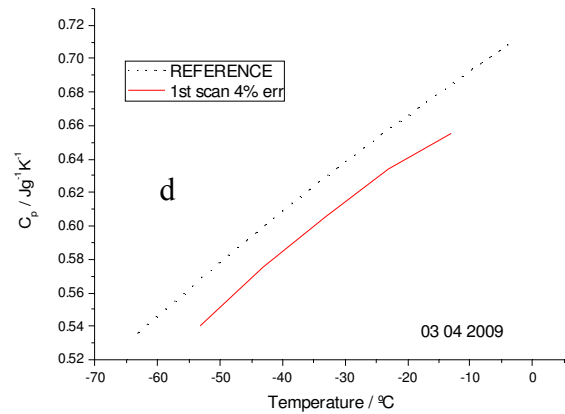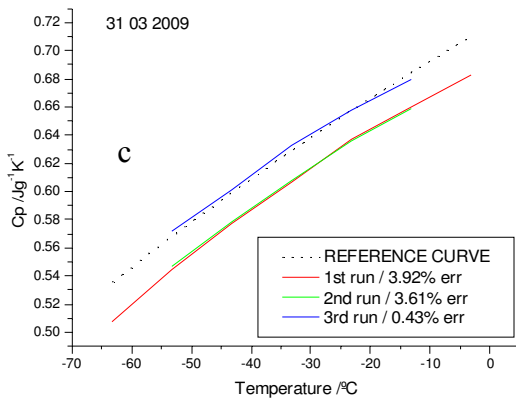
c) 2$^{nd}$ scan immediately followed 1$^{st}$ scan. Between 2$^{nd}$ and 3$^{rd}$ scans there was an ADSC scan
d) 1$^{st}$ scan was made after some resin scans.
Standard capsules were used in all cases.
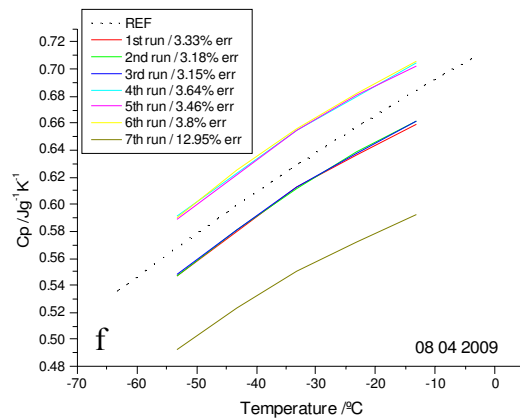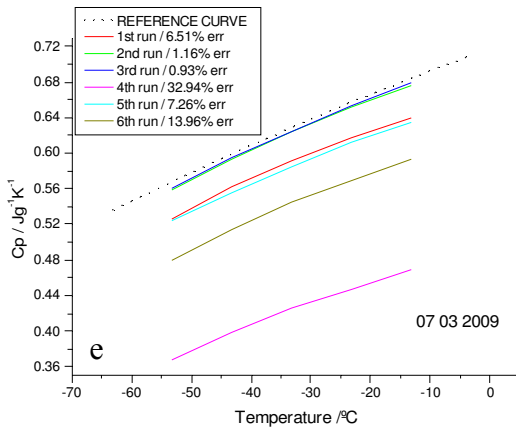


e) 2$^{nd}$ scan immediately followed 1$^{st}$ scan  and 3$^{rd}$ scan immediately followed 2$^{nd}$ scan. PIN capsules were used for scans 1$^{st}$, 2$^{nd}$ and 3$^{rd}$.  4$^{th}$ scan standard. 5$^{th}$ scan with PIN.
6$^{th}$ scan standard capsules.
f) 2$^{nd}$ scan immediately followed 1$^{st}$ scan  and 3$^{rd}$ scan immediately followed 2$^{nd}$ scan. Standard capsules were used for scans 1$^{st}$, 2$^{nd}$ and 3$^{rd}$. 4$^{th}$ to 6$^{th}$ with PIN, followed. 7th scan light 20μL capsules

Figures A2.1 from a) to f). Specific heat capacity versus temperature of different sapphire samples obtained from TOPEM experiments performed in different days as indicated in the inset. The black dotted line is the real specific heat capacity of Sapphire obtained from the Standards. A scan which follows another scan implies that the sample is not taken out of the oven.

As can be clearly seen in the different graphs from Figures A2.a to A2.f, there is a displacement in the value of the heat capacity measured compared with the real value

157

expected. The deviation of the data obtained does not depend on the day of the run; the process of changing the sample (i.e. open the furnace, change the sample and close the furnace again) has more effect on the random shift observed in the data than does the day on which the run was performed. It should be pointed out here that there is an important difference between the calorimeter used for this study and the calorimeter used for the rest of the work presented in this thesis. In these experiments on sapphire, the change of the sample was not made automatically with a robot; instead, the user has to change the sample manually, and hence some possible variations in the measured values of the heat capacity may be due to a different positioning of the sample in the centre of the sensor. The use of capsules with a pin in the base ensures that the sample is placed always in the centre of the sensor, and therefore a better approximation would be expected using this type of capsule, as is shown in Figure A2.2, although there was found again a random deviation in the measured curves.

*TYPE OF CAPSULE*

The results of the scans made with the capsules with a pin are shown in Figure A2.2 together with the results of the scans made with light capsules of 20 µl
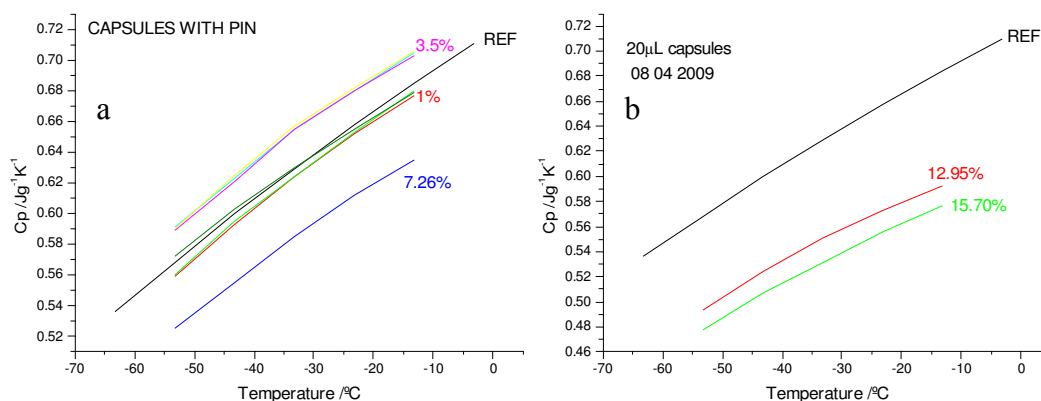


Figure A2.2 Heat Capacity of different Sapphire samples versus Temperature for TOPEM experiments performed with different type of capsules as indicated in the inset. a) Capsules with PIN. b) Light aluminium Capsules 20 µl.

158

containing lighter samples with worse thermal contact which would give, as was observed, worse results.

The data obtained are better in the case of the capsules with a pin but still remains changing for each scan, and also without a clear reason. It is also remarkable that the displacement, in the majority of cases, is below the real value.

*ADSC SCANS*

Two different scans on different days were made also in Alternating DSC (ADSC). The results can be seen in Figure A2.3; the large deviation observed at the lower temperatures for the first scan is an artefact due to poor control in the temperature programme as was indicated in the experiment window during the scan. There is again a deviation of the data as for the case of the TOPEM measurements.
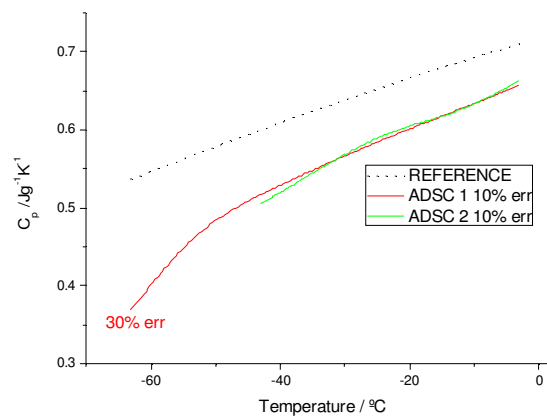


Figure A2.3. Heat capacity of the same sapphire sample versus temperature obtained from ADSC measurements.

*EXPERIMENTAL PARAMETERS*

There should be no dependence of the heat capacity on the experimental parameters in the region of linearity. Nevertheless, as a check on this, two different

heating rates and/or switching time ranges were studied to determine the effect of these experimental parameters. As expected, no systematic effect was observed in any case, as illustrated below.

Figure A2.4 shows the result obtained for experiments performed with a pulse amplitude of 0.5 K, a switching time range from 15-30 s to 15-120 s, and two different heating rates of 1K/min and 2 K/min. In the same way as for the previous results, no correlation between the random shift in the curves and the different selected parameters could be observed.
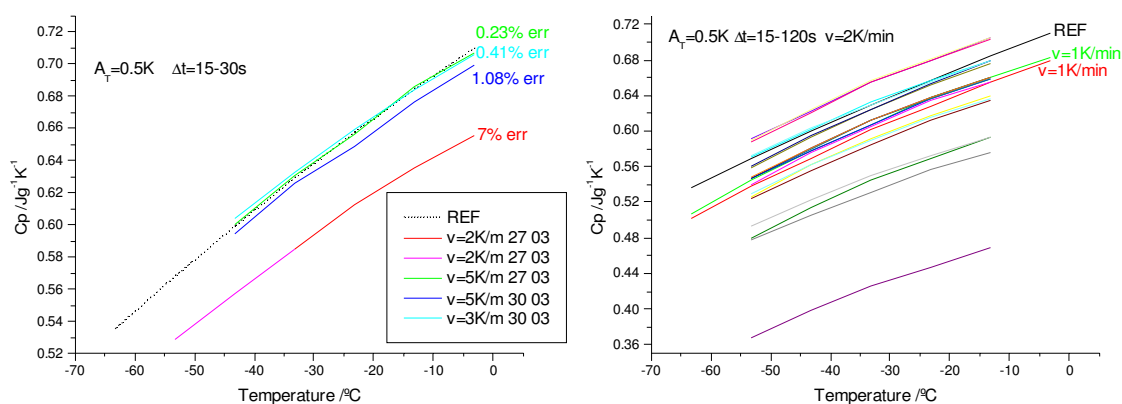


Figure A2.4. Heat capacity of different sapphire samples versus temperature obtained from TOPEM experiments performed with different switching time ranges (15-30 s in the left-hand graph, 15-120 s in the right-hand graph) as indicated in the inset. The effect of heating rate is also shown (all curves have a heating rate of 2 K/min except for two curves indicated in the right-hand graph).

In order to verify that the results did not depend on the particular calorimeter used, a different calorimeter, specifically the calorimeter used for the rest of the studies presented here, with a robot to insert the sample inside the furnace, was also used, together with the same sample of sapphire and a standard capsule. A similar scatter in the curves was observed (though these results are not presented here), with no systematic variation, indicating that the measurements did not depend on the particular calorimeter employed.

### *Comparison with results obtained with a power-compensated calorimeter: PYRIS*

Analogous to the previous work, a short similar study was also made with a PYRIS calorimeter. The main difference between the PYRIS calorimeter (Perkin Elmer) and the Mettler Toledo instrument is that PYRIS is a power-compensation calorimeter, with two separate heaters for the sample and the reference. The purpose of this study was to determine whether the PYRIS gave more accurate measurements of heat capacity.

In this case only two samples were prepared: one sample was similar to the TOPEM samples used with little crystals of sapphire sealed in a capsule and with small weight and the second one, a solid and heavier disc of sapphire. The temperature program was from -50 ºC to 0 ºC in Isostep mode. The temperature program for an Isostep experiment consists of a large number of short dynamic steps (temperature ramps) each of which starts and ends with an isothermal segment. The analysis of the response allows the heat capacity to be determined. The increase in temperature between the isothermal segments was selected to be 1K, the heating rate for these temperature ramps was 5 K/min, and the isothermal segments had a duration of 1.5 minutes.

The results are all summarized in the same Figure A2.5. All the curves displayed are from the same sample of sapphire crystals, except those two indicated as "DISC". It can be clearly observed that the results for the crystals are very similar to that obtained with TOPEM due to the bad thermal contact of the sample.
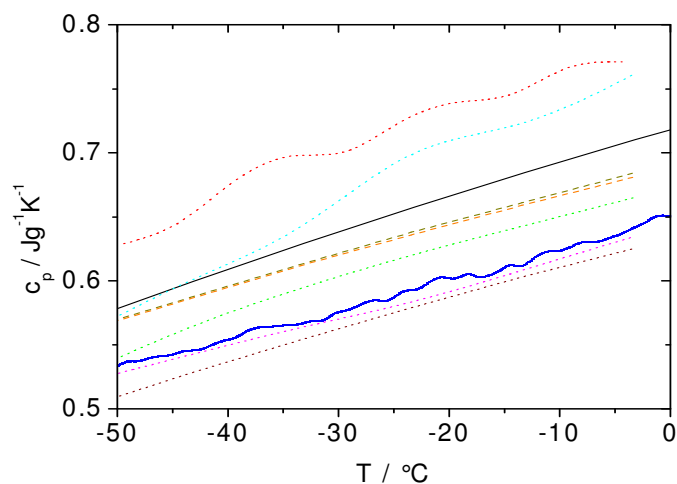
Figure A2.5. Heat capacity of two different sapphire samples versus temperature obtained from Isostep experiments performed in a PYRIS calorimeter. Dash lines correspond to the solid disc of Sapphire the rest of the dot line curves correspond to the same sample prepared with sapphire crystals. Continuous line corresponds to the reference values. The same experimental method was used for all the scans.


**Conclusion**


Different measurements of the heat capacity of sapphire were made under various conditions and compared with reference values, in order to check the accuracy of the calorimeter. Different samples were prepared and different experimental parameters were selected. In all cases a random shift in the value of the heat capacity was observed; in the majority of the experiments the measured heat capacity fell below the reference value. Also, in virtually all cases the magnitude of the displacement was independent of temperature, so that the curves for different experiments are essentially parallel. It was not possible to relate this shift with the date of measurement, the calorimetric technique used, or the experimental parameters selected, although there is a clear change in the magnitude of the shift each time the sample is changed in the furnace that leads to relate the shift with the heat transfer from furnace to sample. The capsules with a pin in their base appear to give better

results. Nevertheless, in the majority of cases the experimental results are less than 10% different from the reference value. A better signal is obtained with the use of a solid disc with a better thermal contact.

# Appendix 3. MATLAB programmes for the simulations

### *A3.1. Isothermal Cure*

```
% This programme calculates the isothermal cure kinetics by
conventional DSC assuming:
% Kamal's semi-empirical equation for the reaction rate;
% WLF variation of diffusion rate constant at Tg;
% Arrhenius dependence for reaction rate constants;
% di Benedetto equation for dependence of Tg on alpha;
% experimental values for temperature and alpha dependence of
Cpl and Cpg;
% Rabinowitsch equation for combination of diffusion and
chemical rate constants;
% equation for Cp during vitrification adapted from diffusion
factor of Cole et al and mobility factor of Van Assche.
% The calculations are compared for the reaction with and
(unrealistically)
% without vitrification.

clear

% Input values
tcuremin=input('cure time [min] ='); % input isothermal cure
time in minutes
tcures=tcuremin*60; % isothermal cure time in seconds
Tc=input('cure temperature [°C] ='); % input cure temperature
in °C

% Exponents in Kamal equation
m=0.23;
n=1.43;

% WLF constants
C1=2.303*17.44;
C2=51.6;

% Activation energies and pre-exponentials for rate constants
in Kamal equation
E1=41500; % for k1 [J/mol]
E1c=51800; % for k1c [J/mol]
A1=10^3.4; % for k1 [1/s]
A1c=10^3.6; % for k1c [1/s]
```

```matlab
% Other constants
kdg0=0.0051; %diffusion rate constat at Tg probe
%kdg0=3.8*10^(-5); % diffusion rate constant at Tg [1/s] from
Wise et al (1997)
%kdg0=0.51; % diffusion rate constant at Tg [1/s] from
Wisanrakkit & Gillham (1990)
r=0.33; % lambda in di Benedetto equation
dt=0.5; % time step [s]
num=tcures/dt; % number of steps in calculation
H=520; % total heat of reaction [J/g]
a(1)=0; % initial degree of cure
ac(1)=0; % initial degree of cure for (unrealistic) chemical
reaction only

% Allowing for frequency dependence of cure temperature
per=input('modulation period [s] ='); % input modulation
period in seconds
freq=1000/per; % frequency [mHz]
dHonR=100; % reduced activation energy [kK]
T0s=Tc+273; % cure temperature in K
T0=1/(1/T0s-(log(1000/60)-log(freq))/(dHonR*1000)); %
equivalent cure temperature at new frequency [K]
Tg0s=-15+273; % Tg of unreacted resin for period of 60s, taken
as standard [K]
Tginfs=80+273; % Tg of fully cured resin for period of 60s,
taken as standard [K]
%Tg0=1/(1/Tg0s+(log(1000/60)-log(freq))/(dHonR*1000)); % Tg of
unreacted resin at new frequency [K]
%Tginf=1/(1/Tginfs+(log(1000/60)-log(freq))/(dHonR*1000)); %
Tg of fully cured resin at new frequency [K]

tic

flag=0;
flagc=0;

% Loop for time steps
    for j=1:num
    t(j)=dt*(j-1); % time
    T(j)=T0; % temperature
    k1(j)=A1*exp(-E1/(8.314*T0s)); % Arrhenius rate constant
k1
    k1c(j)=A1c*exp(-E1c/(8.314*T0s)); % Arrhenius rate
constant k1c

    % Calculations for chemical reaction only
```

```
    Tgc(j)=((1-ac(j))*Tg0s+r*ac(j)*Tginfs)/(1-ac(j)+r*ac(j));
% Tg dependence on degree of cure
        if T0<Tgc(j) & flagc==0 % assumes vitrification when
Tg reaches Tcure
        tvc=t(j); % vitrification time for chemical reaction
only
        flagc=1;
        end
    Cplc(j)=0.00183*(T(j)-273)+1.91; % experimental values
    sCpgc(j)=0.00262*ac(j)+0.00236;
    dCpgc(j)=0.629*ac(j)+0.527;
    Cpgc(j)=sCpgc(j)*(T(j)-273)+dCpgc(j);

    dac(j)=(k1(j)*(ac(j))^m+k1c(j))*((1-ac(j))^n)*dt; % Kamal
equation
    ac(j+1)=ac(j)+dac(j); % degree of cure

    % Calculation of heat flow
    HFc(j)=H*(dac(j)/dt); % heat flow in W/g

    % Calculations when vitrification occurs (diffusion)
    Tg(j)=((1-a(j))*Tg0s+r*a(j)*Tginfs)/(1-a(j)+r*a(j)); % Tg
        if T0<Tg(j) & flag==0 % assumes vitrification when Tg
reaches Tcure
        tv=t(j); % vitrification time
        tvm=tv/60 % vitrification time in minutes
        av=a(j) % degree of cure at vitrification
        v=j; % element for which vitrification occurs
        flag=1;
        end

    kd(j)=kdg0*exp((C1*(T0s-Tg(j)))/(C2+T0s-Tg(j))); % WLF
equation for diffusion rate constant Cpl(j)=0.00183*(T(j)-
273)+1.91;
    Cpl(j)=0.00183*(T(j)-273)+1.91;
    sCpg(j)=0.00262*a(j)+0.00236;
    dCpg(j)=0.629*a(j)+0.527;
    Cpg(j)=sCpg(j)*(T(j)-273)+dCpg(j);
    Cpgi(j)=(0.00262+0.00236)*(T(j)-273)+(0.629+0.527);

    K1(j)=1/(1/kd(j)+1/k1(j)); % Rabinowitsch equation for K1
    K1c(j)=1/(1/kd(j)+1/k1c(j)); % Rabinowitsch equation for
K1c
    da(j)=(K1(j)*(a(j))^m+K1c(j))*((1-a(j))^n)*dt; % Kamal
equation
    a(j+1)=a(j)+da(j); % degree of cure
```

167

```matlab
    % Calculation of heat flow
    HF(j)=H*(da(j)/dt);

    % Calculation of Cp
    kv(j)=(K1(j)*(a(j))^m+K1c(j))/(k1(j)*(ac(j))^m+k1c(j)); %
should we use this or the next line???
    %kv(j)=K1(j)/k1(j); % diffusion factor [Cole et al,
Macromolecules 24, 3098 (1991)]
    Cp(j)=Cpg(j)+kv(j)*(Cpl(j)-Cpg(j)); % adaptation of Van
Assche mobility factor equation
    end

da(num+1)=da(num);
dac(num+1)=dac(num);

figure(1)
zoom on
plot(t,HF,'-',t,HFc,':')
xlabel('time,s')
ylabel('Heat Flow')
hold on

figure(2)
zoom on
plot(a,da,'-',ac,dac,':')
xlabel('Conversion')
ylabel('Rate of conversion')
hold on

figure(3)
zoom on
plot(t,Cp,'-',t,Cpl,':',t,Cpg,'-.')
xlabel('Time,s')
ylabel('Cp,J/gk')
hold on

figure(4)
plot(t,T,'-',t,Tg,':',t,Tgc,'-.')
xlabel('Time,s')
ylabel('Tg,K')
hold on

figure(5)
plot(t,kv)
xlabel('Time,s')
ylabel('K1/k1')
hold on
```

168

```
%dTgdalpha=((1-a(v))*Tg0+r*a(v)*Tginf)*(1-r)/(1-
a(v)+r*a(v))^2+(r*Tginf-Tg0)/(1-a(v)+r*a(v));
%dalphadt=(K1(v)*(a(v))^m+K1c(v))*((1-a(v))^n);
%dTgdt=dTgdalpha*dalphadt;

toc
time=toc
```

### *A3.2. Non - Isothermal Cure*

```
% This programme calculates the non-isothermal cure kinetics
by conventional DSC assuming:
% Kamal's semi-empirical equation for the reaction rate;
% WLF variation of diffusion rate constant at Tg;
% Arrhenius dependence for reaction rate constants;
% di Benedetto equation for dependence of Tg on alpha;
% experimental values for temperature and alpha dependence of
Cpl and Cpg;
% Rabinowitsch equation for combination of diffusion and
chemical rate
% constants;
% ?? equation for Cp during vitrification.
% The calculations are compared for the reaction with and
(unrealistically)
% without vitrification.clear

clear

% Input values
Tstart=input('Starting temperature [°C]='); % input starting
temperature in °C
Tstart=Tstart+273; % temperature in K
Tfinal=input('Final Temperature [°C]='); % input final
temperature in °C
Tfinal=Tfinal+273; % temperature in K
b=input('Heating rate [K/min]='); % input heating rate in
K/min
b=b/60; % heating rate in K/s

% Exponents in Kamal equation
m=1;
n=1.5;

% WLF constants
C1=40.2;
C2=51.6;

% Activation energies and pre-exponentials for rate constants
in Kamal equation
E1=41500; % for k1 [J/mol]
A1=10^3.4; % for k1 [1/s]
E1c=51800; % for k1c [J/mol]
A1c=10^3.6; % for k1c [1/s]

% Other constants
```

```matlab
kdg0=0.0051; % diffusion rate constant at Tg0 [1/s]
r=0.5; % lambda in di Benedetto equation
dt=5; % time step [s]
runtime=(Tfinal-Tstart)/b; % total run time [s]
runtime=round(runtime); % integer of runtime
num=runtime/dt; % number of steps in calculation
H=520; % total heat of reaction [J/g]
a(1)=0; % initial degree of cure
ac(1)=0; % initial degree of cure for (unrealistic) chemical
reaction only
Tg0=-15+273; % Tg of unreacted resin [K]
Tginf=80+273; % Tg of fully cured resin [K]
dHonR=150; %reduced activation energy [kK] for freq dependence
of cure T
tic

% Loop for time steps
for j=1:num
    t(j)=dt*(j-1); % time
    T(j)=Tstart+b*t(j);
    k1(j)=A1*exp(-E1/(8.314*T(j))); % Arrhenius rate constant
k1
    k1c(j)=A1c*exp(-E1c/(8.314*T(j))); % Arrhenius rate
constant k1c

    % Calculations for chemical reaction only
    Tgc(j)=((1-ac(j))*Tg0+r*ac(j)*Tginf)/(1-ac(j)+r*ac(j)); %
Tg dependence on degree of cure
    Cplc(j)=0.00183*(T(j)-273)+1.91;
    sCpgc(j)=0.00262*ac(j)+0.00236;
    dCpgc(j)=0.629*ac(j)+0.527;
    Cpgc(j)=sCpgc(j)*(T(j)-273)+dCpgc(j);

    dac(j)=(k1(j)*(ac(j))^m+k1c(j))*((1-ac(j))^n)*dt; % Kamal
equation
    ac(j+1)=ac(j)+dac(j); % degree of cure
    HFNc(j)=H*(dac(j)/dt); % non-reversing heat flow [W/g]
    HFRc(j)=Cplc(j)*b; % reversing heat flow, liquid heat
capacity [W/g]
    HFc(j)=HFNc(j)+HFRc(j); % heat flow in W/g

    % Calculations when vitrification occurs (diffusion)
    Tg(j)=((1-a(j))*Tg0+r*a(j)*Tginf)/(1-a(j)+r*a(j)); % Tg
    kd(j)=kdg0*exp((C1*(T(j)-Tg(j)))/(C2+T(j)-Tg(j))); % WLF
equation for diffusion rate constant
    Cpl(j)=0.00183*(T(j)-273)+1.91;
    sCpg(j)=0.00262*ac(j)+0.00236;
    dCpg(j)=0.629*ac(j)+0.527;
```

```
    Cpg(j)=sCpgc(j)*(T(j)-273)+dCpgc(j);
    Cpgi(j)=(0.00262+0.00236)*(T(j)-273)+(0.629+0.527);

    % combined chemical and diffusion rate constants
    K1(j)=1/(1/kd(j)+1/k1(j)); % Rabinowitsch equation for K1
    K1c(j)=1/(1/kd(j)+1/k1c(j)); % Rabinowitsch equation for
K1c
    da(j)=(K1(j)*(a(j))^m+K1c(j))*((1-a(j))^n)*dt; % Kamal
equation
    a(j+1)=a(j)+da(j); % degree of cure

    % Calculation of heat flows
    HFN(j)=H*(da(j)/dt); % non-reversing heat flow [W/g]

    %kv(j)=K1(j)/k1(j); % should we use this or the next
line???
    kv(j)=(K1(j)*(a(j))^m+K1c(j))/(k1(j)*(ac(j))^m+k1c(j)); %
diffusion factor [Cole et al, Macromolecules 24, 3098 (1991)]

    % Calculation of specific heat capacity
    Cp(j)=Cpg(j)+kv(j)*(Cpl(j)-Cpg(j));

    HFR(j)=-Cp(j)*b; % reversing heat flow
    HF(j)=HFN(j)+HFR(j); % total heat flow


end

figure(4)
zoom on
plot(T,T,'--',T,Tg,':')
xlabel('Temperature,K')
ylabel('Tg,K')
hold on

figure(7)
zoom on
plot(t,T,'-',t,Tg,':',t,Tgc,'--')
xlabel('time,s')
ylabel('Temperature,K')
hold on

t(num+1)=dt*num;
T(num+1)=Tstart+b*t(num+1);

%Determination of vitrification times
```

172

```matlab
    for nf=1:9
    freq(nf)=10^((nf-1)/4); %frequency mHz
    per(nf)=1000/freq(nf); %period s

    for i=1:num
        Tf(i)=1/(1/T(i)-(log(1000/60)-
log(freq(nf)))/(dHonR*1000));
    end

    for i=1:num
            Tdiff=Tf(i)-Tg(i);
        if Tdiff<=0;
            v(nf)=i;
            tv(nf)=t(i);
            tvm(nf)=tv(nf)/60;
             break;
        end

    end
    for i=v+1:num
            Tdiff=Tf(i)-Tg(i);
        if Tdiff>0;
            dv(nf)=i;
            tdv(nf)=t(i);
            tdvm(nf)=tdv(nf)/60;
            break;
        end

    end


%T(num+1)=T(num);
%Tf(num+1)=Tf(num);
%Tg(num+1)=Tg(num);
%Tgc(num+1)=Tgc(num);
%figure(8)
%zoom on
%plot(t/1000,T,'-',t/1000,Tg,':',t/1000,Tgc,'--',t/1000,Tf,'-
')
%xlabel('time,ks')
%ylabel('T,K')
%hold on


 %T(num+1)=T(num);
 %Tf(num+1)=Tf(num);
 %Tg(num+1)=Tg(num);
```

```matlab
 %figure(8)
 %zoom on
 %plot(t,T,'-',t,Tf,':',t,Tg,'--')
 %xlabel('time,s')
 %ylabel('T,K')
 %hold on

%figure(9)
%zoom on
%plot(T,Tf,':',T,Tg,'-')
%xlabel('T,K')
%ylabel('T,K')
%hold on

end




%da(num+1)=da(num);
%dac(num+1)=dac(num);

%figure(1)
%zoom on
%plot(T,HF,'-',T,HFc,':')
%xlabel('Temperature,K')
%ylabel('Heat Flow,W/g')
%hold on

%figure(2)
%zoom on
%plot(a,da,'-',ac,dac,':')
%xlabel('Conversion')
%ylabel('Rate of conversion,1/s')
%hold on

%figure(3)
%zoom on
%plot(T,Cp,'-',T,Cpl,':',T,Cpg,'-.',T,Cpgi,'--')
%xlabel('Temperature,K')
%ylabel('Cp,J/gK')
%hold on


%figure(5)
%zoom on
%plot(T,kv)
```

174

```
%xlabel('Temperature,K')
%ylabel('K1/k1')
%hold on


%figure(6)
%zoom on
%plot(T,da)
%xlabel('Temperature,K')
%ylabel('da/dt,1/s')
%hold on

toc
time=toc
```

```
%xlabel('Temperature,K')
%ylabel('K1/k1')
%hold on

%figure(6)
```

*Appendix 4. Published Articles*

1. *"TOPEM, a new temperature modulated DSC technique - Application to the glass transition of polymers"*. I. Fraga, S. Montserrat and J.M. Hutchinson; Journal of Thermal analysis and Calorimetry. Volume: 87 Issue: 1 Pages: 119-124. Published: 2007

2. *"Vitrification during the isothermal cure of thermosets. Part I. An investigation using TOPEM, a new temperature modulated technique"*. I. Fraga, S. Montserrat and J.M. Hutchinson; Journal of Thermal analysis and Calorimetry. Volume: 91 Issue: 3 Pages: 687-695. Published: 2008

3. *"Vitrification during the Isothermal Cure of Thermosets: Comparison of Theoretical Simulations with Temperature-Modulated DSC and Dielectric Analysis"*. I. Fraga, S. Montserrat, and J.M. Hutchinson; Macromolecular Chemistry and Physics. Volume: 209 Issue: 19 Pages: 2003-2011. Published: 2008

4. *"Vitrification and devitrification during the non-isothermal cure of a thermoset. A TOPEM study"*. I. Fraga, J.M. Hutchinson, and S. Montserrat; Journal of Thermal analysis and Calorimetry. DOI: 10.1007/s10973-009-0601-7.

5. *"Vitrification and Devitrification during the Non-Isothermal Cure of a Thermoset. Theoretical Model and Comparison with Calorimetric Experiments"*. I. Fraga, S. Montserrat and J.M. Hutchinson; Macromolecular Chemistry and Physics. DOI: 10.1002/macp.200900322.

*Other publications:*

1. *"Vitrification during the isothermal cure of a thermoset studied by TOPEM®"*. UserCom num 29. ME-51725173. Edited by Mettler-Toledo AG Analytical, Switzerland.

2. *"Vitrification and devitrification during the non-isothermal cure of a thermoset studied by TOPEM®"*. In press, Future UserCom num 30 edited by Mettler-Toledo AG Analytical, Switzerland.

### *Appendix 5. Conferences*

1. *CALCAT 06. CALORIMETRY AND THERMAL ANALYSIS CONFERENCE. In memoriam of Prof. Lisardo Núñez Regueira*. Santiago de Compostela (Spain). 9th-12th July 2006.
   Poster: The glass transition by TOPEM®, a new modulated DSC technique.

2. *X Reunión GEP*. Sevilla (Spain). 16th-20th September 2007.
   Poster: Estudio de la vitrificación en el curado isotérmico de un sistema epoxi-amina mediante TOPEM. (Study of the vitrification during the isothermal cure of an epoxy-diamine system by TOPEM.)

3. *MEDICTA 2009. 9th Mediterranean Conference on Calorimetry and Thermal analysis.* Marseille (France). 15th-18th June 2009.
   Oral Presentation: Vitrification and Devitrification during the non-isothermal cure of a thermoset studied by TOPEM. Comparison of experimental and simulated results.